The impact of spatial network topologies on the adaptive evolution of *Pseudomonas aeruginosa* metapopulations

Partha Pratim Chakraborty

A thesis submitted

in partial fulfillment of the requirements for the

Doctorate in Philosophy degree in Biology

Department of Biology

Faculty of Science

University of Ottawa

Abstract

Whether and how the spatial arrangements of populations can influence their dynamics of adaptation is not well understood. This is primarily because different theoretical frameworks comparing the dynamics of spread of a beneficial mutation in spatially structured and fully connected (well-mixed) populations often make contrasting predictions. Although classical population genetic theories find little to no impact of spatial structure on adaptation, Evolutionary Graph Theory (EGT) models that treat spatially structured populations as graphs show that specific patterns of connectivity or network topologies of a population can accelerate or decelerate adaptation compared to well-mixed populations. This thesis aims to improve our understanding about the impact of network topology of spatially structured populations on their dynamics of adaptive evolution.

To do this, I first review the experimental literature till date and find that restricted migration in a spatially structured population tends to slow down the pace and extent of adaptive evolution when compared to a well-mixed population. I also find that there are no direct empirical tests that assess the impact of network topologies of populations on their adaptation. EGT predicts that certain topologies, specifically a four-patch star with bidirectional migration through a central hub to each of three peripheral populations, can accelerate the rate at which a beneficial mutation spreads through a population relative to an unstructured, well-mixed population. I directly test this prediction by tracking the

dynamics of a beneficial mutation as it spreads in a four-patch metapopulation of *Pseudomonas aeruginosa* propagated by either star or well-mixed topology. I find that star topologies can accelerate adaptation but only when there is a high chance that the rare beneficial mutation will be lost to genetic drift. Next, I evaluate whether star topologies can still accelerate adaptation when more than one beneficial mutation is competing for fixation in a microbial population. I propagate clonal four-patch metapopulations of *Pseudomonas aeruginosa* by either star or well-mixed topologies under high or low beneficial mutation supply rate, as they adapt to the fluoroquinolone drug ciprofloxacin. I find that star topology can accelerate adaptation only when the beneficial mutation supply rate is kept low. By performing whole genome sequencing of the evolved metapopulations, I show that star topologies achieve this acceleration under low mutation supply because they substitute rare beneficial mutations with a higher repeatability than well-mixed topologies. In other words, evolution is accelerated because rare beneficial mutations are less likely to be lost in star topologies, not because the strength of selection itself increases.

In sum, this thesis has successfully answered both the ‘whether’ and ‘how’ the network topologies of spatially structured populations can influence their dynamics of adaptive evolution. My work emphasizes the importance of including spatial structure as a key ecological complexity in evolutionary models of adaptation to more accurately predict the dynamics of adaptation in natural metapopulations, to improve the evolutionary forecasting and control of the spread of pathogenic and antibiotic resistance genes in

spatially structured microbial populations such as biofilms, or through more complex transportation and hospital networks.

Résumé

L'impact de l'arrangement spatial des populations sur les dynamiques d'adaptation demeure mal compris. Ceci est dû au fait que les prédictions théoriques sur la propagation de mutations bénéfiques dans des populations spatialement structurées, opposées à des populations entièrement connectées, sont souvent contradictoires. Parmi les différentes théories, les modèles dérivés de la théorie classique de la génétique des populations ne prédisent aucun ou peu d'impact de l'arrangement spatial sur les dynamiques d'adaptation. Au contraire, la Théorie Évolutive des Graphe (EGT), traitant les populations spatialement structurées comme des graphes, prédit que certains motifs de connectivité ou de topologies de réseau entre dans ces populations peuvent accélérer ou ralentir l'adaptation par rapport aux populations entièrement connectées. La thèse ici présentée vise à améliorer notre compréhension sur ce sujet et ses différentes théories en testant expérimentalement leurs prédictions.

Je passe d'abord en revue la littérature expérimentale publiée jusqu'à présent. La première constatation est que la migration restreinte dans une population spatialement structurée a tendance à ralentir le rythme et l'ampleur de l'évolution adaptive par rapport à une population bien mélangée. Je constate également l'absence de tests empiriques visant à observer les prédictions des différentes théories sur l'impact des topologies de réseaux de population sur leur adaptation.

EGT prédit que certaines topologies, en particulier une étoile a quatre patchs avec une migration bidirectionnelle à travers un hub central vers chacune des trois populations périphériques (sans migration direct entre ces populations périphériques), peuvent accélérer le taux de propagation d'une mutation bénéfique dans une population par rapport à un système avec migration direct entre chacune des populations (bien mélangée). Je teste empiriquement cette prédiction en suivant la dynamique d'une mutation bénéfique à travers sa propagation dans une métapopulation à quatre patchs de la bactérie Pseudomonas aeruginosa structurée en étoile ou bien mélangée. L'expérience démontre que la topologie en étoile peut accélérer la propagation de la mutation bénéfique, mais seulement sous certaines conditions qui confère à la rare mutation bénéfique une haute probabilité d'être perdue par dérive génétique.

Dans le prochain chapitre, j'évalue expérimentalement si la topologie en étoile peut accélérer l'adaptation lorsque plus d'une mutation bénéfique apparaissant de novo rivalisent pour fixation génétique dans une population microbienne. Je propage des métapopulations clonales à quatre patchs de P. aeruginosa structurées en étoile ou bien mélangées, à des différentes grandeurs de populations (petite ou grande) et taux de migrations (bas et élevé). Cette propagation et évolution expérimentale se déroule alors que les métapopulations s'adaptent à l'antibiotique fluoroquinolone ciprofloxacine. Cette deuxième expérience démontre que la topologie en étoile accélère seulement l'adaptation lorsque le taux de migration (le taux d'approvisionnement de mutation bénéfique entre les patchs) dans le système est bas. En effectuant le séquençage du génome complet des métapopulations évoluées, je démontre que ce résultat est causé

par la substitution en grande répétabilité de mutations rares et bénéfiques dans ces populations comparées aux populations bien mélangées. En d'autres termes, l'évolution est accélérée parce que les mutations bénéfiques rares ont moins de chances d'être perdues dans la topologie en étoile, et non parce que la force de sélection naturelle elle-même augmente.

En résumé, cette thèse offre des réponses aux questions du 'si' et du 'comment' les topologies de réseaux des populations structurées spatialement peuvent influencer les dynamiques de l'évolution adaptive. Mon travail souligne l'importance d'inclure la structure spatiale en tant que condition écologique clé dans les modèles d'évolution pour prédire de façon plus précise les dynamiques d'adaptation dans les métapopulations naturelles. Ceci a des implications directes pour les prévisions et le contrôle de la propagation et l'évolution de gènes pathogéniques et de résistance aux antibiotiques dans les populations naturellement structurées, telles que les biofilms, ou à travers des réseaux de transport et d'hôpitaux complexes.

Acknowledgement

I would like to extend my gratitude to a number of people whose help and support over the years has enabled me to successfully complete this degree.

First and foremost, I would like to thank my PhD supervisor Rees Kassen, who did not only guide me through the scientific adventures but also made it a very enjoyable experience. In the last five years, countless time I have knocked on Rees's office door or sent him lots of 'can we meet?' emails with concerns of various shapes and forms, and there was never a time he did not help while keeping a smile on his face. It is kind of embarrassing to admit that I was unaware of the existence of the entire field of experimental evolution until a very hot afternoon of April 2016, when for the first time I picked up Rees's book. You have changed my perspectives even before you met me and continue to do so till today. Through the PhD, you have encouraged me, kept me on track whenever I digressed (which I did, a lot), showed immense confidence in me, have been really patient and for that, I cannot thank you enough. I am really glad to have had you as my PhD supervisor.

A big thank you to all past and present members of the Kassen lab clan with whom I temporally overlapped. I am immensely grateful to Aaron Hinz for getting me up to speed in laboratory techniques in the early days and invaluable advice on experimental designs. Thank you Felipe Dargent and Noah Houpt for many fruitful scientific conversations, and Noah for his help in making *that* video. Thanks to Sonal Shewaramani for relentlessly

answering my millions of questions about wet-lab and bioinformatic techniques. Thanks to Angela Alonso for sharing the international graduate student journey with me every step of the way, for her help on setting up the bioinformatic pipeline and Compute Canada lessons. Thanks to Keaton Sinclair for asking me to be hopeful when I was not. Thanks to Alex Hicks and Caio Gomez Tavares Rosa for injecting extra positive energy into the lab every day, and also to Justin Gupta for showing us that there are no limits to how big an experiment can be. I have learned a lot of things from each and every one of you, and I thank you for your support throughout the span of my time in the lab.

I also would like to thank the University of Ottawa for all financial support received during my PhD and also Rees for generously covering all research costs and traveling expenses to domestic and international conferences. Special thank you to my thesis committee members Alex Wong, Heather Kharouba and Andrew Pelling, for critical feedback and discussions. Thanks to Justin Gupta for translating the thesis abstract to French.

I would not be able to be here today if it were not for the unwavering encouragement and support from my parents, Maitrayee and Pradip Chakraborty. Me staying so far away from home has not always been easy on all of us but you have helped me concentrate by providing continuous moral support. Also, I would like to thank my mother- and father-in-law Sharmila Roy and Shyamal Roy for their enthusiasm and confidence in me since the days of my Masters. And, finally the most important person in life, my wife Shamayita, I owe everything to you. Everything.

Dedication

This thesis is dedicated to my beloved grandmother. You are not with me today but your encouragement and wisdom still illuminates every choices that I make in life. This thesis is for you.

Table of Contents

Abstract ii

Résumé v

Acknowledgement viii

Dedication x

List of figures xiii

List of tables xiv

Chapter 1: Introduction 1

Chapter 2: The impact of spatial structure on adaptive evolution: a review 6

- Abstract 7
- Introduction 8
- Theoretical modeling of evolution in spatially structured conditions 12
- Experimental implementations of spatial structure and spatial heterogeneity 19
- Literature search 22
- Experimental tests of theoretical predictions 27
- Spatial self-organization or *de novo* emergence of spatial structure in microbial communities 32
- Spatial structure and cancer evolution 34
- Conclusion 35
- Outstanding questions: 36

Chapter 3: Experimental evidence that network topology can accelerate the spread of beneficial mutations 38

- Abstract: 39
- Lay summary: 40
- Main text: 41
- Results: 47
- Discussion: 60
- Methods: 62

Chapter 4: Network topology accelerates de novo evolution of antibiotic resistance in *Pseudomonas aeruginosa* metapopulations 68

- Abstract 69
- Introduction 70
- Results: 77

Discussion 88
Materials and methods 93
Chapter 5: Network topology increases genetic parallelism during de novo evolution of antibiotic resistance in *Pseudomonas aeruginosa* metapopulations 100
Abstract 101
Introduction 102
Results 107
Discussion 116
Methods 122
Chapter 6: General conclusions 127
Appendix A: 130
Appendix B: 147
Bibliography 158

List of figures

Figure 2.1 Spatial structure and spatial heterogeneity 11
Figure 2.2 Experimental implementation of spatial structure and spatial heterogeneity 19

Figure 3.1 Network topologies and experimental design..... 43
Figure 3.2 The proportion of cip^R mutant in replicate metapopulations propagated by either star (blue) or well-mixed (red) networks with unweighted migration. 47
Figure 3.3 The proportion of cip^R mutant in replicate metapopulations propagated on either star (blue) or well-mixed (red) networks with weighted migration 52
Figure 3.4 The proportion of the cip^R mutants in the constituent subpopulations of each replicate metapopulation propagated as either star (both panel A and B, first row) or well-mixed (both panel A and B, second row) networks with unweighted migration of 0.001% (~100 individuals).. 54
Figure 3.5 The proportion of the cip^R mutants in the constituent subpopulations of each metapopulation propagated by either asymmetric star or well-mixed networks under high (panel A: 1% or 10^5 individuals) and low (panel B: 0.001% or 10^2 individuals) weighted migration. 57
Figure 3.6 The proportion of cip^R mutant in replicate metapopulations propagated on either an inward star (blue) or well-mixed (red) networks with low population size (10^5 CFU/mL) and low migration rate (10^3 CFU/mL)..... 59

Figure 4.1 Design for de novo evolution experiment. 75
Figure 4.2 Dynamics of adaptation in large metapopulations. Fitness trajectories in large metapopulations connected by high and low migration rates (LPHM and LPLM). 77
Figure 4.3 Dynamics of adaptation in small metapopulations. Fitness trajectories in small metapopulations (SPHM and SPLM) connected by high and low migration rates. 79
Figure 4.4 Distribution of fitness effects of isolates in the selection medium. Absolute fitness of evolved end-point isolates in the selection medium (LB supplemented with subinhibitory concentration of ciprofloxacin)..... 81
Figure 4.5 Distribution of fitness effects of isolates in in the permissive medium. 85
Figure 4.6 Ciprofloxacin resistance of evolved isolates..... 87

Figure 5.1 Genetic changes detected in the evolved metapopulations 111

List of tables

Table 2.1 Experimental tests of spatial structure on adaptive evolution in microbes..... 24
Table 2.2 Experimental tests of spatial structure on evolution of cooperative behavior 25
Table 2.3 Experimental tests of spatial structure on host-parasite coevolutionary dynamics 26

Table 5.1 Mutational spectrum of the evolved metapopulations..... 109
Table 5.2 Population-level parallelism..... 115

Chapter 1:

Introduction

"Nothing in biology makes sense except in the light of evolution"

- Theodosius Dobzhansky

"Nothing (or little) makes sense in ecology and evolution without a spatial perspective"

- Hanski and Gaggiotti (2004)

Adaptive evolution happens when natural selection increases the frequency of adaptive genetic variation in a population. Therefore, adaptation is a combination of two processes: the introduction of adaptive genetic variation and its incorporation to the population (Bell 2008; Kassen 2014). Adaptive genetic variations are supplied to a population primarily by *de novo* beneficial mutations but in sexually reproducing organisms, the recombination process can also reshuffle any pre-existing genetic variation to provide more fuel for adaptive evolution. Furthermore, in populations connected by migration, genetic variations can be externally introduced by the process of gene flow. Upon its arrival, a beneficial mutation, however advantageous, can be lost from a population due to genetic drift. Only after the beneficial mutation has reached an appreciable frequency where genetic drift cannot lead to its stochastic loss, it comes under the "eye" of natural selection, starts deterministically increasing in frequency until every member of the population possess the mutation or it is "fixed".

What determines the speed of adaptive evolution? Two factors: the rate at which beneficial mutations are introduced and the probability that they will fix in the entire population (probability of fixation). Therefore, the rate and extent of adaptive evolution simply depends on the probability of fixation of beneficial mutations, all else being equal. Due to its quantitative value for measuring adaptation, the probability of fixation is one of the most extensively studied point metrics in evolutionary biology and population genetics literature (Patwa Z and Wahl L.M 2008). There are many factors that influence the probability of fixation, which in turn impacts the dynamics of adaptation. My thesis focuses on one of the much disputed determinants of the probability of fixation - the spatial structure of populations.

Natural populations are spatially structured, meaning they are composed of an array of subpopulations that are arranged in space and connected by migration. This type of arrangement is also known as a metapopulation (Hanski and Gilpin 1997). Despite this well-known ecological complexity, much of evolutionary theory has modeled the dynamics of adaptation in natural populations assuming little to no spatial structure. This is in part because different theoretical approaches make contrasting predictions on the impact of spatial structure on the probability of fixation of a beneficial mutation. In this vein, early population genetic models do not find any role of spatial structure on probability of fixation (Maruyama 1970; Barton and Whitlock 1997). In contrast, models rooted in another mathematical approach known as the Evolutionary Graph Theory (EGT) predict that probability of fixation is dependent on the specific spatial arrangement or the connectivity of a population (Lieberman et al. 2005). EGT imagines populations as graphs where

individuals reside on the vertices and are connected to their neighbors by migration along the edges. EGT predicts that specific topologies of these graphs or populations, can either accelerate or decelerate adaptation by increasing or decreasing the fixation probability of a beneficial mutant. This is an exciting prediction that has remained empirically untested thus far.

In this thesis, I test the theoretical predictions of EGT under realistic experimental conditions. I evolve *Pseudomonas aeruginosa* 4-patch metapopulations by treating four homogeneously mixed subpopulations as nodes and propagate them using network topologies as proposed by EGT. Over the years, experimental evolution has emerged as an effective way to test specific evolutionary hypotheses in the laboratory(Kawecki et al. 2012; Kassen 2014; Lenski 2017; Van den Bergh et al. 2018; McDonald 2019). Specifically, evolutionary biologists have used microbial populations to test theoretical predictions about the dynamics of fitness gain(Barrick et al. 2009; Lang et al. 2013), genetics of adaptation(Good et al. 2017), adaptive diversification(Rainey and Travisano 1998), evolution of novelty (Kassen 2019) and so much more(Kassen 2014). In this thesis, I have used the gram negative opportunistic human pathogen *Pseudomonas aeruginosa* strain 14 (Pa14) as a model organism for all of my experiments. Pa14 causes persistent nosocomial infection in patients with cystic fibrosis and is a priority 1 level pathogen in the WHO list of critical multi-drug resistant pathogens. One major cause of persistent infection created by Pa14 is that they readily become resistant to the antibiotics used to treat them. In all of the experiments performed in this thesis, I have followed the resistance evolution of Pa14 to a widely used fluoroquinolone drug, ciprofloxacin, as an

experimental model of adaptation. The phenotypic and genotypic determinants of evolution of Pa14 resistance to ciprofloxacin is very well studied which have helped me to formulate predictions on the underlying evolutionary dynamics(Wong and Kassen 2011; Wong et al. 2012; Melnyk et al. 2017).

The rest of the thesis is structured as follows. In chapter 2, I review the theoretical literature on the impact of spatial structure on adaptation and the experimental tests of these predictions using microbial populations and communities. I highlight broad qualitative and quantitative trends from the accumulated experimental data and compare these trends with the expectations from theory. In this process, I identify network topology of metapopulations, an aspect of spatial structure, and its influence on the dynamics of adaptation to be empirically understudied. To fill this knowledge gap, in chapter 3, I experimentally test the predictions from EGT that a particular network topology such as a star, where all peripheral subpopulations of a population are only connected through a central “hub”, can accelerate adaptation compared to well-mixed topology. As a proof-of-principle, I identify the experimental conditions necessary to observe a faster spread of a beneficial mutation in star metapopulations of *P. aeruginosa* compared to well-mixed metapopulations and the underlying evolutionary mechanism responsible for this acceleration. The fixation probability of a beneficial mutation depends on the supply rate of beneficial mutations in a population, independently of the network topology. In chapter 4, I study the inter-dependence of mutation supply rate and network topologies on the dynamics of adaptation of *P. aeruginosa* metapopulations as they evolve to mild ciprofloxacin stress. I propagate multiple replicate metapopulations by star and well-

mixed network topologies under different supply rates of beneficial mutations and measure the dynamics of fitness gain, the distribution of fitness effects of substituted beneficial mutations and other phenotypic determinants of adaptation, such as antibiotic resistance. In chapter 5, I investigate the genetic determinants of adaptation by performing whole genome sequencing on a subset of metapopulations evolved in chapter 3. I quantify and compare population-level genetic parallelism (i.e. similar genetic changes in replicate populations as a result of evolution) to elucidate the genetic basis of evolutionary acceleration expected in star topologies. In chapter 6, I provide a general conclusion of all my experimental results and future directions.

Almost all of the experimental work described in this thesis was performed by me. I took a lead role in these projects with the help from my supervisor Dr. Rees Kassen. The contributions of collaborators, wherever applicable, are noted at the beginning of each chapter.

Chapter 2:

The impact of spatial structure on adaptive evolution: a review

Partha Pratim Chakraborty & Rees Kassen

This chapter will be communicated as a review article (manuscript under preparation).

Abstract

Ecology is a potent force driving evolution in natural populations. Evolutionary theory has long debated the impact of a certain kind of ecological complexity - spatial structure or the restricted mixing of genotypes or growth conditions - on the dynamics of adaptation, resulting in many experimentally testable predictions. To evaluate which of these predictions are best supported empirically, we examine the outcomes of selection in spatially complex environments using data from microbial evolution experiments. Three common trends emerge. First, the dynamics of adaptation are slower under spatially structured relative to well mixed conditions. Second, spatial structure contributes to the evolution and maintenance of community interactions and dictates the speed of coevolutionary dynamics. Third, underlying environmental heterogeneity in spatially structured populations leads to adaptive diversification. Taken together, these results underscore the importance of spatial structure for understanding the long-term evolutionary and community dynamics in microbial communities and other clonal populations, such as cancers, with vital implications for human health and medicine.

Introduction

Natural populations are often spatially subdivided, meaning they are spatially separated into multiple subpopulations and connected to each other by migration. Whether and how spatial subdivision influences the outcome of selection during adaptation is one of the oldest debates in evolutionary biology, dating back to the two seminal models of adaptive evolution – R. A. Fisher's "fundamental theorem of natural selection (FTNS)" and Sewall Wright's "shifting balance theory (SBT)" - and how they interpreted the role of ecological complexity in modulating selection (Fisher 1930; Wright 1932; Frank and Slatkin 1992; Coyne et al. 1997; Wade and Goodnight 1998; Svensson and Calsbeek 2012).

The central point of debate stems from different perceptions of the structure of natural populations. In the Fisherian view, selection occurs in a large, panmictic and freely recombining population such that the fitness effect of any given allele can be described by its average fitness improvement over the current wild type when tested against all possible genetic backgrounds. This interpretation implicitly assumes a single global fitness optimum, with natural selection sifting through all extant genetic variance (Fisher 1930; Frank and Slatkin 1992). The Wrightian view, by contrast, sees populations in nature as subdivided into many small populations connected to each other by migration. Due to their small size, genetic drift is strong, leading to stochastic changes in the frequencies of the most abundant genotypes in each subpopulation. The fitness effect of a given allele therefore depends strongly on which genetic background, that is, in which subpopulation, it is located. Consequently, different subpopulations explore the "adaptive landscape" independently of the other subpopulations, potentially leading to the evolution

of different optimal genotypes on distinct local fitness peaks. Adaptation occurs across the larger collection of subpopulations because some peaks have higher absolute fitness than others, and so send out a disproportionately higher number of migrants to the other subpopulations, resulting in an increase in fitness of the entire population (Wright 1932; Svensson and Calsbeek 2012).

The views of Fisher and Wright represent opposite ends of a spectrum for how spatial structure might impact adaptation in natural populations – no spatial subdivision as opposed to complete subdivision but connected through migration. Although both of these views are highly idealized, at first glance most natural populations probably appear closer to Wright's description than Fisher's, being characterized as "population of populations" or metapopulations (Hanski and Gilpin 1997).

The term spatial structure is used in the literature to describe the arrangement of both populations and environments in space. More specifically, spatial structure refers to the restricted movement of individuals or resources as a result of geographical or physical barriers in space. Spatially structured populations are composed of multiple subpopulations that are arranged in space and are connected by migration, a scenario commonly referred to as a metapopulation. It is common to find other terms such as population subdivision or population structure used synonymously with spatial structure in the literature. The core feature common to all these terms is that, due to restricted migration among subpopulations, selection (or competition among genotypes) acts locally within each subpopulation. In a well-mixed population, by contrast, individuals compete

globally (Fig 2.1). The differential scale of competition among genotypes is the core reason why evolutionary outcomes in spatially structured populations are expected to deviate from those in well-mixed populations.

If resources or other features of the environment are also spatially structured, then conditions of growth will vary from place to place, generating divergent selection that can lead to diversification (Kassen 2002, 2014). It is important to remember that the extent to which environmental conditions are spatially structured constitutes a distinct axis of variation separate from that of population subdivision. This distinction has not always been made clear in the literature, where the term ‘spatial structure’ is often used to refer both to population subdivision and spatial variation in conditions of growth. The two are separate concepts, however, whose combinations lead to distinct evolutionary outcomes (Fig 2.1).

To see this, consider the outcomes of selection in each cell of Fig 2.1. A well-mixed population occupying an otherwise uniform environment (lower left cell) is expected to lead to a single, well-adapted specialist whereas a spatially structured population occupying a heterogeneous environment (upper right cell) should lead to the evolution of distinct, coexisting niche specialists. In a well-mixed heterogeneous environment (lower right cell), we might expect a single generalist type to evolve. The outcome of selection in a spatially structured, homogeneous environments (upper left cell) is less clear because it depends to a large extent on whether the views of Fisher or Wright are more accurate representations of how selection happens.

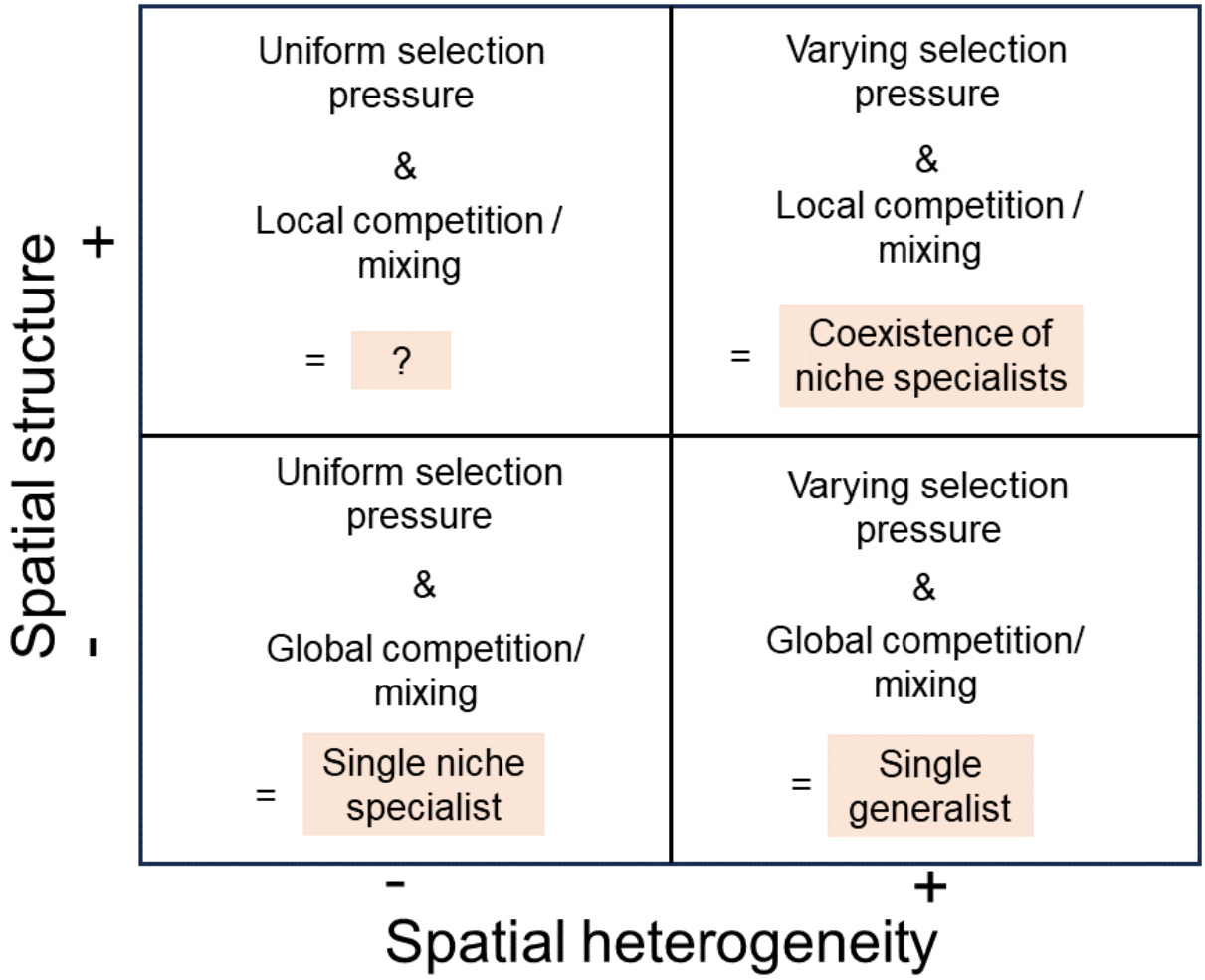

Figure 2.1 Spatial structure and spatial heterogeneity. Each tile shows the mechanism by which each of the components of spatial structure and heterogeneity exerts its effect on evolution. The corresponding expected evolutionary outcomes are represented with orange shading. The dynamics of upper-left tile is undefined.

Our goal in this review is to assemble the large theoretical and empirical literature on the role of spatial structure on adaptive evolution to guide our understanding of the expected evolutionary outcomes under spatially structured conditions. We specifically focus on the data available from microbial evolution studies in the laboratory, as they provide a highly tractable means of directly testing evolutionary theory (Kassen 2014; Lenski 2017; Van den Bergh et al. 2018; McDonald 2019). Moreover, there are two additional reasons to study spatial structure and heterogeneity in microbes: 1) they often occupy environments that are both structured and heterogeneous; 2) we can readily manipulate both dimensions of spatial structure and spatial environmental heterogeneity in the laboratory and study their effects independently and in combination.

Theoretical modeling of evolution in spatially structured conditions

Historically, evolutionary dynamics in spatially structured populations have been studied under different combinations of the three evolutionary forces: migration, selection and genetic drift (Felsenstein 1976; Slatkin 1985, 1987; Barton and Whitlock 1997; Rousset 2004). These studies have been reviewed in the context of the impact of spatial structure on genetic differentiation (Pannell and Charlesworth 2000), genetic divergence and speciation (Barton and Charlesworth 1984), adaptation to local environmental conditions (Lenormand 2002; Kawecki and Ebert 2004) the maintenance of genetic polymorphism (Hedrick 1986; Harrison and Hastings 1996; Charlesworth et al. 2003), evolution of geographical species ranges (Sexton et al. 2009; Angert et al. 2020; Kottler et al. 2021) and genetic equilibrium in clines (Endler 1977). Spatial structure is modeled imagining

space either as a continuum or discrete isolated demes connected by migration, the latter being our main focus because it affords more latitude in specifying the connection between spatial arrangement and dispersal. To be more precise, this literature examines different metapopulation structures (such as the mainland-island, island, classical metapopulation or patchy populations etc.) together with different migration schemes connecting these structures (such as fully connected island model vs. stepping-stone model that only connects immediate neighbors etc.)(Felsenstein 1976). Most models examine evolutionary dynamics by tracking deleterious or neutral mutations with the aim of providing an account for the distribution of extant quantities of genetic variation among subpopulations. Interested readers can consult reviews on the impact of spatial structure on various ecological and demographic processes (Hanski and Gilpin 1997; Tilman and Kareiva 1997; Amarasekare 2003), evolution in metacommunities (Urban et al. 2008) and conservation of endangered species in the presence of gene flow (Aitken and Whitlock 2013; Kelly and Phillips 2016) as entrees into this literature. As our interest is in how spatial structure impacts the dynamics of adaptation, what follows is a brief summary of the most salient models and their predictions.

I. The dynamics of adaptation in spatially structured conditions

The dynamics of adaptation under spatially structured conditions have been studied by at least two classes of models. We have divided these studies according to the predictions they make.

(A) Classical population genetic and cellular automata models

Two point metrics have been frequently studied to determine the impact of spatial structure on the speed of adaptive evolution: 1) the probability of fixation - meaning the likelihood a given beneficial mutation ultimately spreads to all members of the population, and 2) the rate at which beneficial mutations spread or rate of substitution. These efforts started with the investigation of the fixation dynamics of a single beneficial mutation in a spatially subdivided population (Maruyama 1970) and later the original framework has been extended by studying the impact of other factors such as extinction and recolonization dynamics, fluctuating subpopulation size, dominance and the presence of other competing beneficial mutations (Barton 1993; Whitlock 2003; Gordo and Campos 2006; Patwa Z and Wahl L.M 2008). Although the outcomes of these models are sensitive to specific parameters they put forward two interesting predictions. First, when the supply rate of beneficial mutations is low, the fixation probability of a beneficial mutation does not depend on the spatial structure of the population i.e. it is the same as that of a well-mixed population (Maruyama 1970; Slatkin 1981). Second, when multiple beneficial mutations are competing for fixation in the absence of recombination (termed as “clonal

interference")(Gerrish and Lenski 1998), spatial structure increases the fixation time for beneficial mutations and decreases the rate of adaptation and this "cost of adaptation" increases with clonal interference (Gordo and Campos 2006).

(B) Evolutionary Graph Theory models

Recently, the generality of the first prediction stated in the previous paragraph has been challenged by another theoretical framework called the Evolutionary Graph Theory (EGT) (Lieberman et al. 2005; Nowak 2006a). EGT imagines a subdivided population to be spatially arranged as a graph where individuals inhabit each node of the graph and are connected to adjacent neighbors via the connecting edges. Almost 20 years in continuous development, EGT has put forward numerous graph structures that can either increase or decrease the probability of fixation of a beneficial mutation compared to a well-mixed structure (Pavlogiannis et al. 2018; Tkadlec et al. 2021). Lately, there has been a theoretical push to treat these graphs as metapopulations in which populations instead of individuals have been modeled as the nodes and the edges among them have been represented as migration networks (Marrec et al. 2021; Yagoobi and Traulsen 2021). Since EGT is free from the limited use of metapopulation structures and restricted migration as in the earlier population genetic models, the gradual inclusion of relevant population genetic parameters and ecological realism in the EGT could get us closer to a general theory of evolution in spatially structured populations.

II. The evolution of community-level behaviors in spatially structured conditions

The effect of spatial structure on the evolution of community-level interactions such as cooperation has been widely studied. The evolution and maintenance of cooperative interactions represent an evolutionary paradox, since they are exploitable by non-cooperative individuals (or cheaters) that reap the benefits of cooperation but do not themselves invest in cooperative behavior (Maynard Smith 1997). Inclusive fitness (kin selection theory) theory (Hamilton 1963, 1964, 1972; Queller 1992, 1994; Taylor 1992), social evolution theory (Frank 1998) and game theoretical (Nowak and May 1992; Nowak 2006a,b) models have identified spatial structure to be an important condition under which cooperation persists in a population. This is because of limited mixing offered in spatially structured populations direct the benefits back to the cooperators as high population or environmental structure is predicted to keep highly related cooperative individuals at a close proximity and prevent invasion by the cheaters. By clustering cooperative individuals together and keeping their benefits for themselves, spatial structure also has been shown to promote the transition from unicellularity to multicellularity (Michod and Roze 2001; Pfeiffer and Bonhoeffer 2003).

III. Coevolutionary dynamics in spatially structured conditions

There has been a long standing interest in evolutionary ecology to understand the impact of geographical separation on coevolutionary dynamics among species (reviewed in Thompson 2005; Gomulkiewicz et al. 2007). Just as abiotic growth conditions, biotic

interactions are also unevenly distributed in space and such localized ecological interactions have been acknowledged to shape overall patterns of regional and global biodiversity. One of the most extensively studied topics in this context is the antagonistic coevolution between hosts and their parasites (reviewed in Lion and Gandon 2015; Buckingham and Ashby 2022). Spatial structure has been shown to play important roles in various aspects of host-parasite coevolutionary dynamics - promote fluctuating coevolution, increase host defenses and decrease parasite virulence and transmission (reviewed in Buckingham and Ashby 2022). However, these trends are often found to vary depending on specific details of the model, such as the host life-history, migration rates of hosts and their parasites, host defense strategies, and virulence mechanisms etc.(Lion and Gandon 2015). For example, parasites will evolve a decreased virulence when local interactions lead to clonal infections and a prudent exploitation of host (Boots and Sasaki 1999, 2000; Wild et al. 2009). In contrast, spatial structure can also increase virulence when host-colonization is mediated through cooperative secretion of harmful virulence factors (Frank 1996; Buckling and Brockhurst 2008). In other works, spatial structure has also been shown to reduce degree of predation in predator-prey communities (Murrell 2005) or facilitate mutualistic interaction between hosts and their symbionts (Bever and Simms 2000).

IV. Evolution of diversity in both spatially heterogeneous and spatially structured conditions

Evolutionary theory predicts that variable abiotic growth conditions from patch to patch in a spatially structured population can promote the evolution of ecological niche, resource specialization and species diversity (reviewed in Kassen 2002, 2014). This is because divergent selection “pulls-off” subpopulations in different directions. Even when the strength of divergent selection is low, sufficiently low migration among the subpopulations can drive the emergence and maintenance of genotypic and phenotypic diversity through local adaptation (Lenormand 2002; Kawecki and Ebert 2004). As for biotic conditions, models of coevolution implicitly assume spatially variable selection pressures since subpopulations of either interacting partner can evolve along different evolutionary trajectories. We do not review the literature on spatially heterogeneity here further as much of it has already been reviewed elsewhere (reviewed in Kassen 2002, 2014).

For simplicity, most of the theoretical studies summarized here have assumed the study system to be an asexually reproducing organism and even if they did not, the predictions are quite generalizable that they apply to both sexual and asexual organisms. Experimentalists have taken advantage of this fact and tested these predictions through experimentally evolving microbes in the laboratory under controlled conditions. As a result, empirical literature studying the impact of spatial structure and spatial environmental heterogeneity on many aspects of the evolutionary dynamics in microbial

communities ranging from their rates of adaptation to adaptive diversification has grown, albeit slowly, over the last few decades which we discuss below.

Experimental implementations of spatial structure and spatial heterogeneity

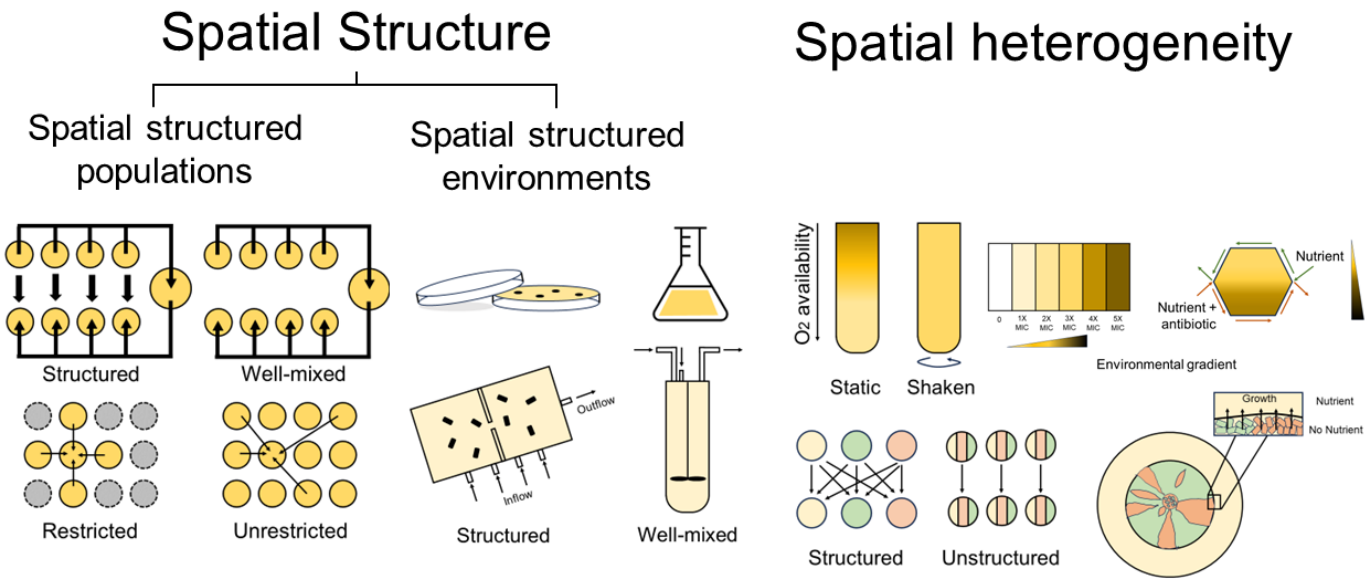

Figure 2.2 Experimental implementation of spatial structure and spatial heterogeneity Different definitions and experimental implementations of spatial structure used in the microbial evolutionary ecology literature**.**

Evolutionary ecologists have manipulated both dimensions of spatial structure (populations and environments) in the context of microbial evolution experiments. These experimental implementations of spatially structured conditions and their comparable well-mixed controls are schematically shown in Figure 2.2. Limited mixing of populations

or resources has been achieved most commonly in two ways. First, population subdivision has been mimicked by experimentally creating a metapopulation structure (Miralles et al. 1999; Kryazhimskiy et al. 2012; France and Forney 2019). Here, each subpopulation is grown in well-mixed liquid environments but they are connected to each other by limited migration. In this case, a metapopulation where subpopulations are fully connected to each other has been used as a well-mixed control. Additionally, the impact of local migration compared to global migration has been tested similarly adhering to the metapopulation structure but carefully controlling the source location of immigrants (Kerr et al. 2006; Nahum et al. 2015). Second, the physical structure of the environment has been manipulated to restrict mixing. In this case, the growth medium has either been completely or partially solidified to limit migration and flow of nutrients (Korona et al. 1994; Habets et al. 2006; Perfeito et al. 2007b; Susan F. Bailey et al. 2021). With the advent of microfabrication techniques, microfluidic chambers have also been frequently used to create physical barriers (Keymer et al. 2006; Hol et al. 2013; Nagy et al. 2018). To differentiate this evolutionary dynamics from a well-mixed conditions unstructured environment such as a liquid growth medium or a chemostat have been used.

Microbes grow as sessile masses such as biofilms in natural environments. Therefore, the complexity of the spatial structure of a biofilm often has been mimicked by using biofilm flow chambers where microbes grow on glass surfaces or growing them on solid nutrient plates as dense colonies (Hansen et al. 2007; Ponciano et al. 2009; Kim et al. 2014; Mitri et al. 2016; France et al. 2019a) or more recently with the use of microfluidic constructs (Keymer et al. 2008; Lambert et al. 2011; Nadell et al. 2017; Dal Co et al.

2019a,b). It is important to mention that, the use of these implementations depends on the experimental questions and each one of them affords the experimenter with control over different dimensions of parameter space. For example, in experimental models of population subdivision migration rates can be controlled precisely but controlling the flow of nutrients in each well-mixed subpopulation is not possible. Contrastingly, growth on a solid medium can keep intact population structure and limit nutrient movement but not control for exact migration rate. In microfluidic devices it is possible to control both the ecological and population genetic parameters. However, implementation of microfluidic devices is not mainstream in experimental evolution literature as of yet (Nagy et al. 2018).

Experimental manipulations of spatial environmental heterogeneity have been achieved by simply creating variability in growth conditions across space in the form of spatial gradients or changing environments in coarse-grained or fine-grained ways (Fig 2.2) (Zhang et al. 2011; Bailey and Kassen 2012; Baym et al. 2016). In this respect, spatially structured environments have often been regarded as spatially heterogeneous even if the experimenter did not explicitly change the growth conditions (Korona et al. 1994; Habets et al. 2006). This is because of two reasons: microbes can themselves manipulate their own surrounding environment by secreting metabolites and the physical structure of the environment often prevents the uninterrupted flow of nutrients, both of which can create localized heterogeneity in the growth environment. As a control, a homogeneous or "mass-action" growth medium has been used.

Literature search

We searched two major biology databases: ISI Web of Science and Google Scholar using keywords such as “spatial structure”, “spatial heterogeneity”, ”adaptation”, ”diversi*”, “experimental evolution”, “microb*”, “migration”, “dispersal”, “gene flow” and different combinations thereof. We filtered the studies using three criteria. First, the study must be an experimental evolution study spanning several generations of growth where spatial structure or spatial heterogeneity has been actively manipulated to test a theoretical prediction (i.e. not an observational study). Second, the study was performed using microbes (e.g. bacteria, virus, nematodes etc.). Third, the study has a well suited control to differentiate the impact of spatial structure or spatial heterogeneity and if not, the experimental expectation in the well-mixed or unstructured condition is unambiguous and well established. For studies on spatial heterogeneity, we have adhered to an earlier consideration of counting resource mixtures as a form of spatial heterogeneity (Kassen 2002) but also have included experiments that manipulate growth conditions in discrete patches connected by migration. We would be immensely grateful if the readers update us on the studies that we might have overlooked in our literature search.

After the literature search, the research articles were divided into 3 main themes: studies that investigate (1) the dynamics of adaptation and (2) the evolution of community dynamics and coevolution under spatially structured conditions, and finally studies that focus on (3) the evolution and maintenance of diversity in spatially heterogeneous environments. Following this screening, the evolutionary responses under spatially structured conditions were collected and compared with well-mixed conditions. A plus

('+') or a minus ('-') sign indicates that spatial structure increases or decreases the adaptive response compared to a comparable well-mixed control. Not applicable ('NA') indicates where the data from corresponding well-mixed control is not available. A question mark ('?') indicates that the comparison between spatially structured and well-mixed control is not available. Same procedure was carried out for studies dealing with spatial heterogeneous and homogeneous conditions. The resulting data is available as Table 2.1-2.3.

Table 2.1 Experimental tests of spatial structure on adaptive evolution in microbes

Spatial structure	Well-mixed/unstructured reference	Study organism	Length of experiment	Signs of adaptation in spatially structured conditions	Measure of adaptation	Reference
Solid agar growth medium	Liquid culture (shaken flask)	*Ralstonia spp.* (comamonas sp.)	1000 generations	? (Did not compare)	Fitness	Korona et al. 1994
Increasing migration rate	NA	Vesicular stomatitis virus	25 daily transfers (~100 generations)	-	Fitness	Miralles et al. 1999
Variable migration rate	100% migration	*Saccharomyces cerevisiae*	550 generations	-	Fitness	Kryazhimskiy et al. 2012
Local migration(from adjacent subpopulation)	Global migration (from any subpopulation)	*Escherichia coli*	36 daily transfers	+	Fitness	Nahum et al. 2015
Variable migration rate	100% migration	*Escherichia coli*	21 daily transfers (~150 generations)	No change	Fitness	France and Forney 2019
Biofilm flow chamber	Liquid culture (shaken test tube)	*Escherichia coli*	75 days in biofilm or 25 days in liquid	-	Frequency of costly mutations	France et al. 2019a
Solid agar growth medium	Liquid culture (shaken test tube)	*Escherichia coli*	275 generations	-	Fitness	Perfeito et al. 2007b
Solid agar growth medium, (a) complete or, (b) no population structure	Liquid culture (shaken test tube)	*Escherichia coli*	900 generations	-	Fitness	Habets et al. 2006
Solid agar growth medium with intact population structure	Invader and ancestor strains scraped, mixed and competed in liquid media	*Escherichia coli*	5 days (40 generations)	-	Rate of invasion	Habets et al. 2007
Semi solid growth medium (0.2% agar)	Liquid culture (24 well plate)	*Pseudomonas fluorescens*	200 generations	-	Fitness (growth rate)	Susan F. Bailey et al. 2021
Solid agar growth medium	Liquid culture (96 well plate)	*Escherichia coli*	24 hours	-	Frequency of costly mutations	Durão et al. 2020
			10 days (~82 generations in liquid and ~74 generations in solid)	-	Marker divergence, fitness	

Table 2.2 Experimental tests of spatial structure on evolution of cooperative behavior

Spatial structure	Well-mixed/unstructured reference	Study organism	Length of experiment	Sign of adaptation in spatially structured conditions	Measure	Reference
Solid agar growth medium	Liquid culture (shaken flask)	*Salmonella enterica* ser. *Typhimurium* and methionine auxotrophic *E.coli*	4 transfers in structured/ 5 transfers in well-mixed environment	+	Frequency of mutualist partners	Harcombe 2010
Solid agar plates with increasing solidness (viscosity)	Liquid culture (static)	*P. aeruginosa* PAO1 and PAO9 as cheater	36 hours	+	Relative fitness of cooperators (to cheaters)	Kümmerli et al. 2009
Solid agar growth medium	Liquid culture (24 well plate)	*Acinetobacter baylyi* and *Escherichia coli*	24 hours	+	Productivity (cell count)	Pande et al. 2016
NA	Liquid culture (shaken flask)	*Myxococcus xanthus*	1000 generations	+	Social phenotypes	Velicer et al. 1998
Microfluidic device with homogeneous growth conditions	Liquid culture (shaken flask)	*Escherichia coli* and its *rpoS* mutant	upto 7 days	+	Frequency of the *rpoS* mutant	Hol et al. 2013
Solid agar growth medium	NA		3 days	+		Hol et al. 2015
Semi-solid agar growth medium				-		Hol et al. 2015
Microfluidic device with heterogeneous growth conditions	NA		40 hours	+		Lambert et al. 2011
Microfluidic device with heterogeneous growth conditions	NA		3 days	+		Keymer et al. 2008

Table 2. 3 Experimental tests of spatial structure on host-parasite coevolutionary dynamics

Spatial structure	Well-mixed/unstructured reference	Study organism	Length of experiment	Sign of adaptation in spatially structured conditions	Measure	Reference
Unshaken liquid culture (test tube)	Intermittently shaken/ mixed liquid culture (test tube)	*P. fluorescens* isolate SBW25 and SBW25-phi-2 bacteriophage	16 transfers (~120 generations)	-,-	Host resistance, pathogen virulence	Brockhurst et al. 2003
Unshaken liquid culture (test tube)	Constantly shaken liquid culture	*P. fluorescens* isolate SBW25 and PP7 bacteriophage	24 transfers (~ 180 bacterial generations)	No change,-	Host resistance, pathogen virulence	Brockhurst et al. 2006
Metapopulations connected by unrestricted or restricted migration	All subpopulations of the metapopulations mixed and structure destroyed	*Escherichia coli* and T4 coliphage	20 transfers (transfer every 12 hours)	-	Pathogen virulence	Kerr et al. 2006
Metapopulations either isolated or connected by varying topologies with unidirectional dispersal	Global mixing of subpopulations	*P. fluorescens* isolate SBW25 and SBW25-phi-2 bacteriophage	12 transfers (each transfer 48 hours)	+,-	Host resistance, pathogen virulence	Vogwill et al. 2010
Bacterial population grown in the presence of a nematode host on solid agar plates	Liquid culture (falcon tubes)	*P. aeruginosa* PAO1 evolved in the presence of its host *C.elegans*	30 transfers (~200 generations)	+	Pathogen virulence	Granato et al. 2018

Experimental tests of theoretical predictions

With the data from Table 2.1 - 2.3 we statistically test the general trends of the experimental results that assess the role of spatial structure and spatial heterogeneity on different aspects of eco-evolutionary dynamics in microbial populations or communities. Specifically, we test whether the empirically observed frequencies of evolutionary responses are significantly different from what would be expected by chance.

(A) Dynamics of Adaptation

We find that speed of adaptation decreased under spatially structured conditions in 9 out of 11 experimental evolution studies when compared to well-mixed conditions (Table 2.1). Among the rest of the cases, in one of them fitness did not change and in another, fitness increased. These experiments either directly measured a form of relative fitness or tracked the increase in the frequency of beneficial mutations or monitored the persistence of costly (deleterious) mutations in the population. It is clear from this cohort of studies that spatial structure predominantly slows down the speed of adaptation (chi-square test, $\chi 2$ = 11.636, df = NA, p-value = 0.006497, probability calculated with monte-carlo simulation, p = 0.002973, without simulation). This inefficacy of selection under spatially structured conditions can be attributed to the limited access to the beneficial alleles with the highest fitness advantage because of restricted migration. In comparison, less spatial structure or high migration between subpopulations in well-mixed conditions can supply more large effect beneficial mutations and speed up the dynamics of adaptation by

accelerating their rate of substitution. One exception to this common trend is the study by Nahum *et al.* (2015) where *E. coli* metapopulations propagated with spatially structured or restricted migration (migration from adjacent subpopulations) achieved higher relative fitness than the metapopulations with unstructured or unrestricted migration (migration from any subpopulation) (Nahum et al. 2015). Although, both in their experiment and computer simulations, unrestricted metapopulations were leading the adaptive dynamics in the beginning, they were eventually "overtaken" by their restricted counterparts. Computer simulations explain this pattern being consistent with the adaptive dynamics in a rugged fitness landscape filled with epistatic interactions where subpopulations independently search for optimum fitness peaks, as described in Wright's SBT. However, reports like this that show spatial structure might even speed up adaptation remain extremely rare.

In this context, it is prudent to mention that there is another suite of studies that has used theoretical models, simulations and microbial (*S. cerevisiae* and *E. coli*) competition experiments to highlight the importance of genetic drift in spatially expanding populations (Hallatschek et al. 2007; Korolev et al. 2010, 2012; Bosshard et al. 2017). For an expanding microbial population growing on a solid surface as a dense colony, most of its growth happens at the colony frontiers or in the direction of space and resource availability (Mitri et al. 2016). Thus, the genetic makeup of the progeny is largely determined by only a small fraction of the whole population that is proliferating at the growth frontier. Furthermore, physical bottlenecks at the growing front rapidly reduce genetic diversity, increase genetic drift and decrease the efficacy of purifying selection (Excoffier and Ray

2008; Excoffier et al. 2009). These studies have found that spatial expansion can lead to faster spread of existing beneficial mutations (Gralka et al. 2016), the retention of costly (deleterious) mutations and their subsequent compensatory evolution (Aif et al. 2022). Additionally, more mutations had a higher chance of “surfing”, i.e. establish and grow at the edge of spatially expanding colonies due to strong population bottlenecks, than in liquid well-mixed conditions (Fusco et al. 2016). It is increasingly clear that surface associated microbial growth can be largely dictated by stochastic events such as genetic drift or spatial positioning of a beneficial mutation, and less by the fitness of an individual (Kim et al. 2014; Kayser et al. 2019). This is also apparent in another study where better adapted and more resistant lineages of *E. coli* expanding towards an increasing antibiotic gradient were often physically annihilated by lesser adapted lineages (Baym et al. 2016). These instances demonstrate the importance of chance and positioning in the evolutionary dynamics of surface associated microbial growths such as biofilms.

(B) Community and coevolutionary dynamics

As expected from theory, intraspecies and inter-species cooperation was clearly supported under spatially structured conditions (8 out of 9 studies, $p = 0.039$, binomial test) (Table 2.2). These studies investigate the maintenance of cooperative behavior through one of the following mechanisms: (a) the stabilization of mutualistic interactions between microbial partners (Harcombe 2010; Pande et al. 2016), (b) the promotion of social behaviors by restricting the fitness advantage to the cooperators (Velicer et al. 1998; Kümmerli et al. 2009) and (c) coexistence due to weakened competition dynamics

(Keymer et al. 2008; Lambert et al. 2011; Hol et al. 2013, 2015). However, in some of these cases the experimental implementation of spatial structure was found to have the same competitive outcomes (coexistence or collapse) via different underlying mechanisms or same implementation led to idiosyncratic outcomes (Hol et al. 2015). Please note that all of these studies follow the community dynamics for a short duration (for hours to days) as microbial experimental systems are susceptible to invasion by cheats in the longer term (However, please see Kerr et al. 2002 for coexistence in a non-transitive “rock-paper-scissor” system). Spatial structure also promoted cooperation and resilience in synthetic cooperator-cheater communities (MacLean and Gudelj 2006; Bachmann et al. 2013; Datta et al. 2013; Van Dyken et al. 2013; Limdi et al. 2018), the stabilization of syntrophic relationships in synthetic multispecies communities (Kim et al. 2008) and shaped the evolution of altruistic traits in bacteria, such as lethal bacteriocin synthesis (Chao and Levin 1981). However, we did not add these studies to the statistical analyses due to the study system specificity of the results. Additionally, spatial structured environment supported the evolution of the composition and productivity of an inter-species microbial community (Hansen et al. 2007). Spatial structure in the form of unmixed metapopulations was also shown to facilitate evolutionary transition to individuality by minimizing competition between cells and enhancing group-level fitness in an experimental model system of multicellularity (Rose et al. 2020).

We did not find sufficient microbial experimental evolution studies to formally conduct a statistical test on how spatial structure impacts coevolutionary dynamics (metrics such as host resistance, pathogen virulence or infectivity etc.) (Table 2.3). However, in 4 out of

the 5 total cases, the pathogen evolved lower virulence under spatially structured conditions, as predicted from theory (Brockhurst et al. 2003, 2006; Kerr et al. 2006; Vogwill et al. 2010). In one of them, the rate of coevolution was faster when spatial structure was low (or mixing was high) (Brockhurst et al. 2003). Interestingly, the only other study where lower virulence was shown to evolve under well-mixed conditions highlights that certain virulence mechanisms - in this case, virulence factors as secreted public goods - can be a determining factor for its evolution in spatially structured conditions (Granato et al. 2018). In other studies, spatially structured environments were shown to provide temporary refuge to bacteria and direct the evolution of their resistance mechanisms against phages (Schrag and Mittler 1996; Coberly et al. 2009; Testa et al. 2019; Attrill et al. 2021). Spatially structured environments can also impact phage life-history traits (Roychoudhury et al. 2014) and the evolution of complex bacteria-phage interaction networks and phage speciation through host switch (Shaer Tamar and Kishony 2022).

(C) Adaptive Diversification

Previously, another meta-analysis found that in 12 out of 19 considered cases, selection in spatially structured and/or heterogeneous environments supported more diversity than in unstructured or homogeneous environments (Kassen 2014). We added three more studies to this cohort that show evolution of higher levels of diversity (functional ,morphological or phenotypic) as a result of a heterogeneous structured environment (Venail et al. 2008; Ponciano et al. 2009; Poltak and Cooper 2011). Although, the revised

trend clearly shows that ~68% studies support the prediction that adaptive diversification is favored in heterogeneous environments, it is not statistically significant in a binomial test (15 out of 22 cases, p = 0.1338). Spatial structure also helped retain a higher diversity in a complex microbial consortium comprising 62 strains (Cairns et al. 2018). Spatial heterogeneity coupled with specific modes of population regulation (at the subpopulation or the metapopulation level) can also lead to the evolution and maintenance of polymorphism (Leale and Kassen 2018). However, diversity was transient in this study and ultimately was lost. Additionally, another experiment showed that diversity was lost when populations of *E. coli* evolved in unstructured (liquid) medium were transferred to a structured (solid agar) growth medium owing to plausible loss in cross-feeding interactions in the structured medium (Saxer et al. 2009). For further meta-analysis performed on experimental data regarding the extent of divergent selection, local adaptation or evolution of specialization in spatially heterogeneous environments we would like to invite the readers to consult other reviews (Kassen 2002, 2014; Kawecki and Ebert 2004; Kraemer and Boynton 2017).

Spatial self-organization or *de novo* emergence of spatial structure in microbial communities

The structure of a microbial community is determined by a feed-forward loop between the spatial arrangement and interactions among the community members. Microbial communities grow in spatially structured environments under natural conditions (such as biofilms) and their community interactions (mutualism, cooperation, commensalism,

competition, etc.) are largely a product of the arrangement of the community members in space. At the same time, depending on the type of interactions, the spatial arrangement of the members in the community can also evolve (Lion and Baalen 2008; Nadell et al. 2016). Metabolic interactions (Estrela and Brown 2013, 2018; Momeni et al. 2013; Marchal et al. 2017; Borer et al. 2020), physical shoving due to differential cell shape (Smith et al. 2017), and selective killing of neighbors (McNally et al. 2017) have been identified as some of the factors that can dynamically change the spatial arrangement of a community (reviewed in Yanni et al. 2019). Other factors such as nutrient availability (Mitri et al. 2016) or environmental heterogeneity in terms of physical obstacles (Ciccarese et al. 2020) have also been shown to dictate the self-structuring of these assemblages. Self-structuring is also important in the context of cooperative behavior shown by social amoeba Dictyostelium (Buttery et al. 2012) and Myxococcus (Ramos et al. 2021). Such non-random spatial self-organization has a huge impact for the evolutionary ecology of microbial communities ranging from the optimum functioning of microbial communities in the environment (reviewed in Werner et al. 2014) to the biogeography of microbial infections in humans (reviewed in Stacy et al. 2016; Vega and Gore 2018; Azimi et al. 2022). The underlying eco-evolutionary mechanisms for the emergence of spatial self-organization within microbial communities is a burgeoning field of research and its progress has been comprehensively summarized in other reviews (Cremin et al. 2023).

Spatial structure and cancer evolution

Many parallels can be drawn between the evolutionary dynamics in microbial populations to that of other clonal cell populations, such as cancers (Sprouffske et al. 2012; Korolev et al. 2014). Unique cellular and genetic signatures of different types of cancers are largely dictated by their idiosyncratic evolutionary trajectories and it is one of the main hurdles for designing effective treatment strategies for cancer. Although the development of a tumor starts from a clonal population, its physical architecture in terms of spatial location of cells, cellular dispersal and spatial constraints of growth can further determine its mode of evolution (Lipinski et al. 2016; Yuan 2016; Seferbekova et al. 2023). Recently, a simulation study has shown this is to be the case. In these simulation models, while selection was the strongest in non-spatial cancers such as leukemia, hepatocellular carcinoma evolved almost neutrally. Other glandular cancers diversified genetically, albeit with different outcomes, due to selection acting locally and intensified clonal interference (Noble et al. 2022). In another modeling work, spatial structured growth has been shown to increase the time it takes for a neoplastic cell (i.e. an abnormally growing cell) to substitute sufficient number of driver mutations to develop into cancer (Martens et al. 2011). The research avenue into investigating the impact of spatial structure on cancer evolution still remains in its infancy and we did not come across any experimental studies that test these predictions.

Conclusion

The relative importance of spatial structure on the evolution of populations has been widely contested in the literature. Despite the development of rich theoretical literature on this topic, there has been a paucity of experimental evidence testing the predictions of these theories. Furthermore, the lack of clear definition of different forms of spatial structure has made it difficult to predict the underlying mechanisms and targets of adaptation. We have presented here experimental evidence from nearly the last three decades that points to an unified statement: evolutionary outcomes in spatially structured conditions are quite different than well-mixed conditions. However, the specific dynamics can be idiosyncratic to the implementation of spatial structure. Understanding the impact of spatial structure on adaptive evolution is particularly important for us to interpret the evolutionary dynamics of microbial populations and cancers that inhabit heterogeneous and structured environments. Only by comprehending the ground rules that dictate their evolution can we strategize how to best predict and contain the spread of pathogenic microbes in natural and clinical settings or design effective therapeutic strategies for cancers.

Outstanding questions:

1. The predictions of Evolutionary Graph Theory and the role of network topology of metapopulation on adaptive evolution remain empirically untested. A simple experimental test of EGT could be performed by constructing bacterial metapopulations with different network topologies in the lab and monitoring the spread of a known beneficial mutation in the background of a wild-type. Similar dynamics should be followed in a well-mixed metapopulation as a suitable control.

2. How does the dynamics of adaptation in spatially structured populations depend on the underlying mutation supply rate? The balance between the strength of selection and genetic drift is important in this context and empirical tests are lacking.

3. How are the genetic determinants of adaptation different between spatially structured and well-mixed populations? Is there a difference in the levels of genetic parallelism?

3. What is the length of adaptive walk in spatially structured populations if the fitness effects of substituted mutations in spatially structured populations are different from well-mixed populations? How will these dynamics depend on the ruggedness of the underlying fitness landscape?

4. What is the speed of adaptive dynamics in subdivided populations compared to well-mixed populations when conditions for growth vary in the subpopulations? What if the conditions of growth involve more than nutrients or stress i.e. the presence of predators

or hosts - how fast might anti-predator defense or virulence evolve in a structured population?

5. What is the fate of diversity in spatially structured populations? How does it depend on the connectivity (symmetric or asymmetric migration) among the subpopulations?

7. What is the rate of horizontal gene transfer in structured microbial populations? How does it depend on the cell-cell and metabolic interactions among the participating community members?

Chapter 3:

This chapter is reproduced from:

Experimental evidence that network topology can accelerate the spread of beneficial mutations

Chakraborty, P. P., Nemzer, L. R., & Kassen, R. (2023). *Evolution letters*, 7(6), 447–456.

Collaborator contributions:

Louis Nemzer performed the simulations. Caroline de Ligneris collected experimental data for figure 3.4.

Abstract:

Whether and how the spatial arrangement of a population influences adaptive evolution has puzzled evolutionary biologists. Theoretical models make conflicting predictions about the probability a beneficial mutation will become fixed in a population for certain topologies like stars, in which “leaf” populations are connected through a central “hub.” To date, these predictions have not been evaluated under realistic experimental conditions. Here, we test the prediction that topology can change the dynamics of fixation both *in vitro* and *in silico* by tracking the frequency of a beneficial mutant under positive selection as it spreads through networks of different topologies. Our results provide empirical support that metapopulation topology can increase the likelihood that a beneficial mutation spreads, broadens the conditions under which this phenomenon is thought to occur, and points the way towards using network topology to amplify the effects of weakly favored mutations under directed evolution in industrial applications.

Lay summary:

Most natural populations are spatially structured, meaning they are geographically subdivided and connected by migration. Whether spatial structure impacts adaptive evolution has been less clear, however, as different theoretical approaches to modelling the movement of beneficial mutations in spatially structured populations make contrasting predictions. Our work uses evolution experiments and numerical simulations to help provide clarity. We show that spatial structure can impact the pace of adaptive evolution: certain topologies, specifically a 4-patch star with bidirectional migration through a central hub to each of three ‘leaf’ populations, can accelerate the rate at which a beneficial mutation spreads through a population relative to what happens in an unstructured, well-mixed population. The cause of this acceleration is a reduced probability that beneficial mutations are stochastically lost when they are rare because they get concentrated in the central hub and then disperse outwards to the leaves. Our results offer the first experimental support for models of adaptive evolution in space based on evolutionary graph theory, may help understand the spread of invasive species or pathogens, and could be used to inspire novel topologies to selectively enrich desired traits or biomolecules of interest in industrial applications.

Main text:

The last two decades have seen the development of an empirically grounded theory of mutation-driven adaptation built on the assumption of a large, well-mixed population adapting through mutation to a uniform environment that remains constant in time (Orr 2005a; Martin and Lenormand 2008; Schoustra et al. 2009; Lang et al. 2013; Kassen 2014; Bailey and Bataillon 2016; Tenaillon et al. 2016; Lenski 2017). Yet most natural populations occupy environments that are far more ecologically complex than this theory assumes. One common form of ecological complexity is spatial structure, where a population is composed of a series of subpopulations connected by dispersal (also known as a meta-population). How spatial structure impacts adaptive evolution, and in particular, the dynamics of substitution, in an otherwise uniform environment is not well understood.

By contrast, a rich theoretical literature exists on the effects of different forms of spatial structure on the population genetics of neutral variation (Slatkin 1985; Harrison and Hastings 1996; Hanski and Gilpin 1997; Pannell and Charlesworth 2000) and the interplay between migration and selection in adaptation (Guillaume 2011; Yeaman and Otto 2011; Blanquart et al. 2012). Empirical work has considered the impact of spatial structure through habitat fragmentation on trait evolution (Urban et al. 2008; Cheptou et al. 2017), how population subdivision modulates the extent of adaptive change (Chao and Levin 1981; Korona et al. 1994; Miralles et al. 1999; Habets et al. 2006, 2007; Perfeito et al. 2007b; Zhang et al. 2011; Kryazhimskiy et al. 2012; Nahum et al. 2015; Baym et al. 2016; Bailey et al. 2021b) and community resilience (Limdi et al. 2018). Other work in microbiology has examined the emergence and fate of diversity in spatially structured

environments associated with colony growth or biofilms (Kerr et al. 2002; Nadell et al. 2010, 2016; Steenackers et al. 2016; Celik Ozgen et al. 2018; France et al. 2018, 2019b; Borer et al. 2020; Trubenová et al. 2022) but lacks explicit descriptions of spatial structure, or conflates it with variation in conditions of growth generating divergent selection (Leale and Kassen 2018; Chen and Kassen 2020). Missing, however, are explicit tests of theory on how the spatial arrangement of populations in space impacts the dynamics of adaptive evolution, including the rate of spread of a beneficial mutation and probability of fixation.

Here we explore the impact of network topology – the pattern of connectivity among subpopulations – on adaptive evolution by testing key predictions from two theoretical frameworks, one rooted in classic population genetics and the other in evolutionary graph theory. Population genetic models that track the effects of migration and selection on gene frequencies, often under the simplifying assumption of infinite population size, predict little effect of network topology on the fixation probability of a beneficial mutation (Maruyama 1970; Slatkin 1981). By contrast, models employing evolutionary graph theory (EGT), in which individuals occupy the vertices of a graph and edges represent dispersal routes between neighboring sites, predict that fixation probabilities can change based on how the nodes are connected (Lieberman et al. 2005).

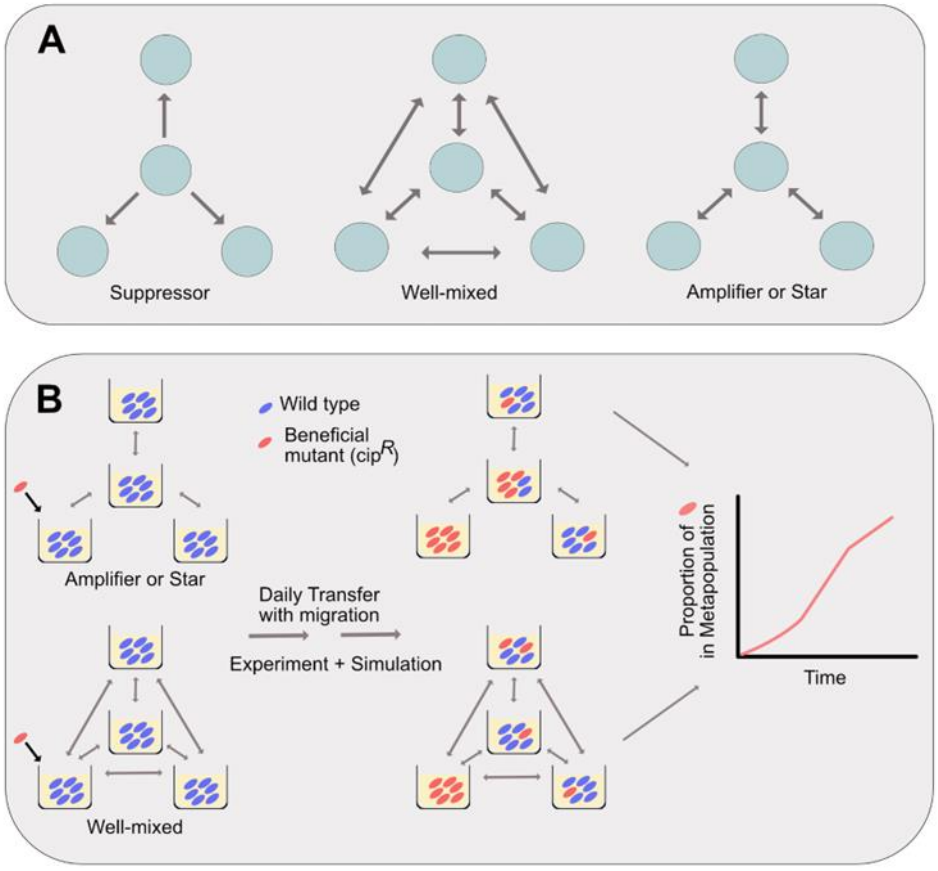

Figure 3.1 Network Topologies and experimental design. A. Three network topologies among four subpopulations. Arrows depict dispersal among subpopulations (green circles). B. Experimental schematics.

To see this more clearly, it is helpful to consider the predictions of each model in one of the simplest possible scenarios, a four deme ‘star’ network composed of satellite ‘leaves’ and a central ‘hub’ (Fig 3.1). Both migration-selection models in population genetics and EGT predict that a rooted ‘star’ network, where one deme supplies more individuals to others than it receives (Fig 3.1A, left panel), can decrease (suppress) fixation probabilities relative to a well-mixed system (Fig 3.1A, middle panel). A beneficial mutant is likely to spread through this topology only if it arises, for the case illustrated, in the hub and selection is substantially stronger than migration. The predictions made by standard population genetic models and EGT differ for star networks with connections clustered in a few vertices (Fig 3.1A, right panel). Relative to a well-mixed system, population genetic models predict no effect of topology on the rate or probability of spread while EGT predicts fixation probabilities can increase, an effect termed amplification, because beneficial mutations arising in a leaf can spread to all other patches via the central hub (Lieberman et al. 2005; Pavlogiannis et al. 2018).

The EGT approach has inspired a rich theoretical literature exploring the potential for ever more complicated network structures to serve as amplifiers of selection (Galanis et al. 2017; Pavlogiannis et al. 2018; Tkadlec et al. 2021), including claims that certain topologies, like the so-called “superstar”, could asymptotically amplify even very small fitness differences. Others (Jamieson-Lane and Hauert 2015; Galanis et al. 2017) tempered these findings by showing that this prediction depends on model details like the ordering of birth and death steps (Hindersin and Traulsen 2015; Tkadlec et al. 2020), and that perfect amplification would require unlimited space and time (Tkadlec et al. 2021). In any case, the central claims of EGT remain untested by experiment in any biological

system, and so its relevance to real-world situations remains uncertain. Moreover, because EGT rests on a stochastic model of evolution in finite populations (Moran 1962) (Moran, 1962) in which individuals occupy the nodes of the graph, the empirical robustness of its predictions to alternative scenarios where nodes are composed of subpopulations, variable rates of dispersal, or migration asymmetries (Houchmandzadeh and Vallade 2011, 2013; Constable and McKane 2014; Adlam et al. 2015; Marrec et al. 2021) remains unclear.

Here, we evaluate the impact of network topology on the fixation dynamics of a beneficial mutation directly through experiment. Specifically, we focus on the spread of an antibiotic resistant mutant through a star topology across a range of dispersal rates, as this is the network structure where EGT and standard population genetics make divergent predictions. The well-mixed topology serves as a control. Our experiment tracks the spread of an initially rare (1:1000) ciprofloxacin-resistant (cip^R) mutant of *Pseudomonas aeruginosa* strain 14 (PA14-*gyrA*) invading four-patch metapopulations varying in topology and dispersal rate (Fig 3.1B). Selection is uniform across all patches, and is imposed by supplementing growth media with subinhibitory concentrations of ciprofloxacin adjusted to provide a ~20% fitness advantage to the resistant mutant. Dispersal occurs during daily serial transfer by first mixing samples from the appropriate subpopulations (see Methods for details) and then diluting the mixture to adjust dispersal rates. Since the theory makes predictions about fixation of a single beneficial mutation, we focus on the first 5 - 6 days (~6.67 generations/day : ~35 - 40 generations) to minimize the opportunity for *de novo* mutations rising to high frequency. We keep track of the frequency of the beneficial mutant over time, which should closely approximate the

probability of fixation because the larger the frequency of a mutant at time *t*, the more likely it is to eventually fix. As such, we use ‘amplification’ here to mean the increased rate of spread of a beneficial mutation *relative* to that expected from the well-mixed case at a given time, rather than the fixation probability itself. We check our experimental results and the correspondence between rate of spread and probability of fixation, with a new agent-based simulation (see Methods and Appendix A) in which an individual is represented by an agent that competes for finite spaces in a node and can disperse along edges. Together, our results allow us to test directly, both *in vitro* and *in silico*, whether network topology modulates the fixation process that drives adaptive evolution, and if so, how this occurs.

Results:

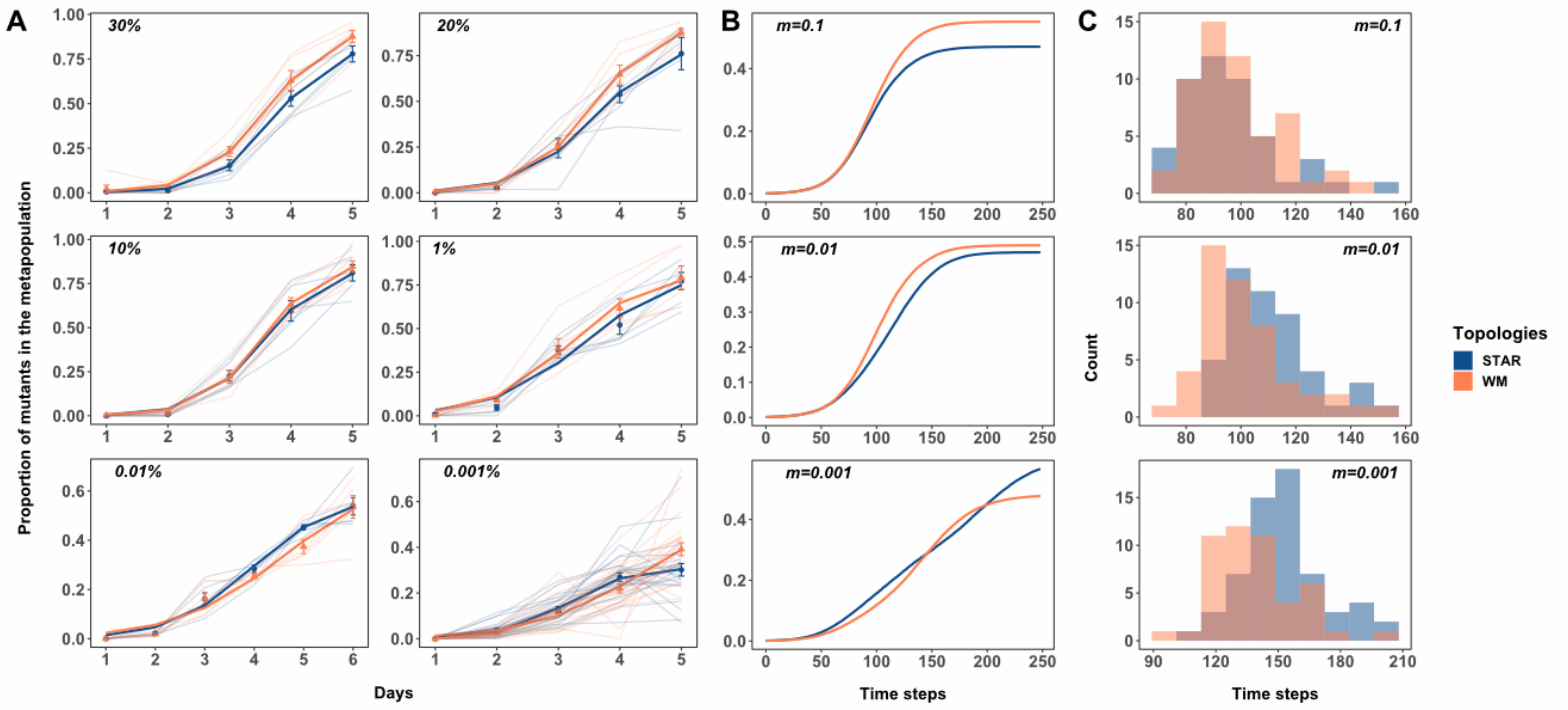

Figure 3.2 The proportion of cip^R mutant in replicate metapopulations propagated by either star (blue) or well-mixed (red) networks with unweighted migration. The bright lines depict the nonlinear least squares (NLS) fit for each metapopulation structure. Panel A shows experimental results; simulation results are shown in Panel B-C. Migration rates are noted in the inset of each plot. Migration rates in the simulation means a low, intermediate, or high value relative to the effective carrying capacity of the patch. Five days in the experiment is equivalent to approximately 5 days or 240 timesteps in the simulation (see methods for details on how time steps in simulations compare to days in experiment). Panel C is histograms from the simulations showing the minimum generations required for the cip^R to reach a frequency of at least 50% in a metapopulation under each combination of network type and migration rate. Each data point represents the mean proportion of all of the replicate metapopulations on that day and error bars represent standard error.

Our results show that the effect of network topology on the spread of the cip^R mutant depends on migration rate (Fig 3.2). The beneficial mutant spreads faster through a well-mixed than a star topology at migration rates above 10% (panel A: final frequency of cip^R in networks with 30% migration: $\chi 2 = 15.348$, $p<0.0001$; 20% migration: $\chi 2 = 9.0148$, $p = 0.0027$) while the rate of spread is statistically indistinguishable at the intermediate migration rates of 10% and 1% (10% migration: $\chi 2 = 0.7082$, $p = 0.4001$; 1% migration: $\chi 2 = 0.2168$, $p = 0.6415$). Below migration rates of 0.01% we see evidence that cip^R spreads modestly faster in a star network than in a well-mixed system, consistent with the prediction from EGT that bidirectional star networks can amplify selection. Notably, the amplification effect is transient, being maximal at intermediate time steps (0.01%: relative frequency of cip^R to WT on Day 5: $\chi^2 =13.825$, $p = 0.0002$ and 0.001%: frequency of cip^R on Day 4: $\chi^2 = 5.2577$, $p = 0.0218$) and disappearing on day 5 or 6, depending on the migration rate (see appendix A), an effect that has not been previously observed in models of EGT.

Our results suggest that star topologies can increase the rate at which a beneficial mutation spreads, although its effects appear limited to very low migration rates. An alternative explanation is that the increased rate of spread in our experiments was due to *de novo* evolution of second-site beneficial mutations in the cip^R background. Three lines of evidence argue against this interpretation. First, there should be no inherent evolutionary advantage to any treatment in our experiment because mutation supply rates, being the product of population size and mutation rate, did not differ across treatments. Second, we observed novel colony morphotypes in the more abundant wild-type background only that, when present, had undulate morphologies indicative of biofilm

formation. Third, we never recovered mutants more resistant than our focal cip^R strain, even after propagating the wild type for ten days under identical conditions (see methods, Appendix A figure A.8), suggesting that spontaneous resistant mutations, if present, remained too rare to influence our results. Our observation that the amplification of an initially rare beneficial mutant occurred in spite of potential competition from *de novo* mutants in the more abundant competitor class thus makes our results even more compelling.

To confirm these results are not an idiosyncratic feature of our biological system, and to provide additional insight into the mechanisms driving amplification, we simulated the population dynamics of selection in metapopulations under the same topologies and migration rates using an agent-based model. The model tracks competition between wild-type and resistant bacteria for a fixed number of spaces in each patch with dispersal along edges between patches, with fitness being given by the probability of being killed by the antibiotic, and population sizes within each patch being allowed to vary between zero and a fixed carrying capacity. Our model thus allows us to capture the dynamics of slow, but nonequilibrium, migration. Simulation (Fig 3.2 panel B-C) and experimental results match closely, with the well-mixed topology being faster at spreading the beneficial mutant than the star network at high migration rates. As in our experimental results, transient amplification was seen under low migration rates (Panel B, Fig. 3.2). Closer inspection reveals amplification is most likely to occur when the expected number of mutant migrants per generation along each edge, at the effective carrying capacity of mutants, is on the order of one. This corresponds to:

$$Expected\ migrants$$

$$= (Migration\ rate)\ X\ (Spaces\ per\ node)\ X\ [1 - Antibiotic/Resistance]$$

$$\sim 1$$

where *Antibiotic* is the antibiotic concentration and *Resistance* represents the reduction in the kill rate of mutants normalized by their growth rate, so that all of them would be killed when (*Antibiotic/Resistance*) ≥ 1. This result suggests that amplification associated with "slow" migration rates is caused by seeding events of mutants into a new subpopulation if and only if the mutants have already successfully colonized a previous subpopulation. Substitution occurs in a more predictable and stepwise fashion under slow, relative to fast, migration rates because beneficial mutants have more time to rise to high frequency in the subpopulation they previously colonized, and so are less likely to be lost due to drift when colonizing a new subpopulation. Moreover, a star network that concentrates incoming migrants into the hub will alleviate genetic drift more than a well-mixed network, and should, in principle, act as a stronger amplifier of selection. By contrast, when migration introduces beneficial mutants at a rate faster than they are lost due to genetic drift, a better connected well-mixed network spreads beneficial mutants faster than a star network where leaves are only connected via the hub.

Recent theoretical work (Marrec et al. 2021; Yagoobi and Traulsen 2021) treating nodes as subpopulations rather than individuals, as in our experiments, shows that migration asymmetry between leaves and hub can potentially amplify fixation probabilities relative to the well-mixed case. Specifically, star networks with net outward or inward migration are predicted to be suppressors or amplifiers of selection, respectively, while those with no asymmetry (balanced) migration should have no advantage over a well-mixed network

in fixing a beneficial mutant (Marrec et al. 2021). Our first experiment (Figure 3.2) adjusted the migration rate, *m*, to ensure all patches receive the same number of mutants. Using the same experimental setup, we can test these predictions by manipulating the relative amount of migration between the hub and the three leaves of the star network in both experiments and simulation.

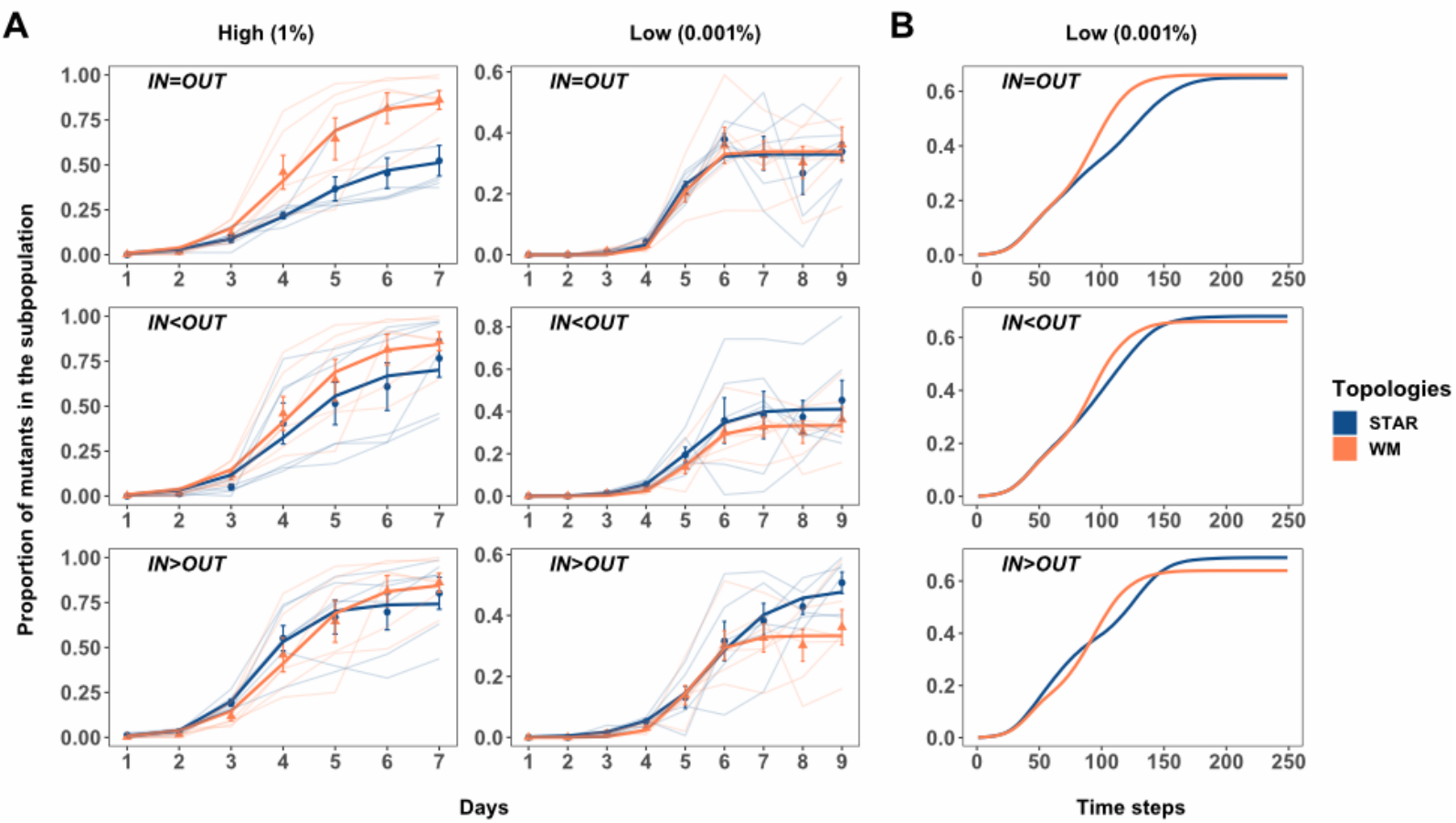

Figure 3.3 The proportion of cip^{R} mutant in replicate metapopulations propagated on either star (blue) or well-mixed (red) networks with weighted migration. Bright lines are the nonlinear least squares (NLS) fit to the two network treatments. Panel A shows results from the experiments under high and low migration rates, whereas Panel B shows the results of the agent based model only under the low migration rate. The respective dispersal asymmetries are provided in the inset of each plot. Each data point represents the mean proportion of all of the replicate metapopulations on that day and error bars represent standard error.

Our results are consistent with the predictions of theory. At high migration rates (Fig 3.3A), the rate at which the cip^R mutant spreads is never statistically significantly higher than that of the well-mixed topology under both forms of asymmetric migration (middle and bottom panels; $\chi^2 = 1.1888$, $p = 0.2756$ (OUT>IN) and $\chi^2 = 0.4124$, $p = 0.5208$ (IN>OUT), respectively; see Appendix A table A.4), and is substantially slower when migration rates were balanced among the nodes (top panel) (IN=OUT: relative frequency of cip^R on Day 9: $\chi^2 = 12.234$, $p = 0.0005$). At low migration rates (Fig 3.3B), however, the dynamics of cip^R spread is indistinguishable (see Appendix A table A.4) from that of the well-mixed case for both balanced migration (top panel, $\chi^2 = 0.1848$, $p = 0.6673$) and net outward migration (middle panel, $\chi^2 = 0.5233$, $p = 0.4694$), as expected from theory. When inward migration exceeds outward migration (bottom panel), however, the cip^R mutants gain a significant advantage in the latter stages of the experiment (IN>OUT: relative frequency of cip^R on Day 9: $\chi^2 = 5.2917$, $p = 0.0214$). The results of our simulations are shown in the panels in Fig 3.3B and agrees with our experimental results closely.

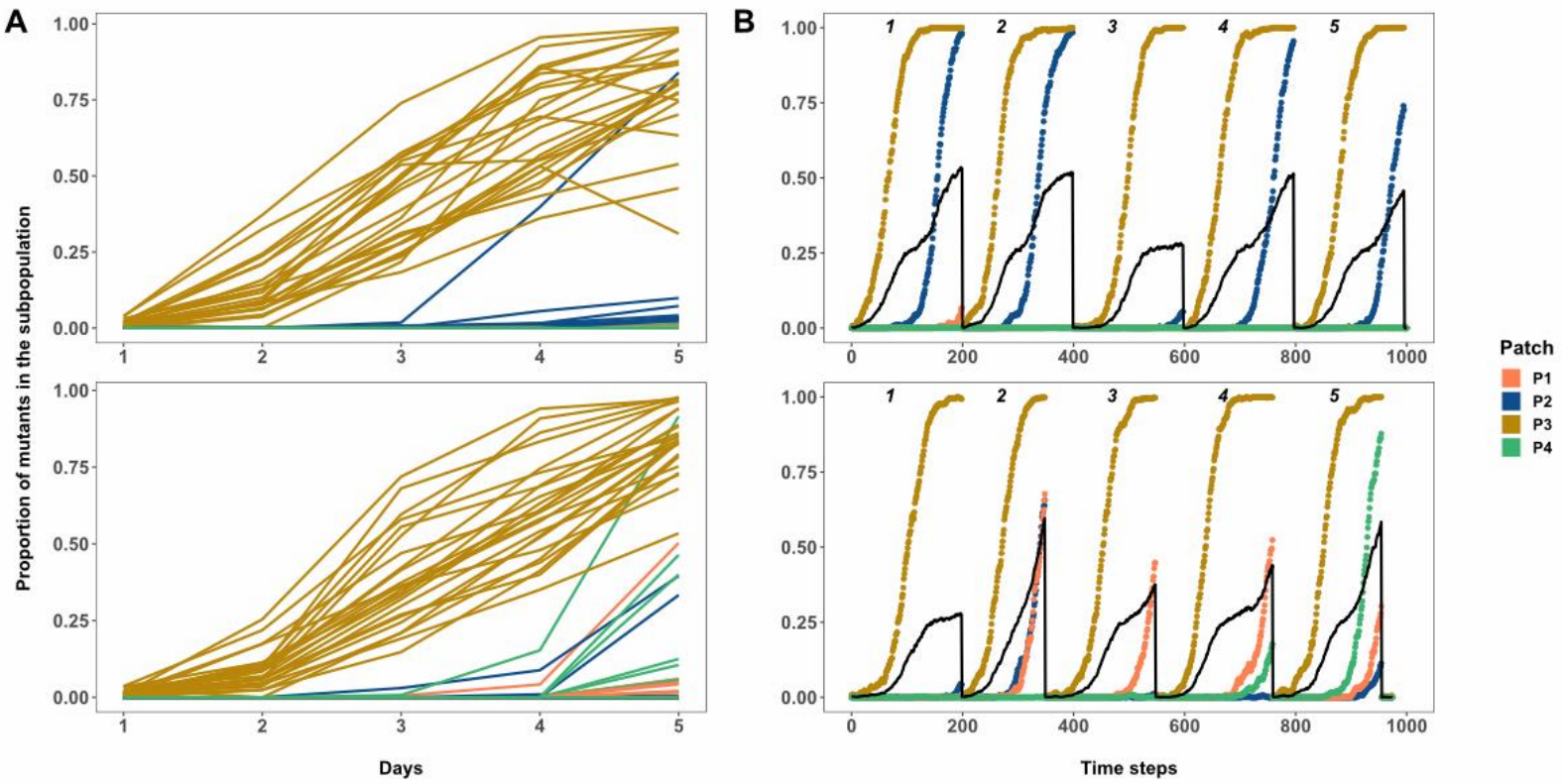

Figure 3.4 The proportion of the cip^R mutants in the constituent subpopulations of each replicate metapopulation propagated as either star (both panel A and B, first row) or well-mixed (both panel A and B, second row) networks with unweighted migration of 0.001% (~100 individuals). Panel A is the data from the experiment and Panel B is the data from the agent based model. Subpopulation nomenclature: P3 = node of introduction of the cip^R mutant, P2 = hub and P1 and P4 = rest of the peripheral leaves. In panel A, cip^R fixation dynamics in four subpopulations of each of the 24 replicate metapopulations under each network are shown (top = star, bottom = well-mixed). The black solid lines in panel B are the overall proportion of cip^R mutants in a metapopulation. In panel B, five replicate instantiations (each run for 200 generations) of the simulation are shown for each network (top = star, bottom = well-mixed).

Whether or not amplification occurs should depend on the balance between two dynamic processes - the rate of fixation within a patch and the rate of dispersal to new patches. When migration rates are fast, an initially rare beneficial mutant cannot reach sufficiently high frequency in its native patch to guarantee dispersal to other patches. Consequently, if it does manage to get dispersed to a novel patch, the beneficial mutant is initially so rare that it is likely to be lost due to drift. Under slow migration, however, selection increases the frequency of a beneficial mutant faster in its native patch than it is dispersed to novel patches, ensuring that it can be repeatedly dispersed to novel patches and so reducing the likelihood of drift loss upon arrival. Amplifying topologies act in a similar way when dispersal is slow, by allowing beneficial mutants to first fix in the patch where they were introduced, and then funneling them through a central hub, so the likelihood of drift loss before other leaves are seeded is reduced. Under well-mixed conditions, migration overwhelms selection such that the constant influx of lower fitness migrants from other patches means the beneficial mutant cannot accumulate to sufficiently high frequency in its focal patch before it is dispersed to other patches, where it is rare and likely to be lost due to drift.

We evaluated this interpretation by examining the dynamics of the cip^R mutant as it spreads among subpopulations in our experiment. Fixation is expected to occur first in the leaf in which the beneficial mutant was initially inoculated followed by, in an amplifying star network, accumulation in the hub and then spread to other leaves of the network. In a well-mixed metapopulation, however, the spread of the cip^R mutant should occur into both hub and leaf subpopulations at the same time. Indeed, when we examine the dynamics of the cip^R mutant in star and well-mixed metapopulations at a low migration

rate (0.001%) where amplification is seen in the former but not the latter, we see the expected patterns (Fig 3.4). The cip^R mutant first fixes in the leaf where it was initially inoculated for both of the networks, as expected. Although there is substantial variation among replicates, our results show that the cip^R mutant spreads differently among the remaining three subpopulations in the two kinds of network: in the star network there is a clear tendency for the mutant to spread from the initial subpopulation to the hub (P2) first, whereas in the well-mixed network the mutant is equally likely to spread to the hub as any additional subpopulation (Fig 3.4A). These experimental results are mirrored closely by those of the simulation (Fig 3.4B).

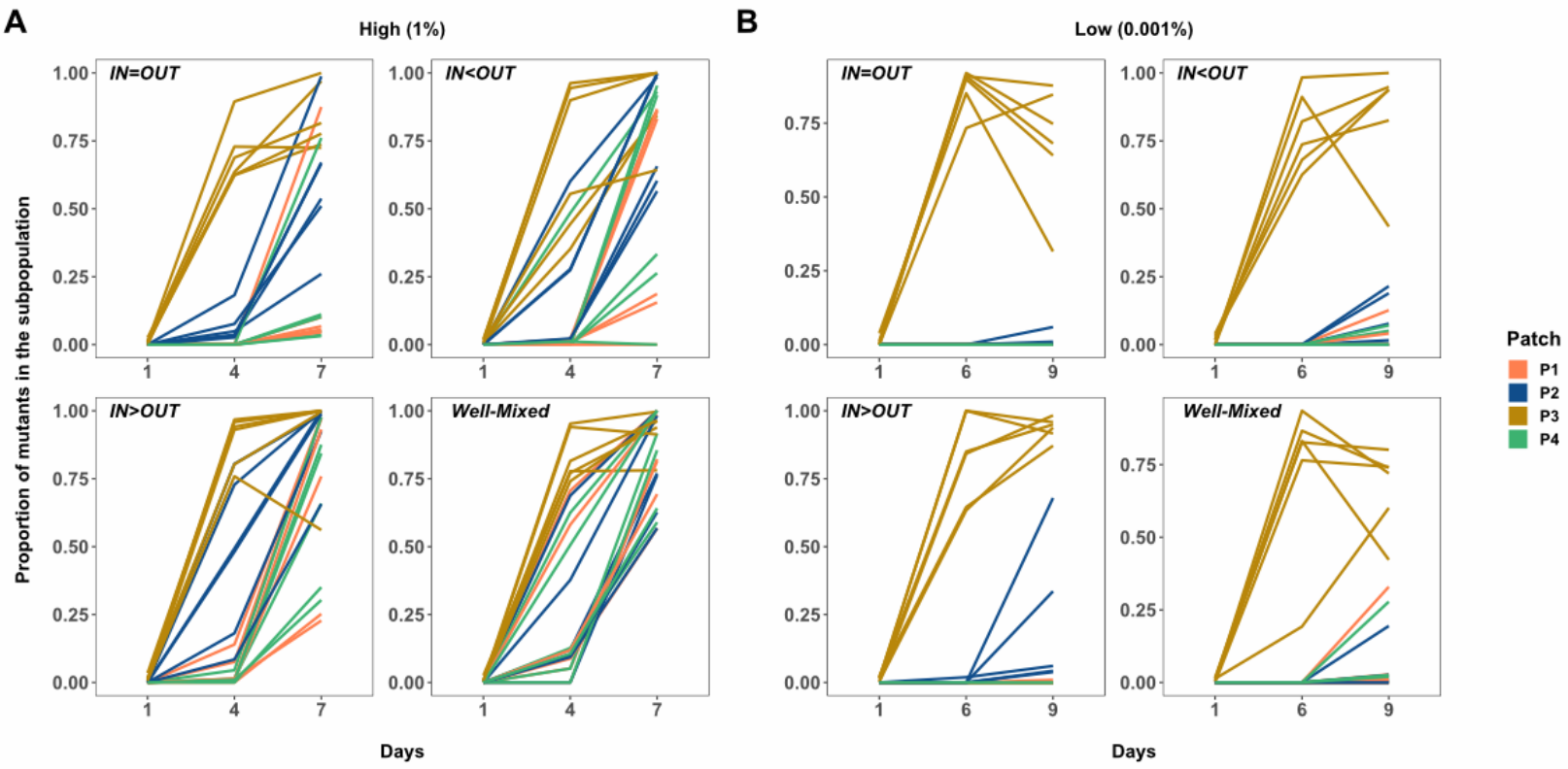

Figure 3.5 The proportion of the cipR mutants in the constituent subpopulations of each metapopulation propagated by either asymmetric star or well-mixed networks under high (panel A: 1% or 10^5 individuals) and low (panel B: 0.001% or 10^2 individuals) weighted migration. Subpopulation nomenclature: P3 = node of introduction of the cip^R mutant, P2 = hub and P1 and P4 = rest of the peripheral leaves. In both panels A and B, cip^R fixation dynamics in four subpopulations of each of the six replicate metapopulations using each of the three asymmetric star networks and the well-mixed network are shown (see plot insets for details) under high and low migration rates, respectively.

We see similar dynamics of spread among subpopulations in our experiments examining migration asymmetry. In well-mixed systems and those star networks where amplification was not observed (high migration rates) the cip^R mutant rapidly spreads into both hub and leaves after near fixation in the patch of introduction (Fig 3.5A). In contrast, the cip^R mutant spreads to the hub first in the most strongly amplifying star topology (IN>OUT), consistent with the idea that beneficial mutants are more likely to avoid stochastic loss due to drift by being concentrated in the hub (Fig 3.5B).

If avoiding “drift loss” under low migration rate is indeed the mechanism for amplification, then imposing more severe drift should increase the magnitude and duration of the observed amplification. We tested this hypothesis by enforcing a stricter bottleneck, and thus stronger drift, during daily transfers and tracking the spread of resistant mutants in a star metapopulation with in-weighted migration (IN>OUT) and a well-mixed metapopulation at a low migration rate (~1000 individuals). The results are consistent with our prediction (Fig 3.6): for intermediate time-points (Day 5 and 6), there was a significantly higher proportion of mutants (Day 5: χ^2 =17.255, p = 3.269e-05, Day 6: χ^2 =16.17, p = 5.79e-05) in the star-like metapopulations compared to the wild-type. In other words, we observed an amplification with a higher magnitude and longer duration (stable for ~30 generations, which was nearly the entire length of our previous experiments). This result is consistent with our hypothesis that the likelihood of drift loss is lower in star-like metapopulations when the migration rate between subpopulations are low and asymmetric migration concentrates mutants through the hub. Our results thus lend strong support to the idea that a reduction in the probability of drift loss is responsible for the amplification effect in star-like topologies. Moreover, this result emphasizes the need for

future theoretical and experimental work to focus on fine-tuning evolutionary forces such as stochastic drift, selection and migration to determine the magnitude of amplification in different topologies.

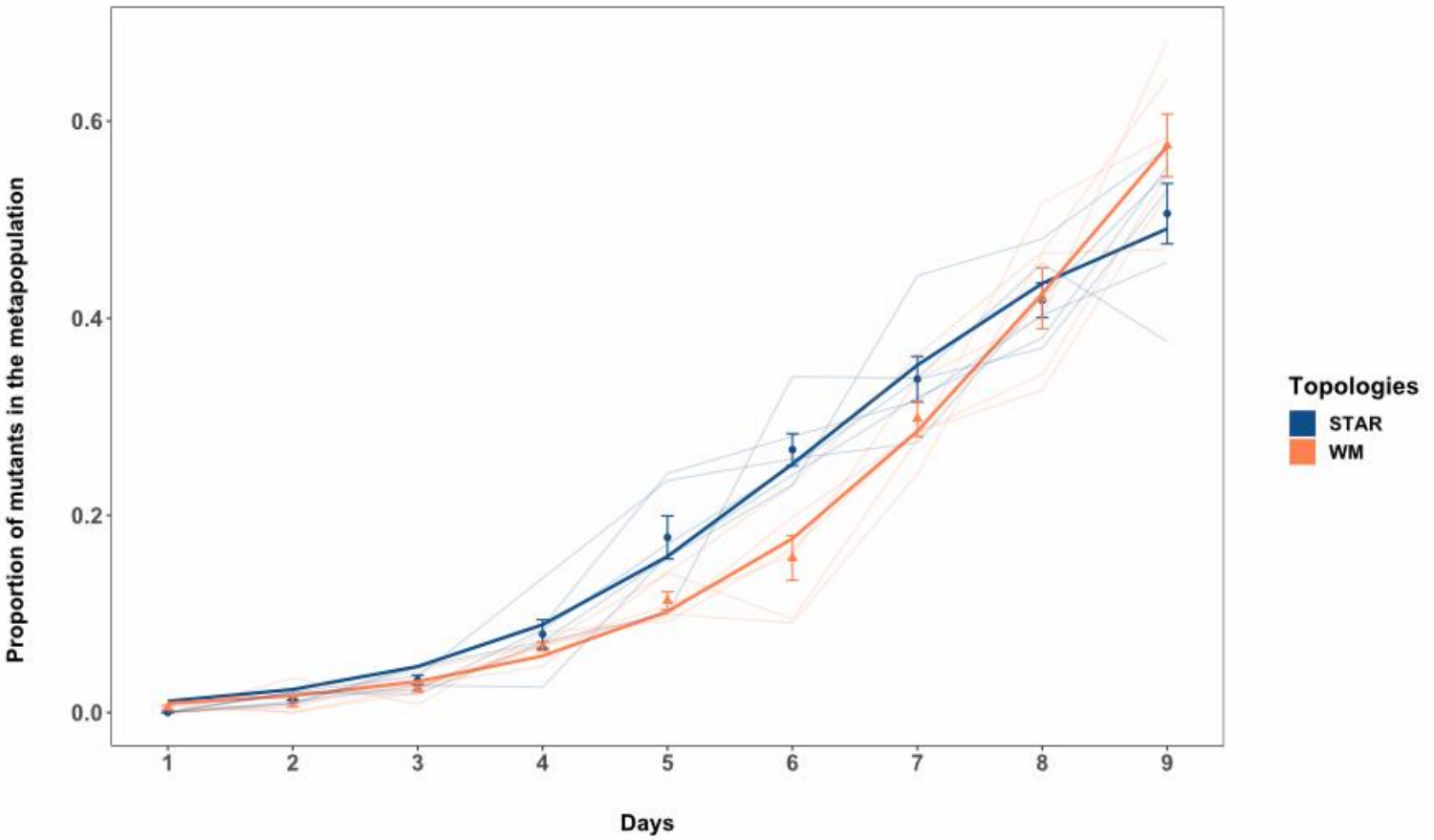

Figure 3.6 The proportion of cipR mutant in replicate metapopulations propagated on either an inward star (blue) or well-mixed (red) networks with low population size (10^5 CFU/mL) and low migration rate (10^3 CFU/mL). Bright lines are the nonlinear least squares (NLS) fit to the two network treatments. Each data point represents the mean proportion of all of the replicate metapopulations on that day and error bars represent standard error.

Discussion:

We have shown experimentally and through simulation that metapopulation structure can impact the dynamics of adaptive substitution. Star metapopulations, in which leaf subpopulations exchange migrants through a central hub, can act as amplifiers of selection leading to faster rates of spread than a comparable well-mixed population where all subpopulations share migrants equally. Amplification is most pronounced when selection is strong relative to migration, a scenario that reduces the probability that a rare beneficial mutant in a newly colonized patch will be lost due to drift, and when the topology of dispersal concentrates the beneficial mutant in a central hub ('inward' > 'outward' migration). In other words, amplification occurs because rare mutants are less likely to be lost, not because the strength of selection itself increases.

This result is remarkable because it was not anticipated by standard theory in population genetics, in which population structure usually has little effect on the probability of fixation for beneficial mutants. This conclusion likely derives from the tradition in population genetics of considering allele frequency changes in the limit of infinite populations and high migration rates. Our results, by contrast, show how stochastic effects associated with finite population sizes can alter the dynamics of adaptive substitution in ways that are consistent with predictions from evolutionary graph theory where individuals are assigned to nodes of a graph. Importantly, our results show that amplification can occur under a broader and arguably more realistic set of conditions where populations, not individuals, occupy the nodes. Our work emphasizes the previously overlooked importance of migration rate and serves as a first step towards bridging these two

approaches, with infinite populations on the one hand and finite populations focused on the dynamics of individuals on the other.

More generally, it will be useful to expand the analytical framework of EGT to include more biological realism and to articulate more precisely the range of conditions under which amplification can occur. It should be possible, for example, to use network topology to amplify the selection of even a slightly favored mutation for the purpose of experimentation or the directed evolution of desired traits in industrial applications. A more comprehensive theory of evolution on structured landscapes will also be important in other aspects of biology, including the spread of invasive species, pathogens, and the resistance factors they possess.

Methods:

The SANCTUM model:

Each node (A_i) has n_i spaces that can each be empty, occupied by a wild-type, or occupied by a mutant. For these experiments, all the n values are set to 1600. For each generation of the simulation, there are three phases: (1) Death, (2) Birth, and (3) Migration. *Death*: An agent is removed during the death step with a probability that depends on the antibiotic concentration divided by its individual resistance. *Birth*: Each agent has a chance of reproducing an identical agent in an empty space of the same node during the birth step. Similar to the Lotka-Volterra model of population growth, the probability of reproduction increases with the number of empty spaces in the node. *Migration*: There is a probability of migration that varies based on the experimental condition. If an agent is selected to migrate, it randomly moves to an adjacent connected node with a probability proportional to the weight of that edge (w). These definitions are interpreted in the model as follows:

$$\text{Effective Carrying Capacity with antibiotic} = (1-Z*A/R)K$$

where Z is first-order kill rate of the mutants by the antibiotic, A is the antibiotic concentration, R is growth rate of mutants, and K is the total number of spaces per node (the unmodified carrying capacity). Using the effective carrying capacity of mutants limited by the antibiotic:

Expected migrants per step per edge = (Migration rate) x (Effective Carrying Capacity)

= (Migration rate) x [(1-Z*A/R)K]

= (Migration rate) x (Spaces per node) x [1-Antibiotic/Normalized Resistance]

Here, R/Z represents the Normalized Resistance, which reflects the balance between the death and growth rates. This value also sets the threshold for A, above which all the mutants would be eliminated. The initial system is randomly seeded with one thousand agents across all nodes, and one of these is selected to be the mutant (not in the hub). Time in the simulation is calculated as below :

Total simulation time = (time equivalent in experiment(days) x 24 hours x 60 minutes)/ t

Where t is the doubling time (generation time) for PA14 ~ 30 mins. Therefore, 5 days of experiment is equivalent to 240 time steps in the simulation. For each simulated condition, the metapopulation fraction is averaged over 100 instantiations. For runs that ultimately fix, the number of generations until the mutants are the majority of agents is also recorded.

Microbial strains and conditions:

For all experiments, clonal populations of *Pseudomonas aeruginosa* strain 14:gyrA (PA14:*gyrA*) and PA14:*lacZ,* isogenic to PA14 except with a point mutation in the *gyrA* gene and an insertion in the *lacZ* gene respectively, were used. Colonies possessing the *lacZ* insertion appear blue when cultured on agar plates supplemented with 40 mg/L of 5-bromo-4-chloro-3-indolyl-beta-D-galactopyranoside (X-Gal), and are visually distinct from the PA14:*gyrA* white colouration. The neutrality of the *lacZ* marker was confirmed in our experimental environments by measuring the fitness of the marked strain relative to the unmarked strain. Populations were cultured in 24-well plates with 1.5 mL of media in each well, in an orbital shaker (150 RPM) at 37°C. The culture media consisted of Luria

Bertani broth (LB: bacto-tryptone 10 g/L, yeast extract 5 g/L, NaCl 10 g/L) supplemented with 20 ng/mL of the fluoroquinolone antibiotic, ciprofloxacin. This concentration of ciprofloxacin confers ~ 20% selective advantage to PA14:*gyrA* relative to PA14:*lacZ* (Appendix A Figure A.7). All strains and evolving populations were frozen at −80°C in 20% (v/v) glycerol.

Evolution experiment:

A single metapopulation consisted of four subpopulations, one subpopulation being located on each of four different 24-well plates. Plate 2 was always assigned as the hub, and plates 1, 3, and 4 were treated as the leaves. This design allows us to track up to 24 replicate populations using just four multi-well plates. The experiment was initiated by inoculating each subpopulation with ~10^7 colony forming units (CFU) per ml of PA14:*lacZ* descended from a single colony picked from an agar plate and grown overnight in liquid LB at 37°C with vigorous shaking (150 RPM). The cip^R mutant, derived from frozen cultures in the same way, was introduced simultaneously into one subpopulation (plate 3) at a density ~10^4 PA14:*gyrA* cells producing an initial ratio of resistant to wild-type cells of ~1:1000 in this subpopulation. Metapopulations were transferred daily following dispersal among subpopulations (see below) by taking an aliquot corresponding to ~10^7 CFUs per mL and inoculating into fresh medium. The population density in each subpopulation reached ~10^9 CFUs, so this transfer regime corresponds to ~6.67 daily generations of growth.

We constructed distinct network topologies by mixing subpopulations prior to serial transfer following the schematic shown in Appendix A figure A.2. Briefly, well-mixed

networks were created by combining equal volume aliquots from all subpopulations into a common dispersal pool, diluting this mixture to the appropriate density to achieve the desired migration rate, and then mixing the dispersal pool with aliquots from each subpopulation (so-called 'self-inoculation') before transfer. Star networks, which involve bidirectional dispersal between the hub and leaves, were constructed in a similar way to the well-mixed situation only now the dispersal pool consisted of aliquots from just the leaves and aliquots from the hub (plate 2) were mixed with 'self-inoculation' samples from each leaf prior to serial transfer. Further details on how each network topology and migration rate were achieved are provided below.

Tracking the spread of resistance:

We tracked the spread of the cipR mutant (PA14:*gyrA*) relative to the wild type (PA14:*lacZ*) by plating samples from each subpopulation as well as a mixture of the entire metapopulation on LB agar plates supplemented with X-gal allowing us to use blue-white screening to track the relative frequency of each type over time.

Statistical analyses:

All statistical analyses were conducted using R statistical software (R Core Team 2020).We used two complementary approaches to analyze our experimental data.

The first models the spread of resistance (see Fig. 3.2 and Fig. 3.3) as a three-parameter logistic growth model using non-linear least squares with a fixed N_0 (NLS) (Nash 2016). This model, as with comparable approaches focused on population growth in resource limited environments, allows us to estimate the rate at which resistance spreads

(equivalent to r_{max} in logistic growth) and the final frequency of cip^R mutants at the end of the experiment (equivalent to the carrying capacity, K, from logistic growth models) in each replicate metapopulation. Contrasts of maximal growth rates between treatments (star or well-mixed) were performed using a linear model (lm function from base R). Comparable contrasts for maximum proportion of resistant mutants fixed on the final day of the experiment used a generalized linear mixed model using methods as described below.

The second approach modeled the change in proportion for the cip^R mutants directly using a generalized linear mixed model (GLMM) with quasi-binomial error distribution (and logit link function), using the glmmPQL function from the MASS package in R (Venables and Ripley 2002). We focus on the main effects of time and network structure (star vs. well-mixed) and their interaction at each migration rate treatment. Logistical constraints prevented us from conducting experiments that manipulate both network structure and migration rate simultaneously, so we elected to run separate experiments at each migration rate to focus on the effect of contrasting network structures, as this is the focus of EGT. Our model treats 'network' as a fixed effect and 'replicate' as a random effect, while accounting for repeated measures through time. This approach produces estimates of the pairwise difference between the slopes (vs time) for the network treatment (for example, - Time:Network star - Time:Network well-mixed) that were further analyzed using the EMTRENDS function from the EMMEANS package (analogous to a Tukey *post hoc* test) (Lenth 2020). These contrasts allow us to determine the magnitude and direction of difference between the star and well-mixed networks for the whole experiment.

The approaches above, which focus on estimating best-fit main effects and interactions, are useful for helping to visualize the dynamics of spread across many instantiations of an inherently noisy process. We additionally focus attention on contrasts between the fraction of cip^R mutants between star and well-mixed treatments at specific days when: (1) the fitted logistic model for the star was higher than that of the well-mixed over the course of the complete experiment; or, (2) when the fitted models reveal a transient "crossover" event at intermediate time steps. We used a GLMM as described above to contrast the fraction of cip^R mutants in star vs well-mixed networks at a particular day, treating replicate as a random factor. The analysis of variance of the GLMMs were performed with the ANOVA function from the car package.

Chapter 4:

Network topology accelerates de novo evolution of antibiotic resistance in Pseudomonas aeruginosa metapopulations

Partha Pratim Chakraborty & Rees Kassen

This chapter will be communicated along with Chapter 5 (manuscript under preparation).

Abstract

How the spatial arrangement of a population impacts adaptive dynamics is one of the most widely contested topics in evolutionary biology. In theory and experiments, certain topologies like stars, in which “leaf” populations are exclusively connected through a central “hub”, have been shown to accelerate the spread of a beneficial mutation compared to a well-mixed topology. However, the dynamics of fixation of multiple contending beneficial mutations has remained unclear in these spatially structured populations. Here, we experimentally assess the impact of mutation supply rate on the capability of network topologies to accelerate the speed of *de novo* antibiotic resistance evolution in *Pseudomonas aeruginosa* metapopulations. Our results suggest that star metapopulation topology can accelerate adaptation at low but not at high mutation supply rates, consistent with the predictions of theory. Overall, our results illustrate the relevance of network topology in understanding the evolutionary dynamics of pathogenic bacteria or other clonal populations, optimize their containment measures or steer accelerated directed evolution of biomolecules of interest for industrial applications.

Introduction

The theory of adaptive evolution in mutation-limited populations has been built under the simplifying assumptions of a large, well-mixed population adapting to a very slowly changing environment by substituting beneficial mutations (Orr 2005c; Martin and Lenormand 2006; Schoustra et al. 2009; Lang et al. 2013; Kassen 2014; Bailey and Bataillon 2016). Yet natural populations are far more ecologically complex than this. They are often spatially structured – meaning they are arranged in space and connected by migration. In that sense, they resemble metapopulations (Hanski and Gilpin 1997). The spatial structure of populations can have profound impact on their micro- and macroevolutionary dynamics (Felsenstein 1976; Slatkin 1985; Harrison and Hastings 1996; Barton and Whitlock 1997; Hanski and Gilpin 1997; Pannell and Charlesworth 2000; Charlesworth et al. 2003; Rousset 2004). Therefore, it is imperative for us to understand how spatial structure influences the adaptive substitution of beneficial mutations, in turn the overall adaptive dynamics, to better explain the short- and long-term evolutionary trajectories of populations in their natural habitats.

However, before bringing spatial structure into the picture, let us consider a simple scenario for a mutation-limited large asexual population that is adapting to a uniform environment. Adaptive dynamics in such a population is by and large determined by the rate of mutation supply that is the product of the effective population size (N_e) and beneficial mutation rate (μ_b) (Desai and Fisher 2007; Desai et al. 2007). Classical population genetic theory, in the limit of strong selection and weak mutation supply rate (otherwise termed as the “SSWM” or Strong Selection Weak Mutation regime), assumes

the waiting time to the next beneficial mutation is sufficiently long that adaptation occurs through a sequential series of substitutions, one beneficial mutation at a time. As mutation supply rates increase, more than one beneficial mutant will be segregating in a large population at the same time leading, in the absence of recombination, to competition among independently derived beneficial mutations for fixation, a phenomenon termed “clonal interference”. Clonal interference decreases the rate at which beneficial mutations fix, in turn slowing the rate of adaptation of the population as a whole (Gerrish and Lenski 1998; Sniegowski and Gerrish 2010).

The existing theoretical and empirical literature on the effect of spatial structure on adaptive dynamics varies among a spectrum of possibilities depending on the mutation supply rate to the population. Under the SSWM or the ‘periodic selection’ regime, theoretical models in the limit of constant population size find no effect of spatial structure on the fixation probability of a beneficial mutation - hence, no effect on the adaptive dynamics (Maruyama 1970; Slatkin 1981). However, when the constant population size criteria is relaxed, spatial structure can impact the probability of fixation, including the time it takes for a beneficial mutant to fix, depending on the migration rate, migration symmetry, effective population size of the individual demes and extinction-recolonization dynamics in structured populations (Barton 1993; Whitlock 2003; Patwa Z and Wahl L.M 2008). Under the “clonal interference” regime, by contrast, spatial structure is predicted to increase the local competition among multiple segregating beneficial mutations, hence, increasing clonal interference and decelerating the dynamics of adaptation even more than a well-mixed population (Gordo and Campos 2006). Accumulated evidence from

experimental evolution studies assessing the impact of spatial structure on the dynamics of adaptation in *E. coli*, *P. fluorescens* and *S. cerevisiae* populations has shown that spatial structure predominantly slows down adaptation (reviewed in Chakraborty and Kassen, manuscript under preparation, Miralles et al. 1999; Habets et al. 2006, 2007; Perfeito et al. 2007; Kryazhimskiy et al. 2012; Bailey et al. 2021). A notable exception to this trend is that spatial structure can speed up adaptation when the underlying fitness landscape is “rugged” or filled with epistatic interactions among beneficial mutations (Nahum et al. 2015). However, reports like this remain rare.

Despite these advances in theory and experiment, the knowledge on the influence of spatial structure on the adaptive evolution in mutation-limited populations is far from complete. Specifically because one aspect of spatial structure, network topology or the pattern of connectivity among subpopulations and its impact on adaptive evolution, remains empirically understudied. Here, two very divergent predictions emerge depending on whether network topology can dictate the fixation probability of a beneficial mutant in a population. Models of classical population genetic theory, often under the simplifying assumptions of infinite population size, predict little to no effect of network topologies on the fixation probability of beneficial alleles (Maruyama 1970; Slatkin 1981). In contrast, models employing evolutionary graph theory (EGT), in which individuals inhabit the vertices of a graph and edges represent dispersal routes between neighboring sites, predict that fixation probabilities can change based on how the nodes are connected (Lieberman et al. 2005). For the simplest case scenario, think of a metapopulation consisting of four inter-connected subpopulations (demes). Evolutionary Graph Theory

predicts that the star network where the three peripheral nodes are connected to a central hub through bi-directional dispersal can “amplify” or increase the fixation probability of a beneficial mutant when compared with a completely connected well-mixed network. This “amplification” effect is attributed to the star networks because they can tip the balance between selection and drift in favor of the former by reducing the probability of stochastic loss of rare beneficial mutations relative to a well-mixed system. This basic prediction holds true for even more fantastical network structures “amplifying” the fixation probability of a beneficial allele (Jamieson-Lane and Hauert 2015; Galanis et al. 2017; Pavlogiannis et al. 2018; Tkadlec et al. 2021). More recent theory has focused on relaxing some of the more restrictive assumptions of the original EGT model, for example by treating each node as a population instead of an individual, to evaluate its generality as an explanation for adaptive evolution in spatially structured populations (Houchmandzadeh and Vallade 2011; Constable and McKane 2014; Adlam et al. 2015; Marrec et al. 2021; Yagoobi and Traulsen 2021). Importantly, amplification can still be observed in these less restrictive scenarios, suggesting that it can be a general effect arising from the topology of dispersal characteristic of star metapopulations.

To our knowledge, there is just one empirical test of the prediction that star networks amplify selection over and above that observed in well-mixed systems. This work showed, in laboratory metapopulations of *P. aeruginosa* adapting to sub-inhibitory concentrations of an antibiotic, that amplification can occur in star networks, although its effects are modest and often transient. The “amplification” observed in this study was due to the star network being able to avoid the loss of the beneficial mutant to genetic drift by first

concentrating it in the hub, prior to dispersing it to the peripheral leaves. Amplification could be prolonged, and its effect size increased, by employing low levels of asymmetric inward migration towards the hub and in the presence of high levels of genetic drift (Chakraborty et al. 2023).

As intriguing as these results are for what they tell us about the dynamics of fixation of a single beneficial mutation in metapopulations, whether amplification occurs in more open-ended instances of adaptation involving multiple contending mutations remains unclear. Recent extensions of the EGT, in the limit of high mutation rate, have found that “amplifying” star networks attain a lower steady state fitness than the well-mixed networks but at low mutation rates, star networks retain their “amplifying” capabilities (Sharma et al. 2023). However, these predictions are made on graphs where individuals occupy the nodes, not populations - hence the empirical robustness of these predictions to alternative scenarios where nodes are composed of populations, remains unclear.

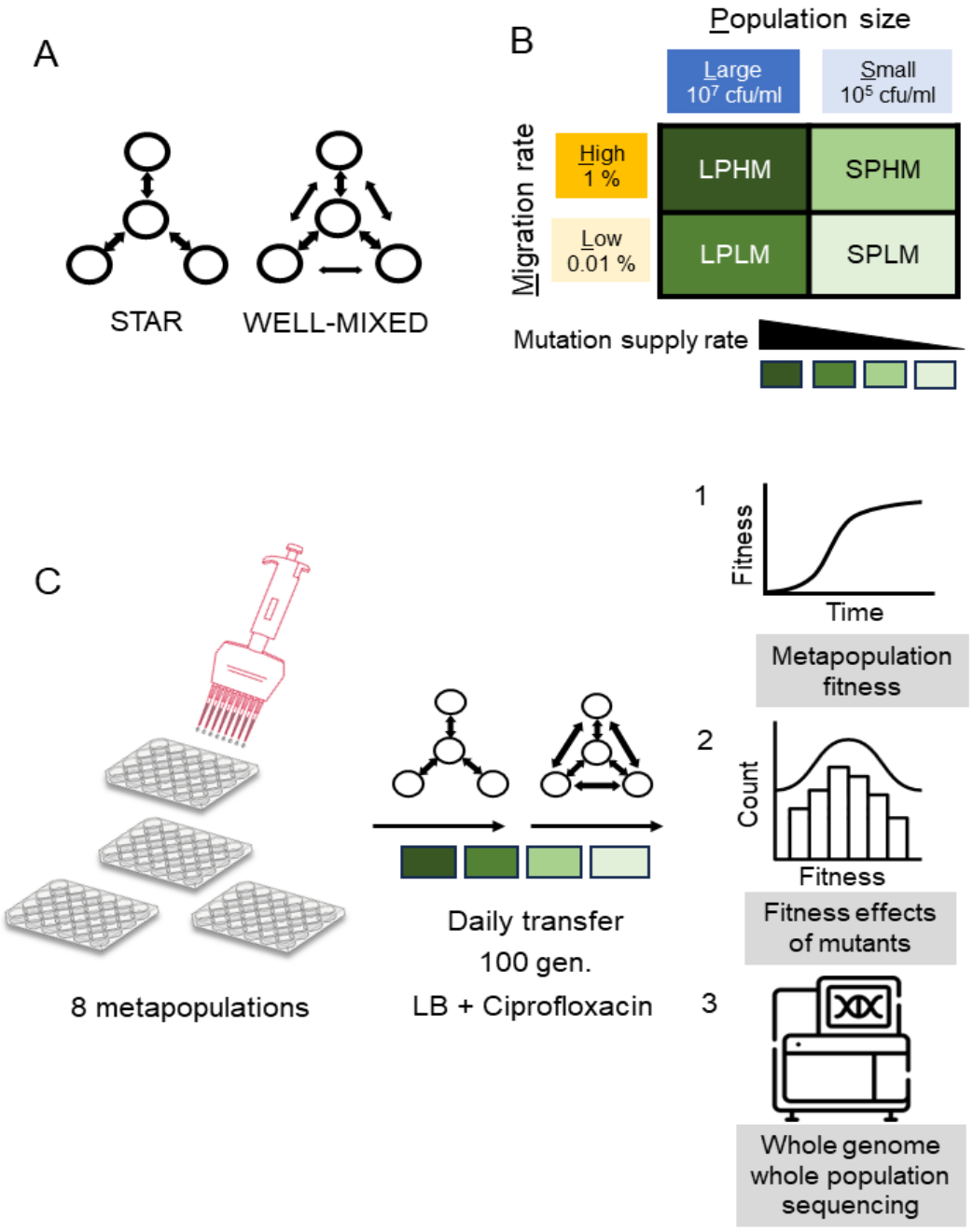

Figure 4.1 Design for *de novo* evolution experiment. (a) Two topologies, Star or Well-mixed, constructed among four subpopulations. Arrows depict dispersal routes among subpopulations (circles). (b) Four combinations of mutation supply rates achieved by manipulating both effective population sizes of the subpopulations and the migration rates among the subpopulations. (c) Experimental evolution setup and subsequent assays performed. Results of objective 3 - whole genome sequencing of the evolved metapopulations - have been reported in chapter 5.

We experimentally test these predictions directly by evolving a total of 64 replicate 4-patch metapopulations of *P. aeruginosa* in the laboratory under four mutation supply rates (combinations of 2 effective population sizes and 2 migration rates), and two network topologies, star and well-mixed (Fig. 1). We selected a star network with asymmetric inward migration for this experiment as it was shown to spread beneficial mutations faster in our earlier work (Chakraborty et al. 2023). In a metapopulation, mutation supply rate can be manipulated at two different levels, at the level of subpopulations - by changing the effective population size of the constitutive subpopulations and at the level of the whole metapopulation - by modifying the rate of migration between the subpopulations. In our experiment, during daily serial transfer of the metapopulations we manipulate mutation supply rate by creating a total of four combinations of effective population size (large and small) and migration rate (high and low, relative to the effective population size). We propagate eight replicate metapopulations by either the star or the well-mixed network under each of these four mutation supply rates for 100 generations as they evolve in the growth medium supplemented by a subinhibitory concentration of ciprofloxacin (40 ng/ml). For mutation-limited adaptation, increased fixation probabilities should increase the rate of adaptation as well. To see how the network topologies impact the rate of adaptation under each mutation supply rate, we measure the fitness gain of each metapopulation every ~25 generations for the duration of the evolution experiment. Additionally, we also measure absolute fitness and minimum inhibitory concentrations of 48 end-point isolates collected from each of the evolved metapopulations to evaluate the fitness effects and antibiotic resistance of substituted beneficial mutations under each network topology and mutation supply rate.

Results:

Star topology speeds up adaptation under low mutation supply

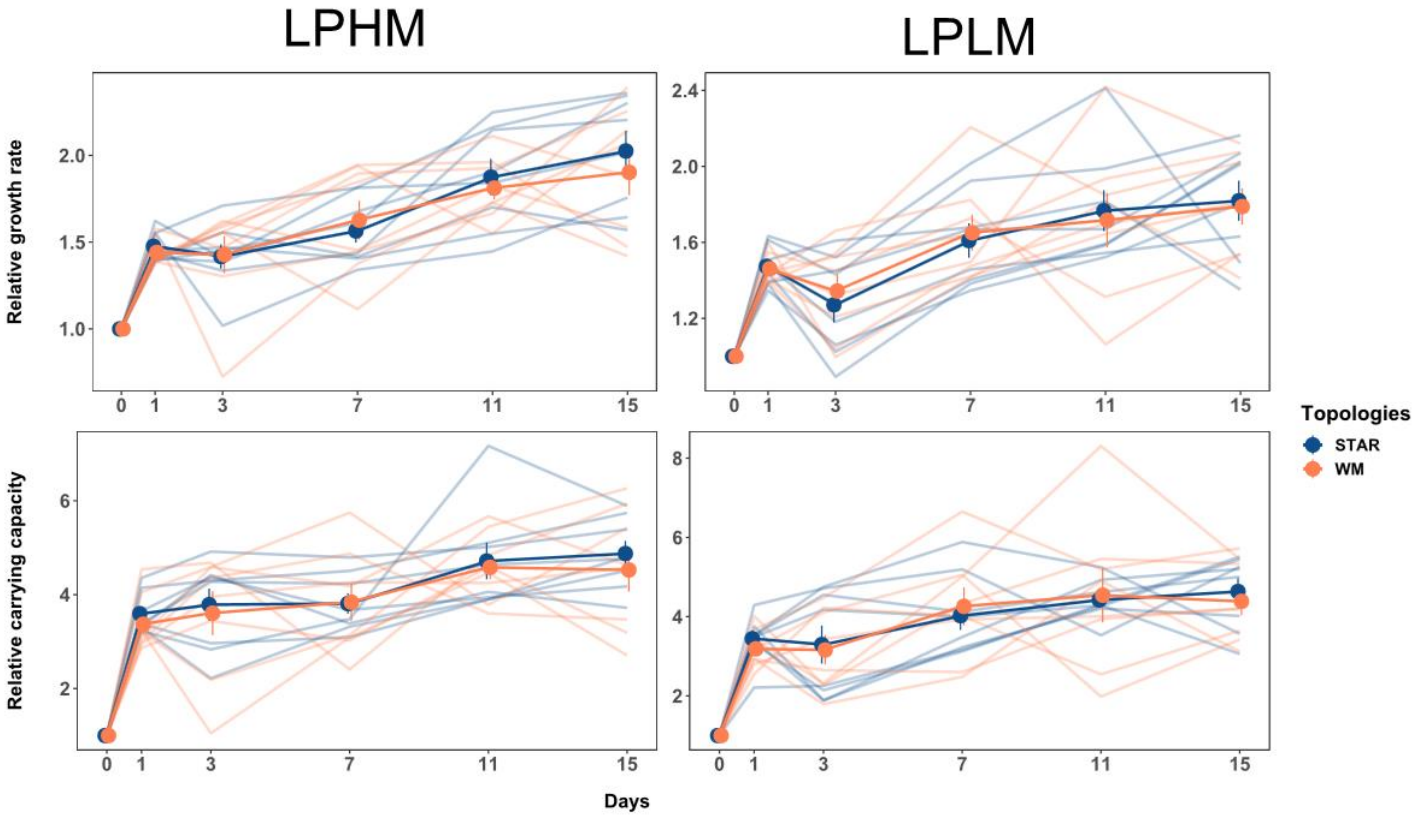

Figure 4.2 Dynamics of adaptation in large metapopulations. Fitness trajectories in large metapopulations connected by high and low migration rates (LPHM and LPLM). Increase in relative growth rate (upper panel) and relative carrying capacity (lower panel) in metapopulations propagated by either the star or the well-mixed topology with the LPHM (left panel) or LPLM (right panel) regime over the experimental time-period. Each point is the mean of 8 replicate metapopulations for a particular day and network topology, error bars show 1 standard error to the mean (SE). For large metapopulations (LPHM and LPLM), approximately 6.67 generations of growth happened per transfer.

We first investigated whether the rate of adaptation of the evolved metapopulations was influenced by their network topologies and mutation supply rate. According to the predictions put forward by EGT, when mutation supply rate is high we should expect a higher steady state fitness in well-mixed topologies but under lower mutation supply it is the star topology that should have a higher steady state fitness. Our results are partially consistent with these predictions. We observe that the rate of increase in fitness depends on the network topologies of the metapopulations but only when the effective population sizes of the constitutive subpopulations are smaller. The rate of increase in fitness is statistically indistinguishable between the star and the well-mixed network topologies at large effective population size in terms of both growth rate (r) (Fig 4.2 upper horizontal panel) and carrying capacity (k) (Fig 4.2 lower horizontal panel) relative to the wild-type ancestor (linear mixed effect model with time as a second order polynomial regressor, main effect of network treatment for relative r: Chisq = 0.0039, p = 0.95 and relative k: Chisq = 0.2678, p = 0.60). Additionally, the rate of migration between the subpopulations does not explain a significant amount of variation in the rate of fitness increase (relative r: Chisq = 0.6350, p = 0.42 and relative k: Chisq = 0.4338, p = 0.51).

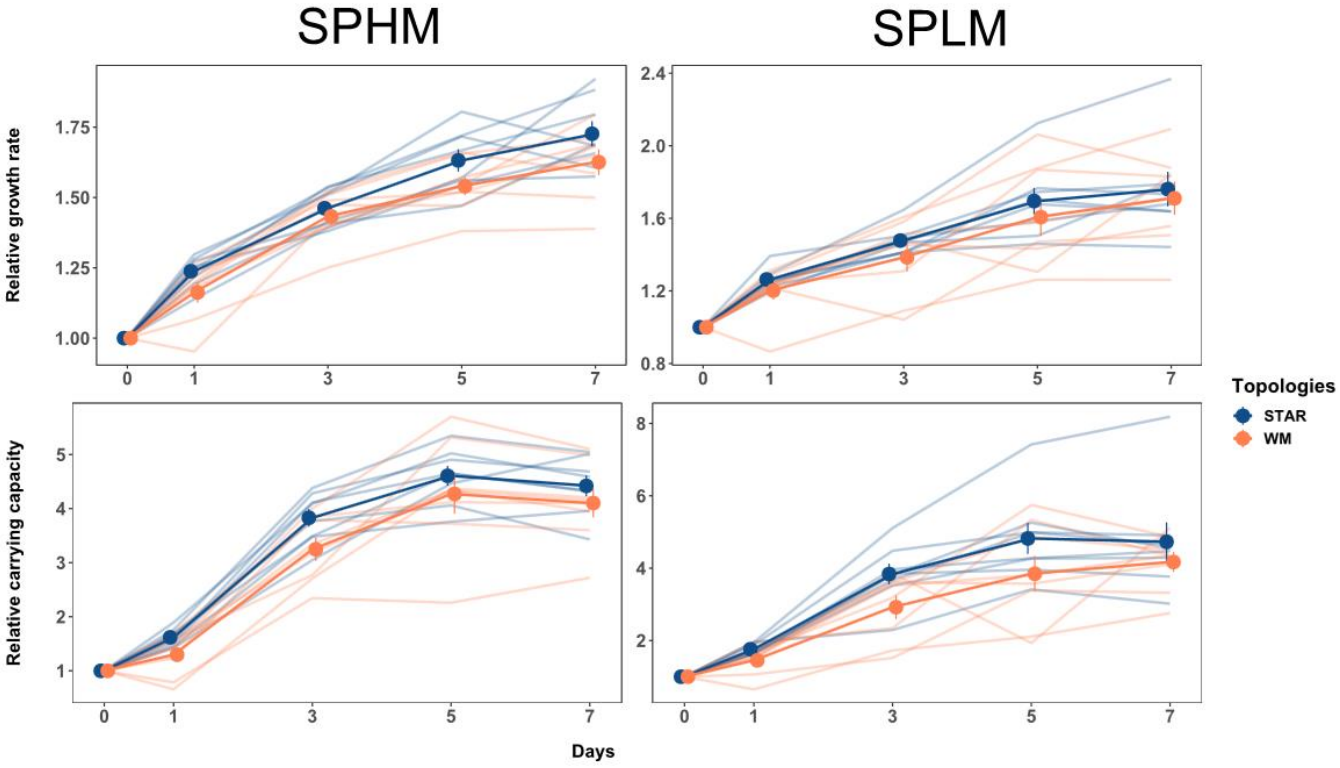

Figure 4.3 Dynamics of adaptation in small metapopulations. Fitness trajectories in small metapopulations (SPHM and SPLM) connected by high and low migration rates. Increase in relative growth rate (upper panel) and relative carrying capacity (lower panel) in metapopulations propagated by either the star or the well-mixed topology with the SPHM (left vertical panel) or SPLM (right vertical panel) regime over the experimental time-period. Each point is the mean of 8 replicate metapopulations for a particular day and network topology, error bars show 1 standard error to the mean (SE). For small metapopulations (SPHM and SPLM), approximately 13.28 generations of growth happened per transfer.

Interestingly, at the smaller effective population size (Fig 4.3), we see evidence that network topology can explain a significant amount of variation in the rate of increase in fitness. This effect is marginally significant for the increase in relative growth rate (Fig 4.3 upper horizontal panel) but significantly higher for the increase in carrying capacity (Fig 4.3 lower horizontal panel) in the star structured metapopulations compared to their well-mixed counterparts (relative r: Chisq=3.3598, p=0.06 and relative k: Chisq=6.6948, p<0.01). Similar as before, we do not uncover any significant effect of migration rate on the rate of increase in fitness (relative r: Chisq=0.1189, p=0.73 and relative k: Chisq=0.0008, p = 0.97). These results lend support to the predictions of EGT that star topologies can retain their “amplifying” feature when mutation supply is low but not when mutation supply is high.

Network topology and mutation supply rate interacts to determine the distribution of fitness effects of the evolved isolates

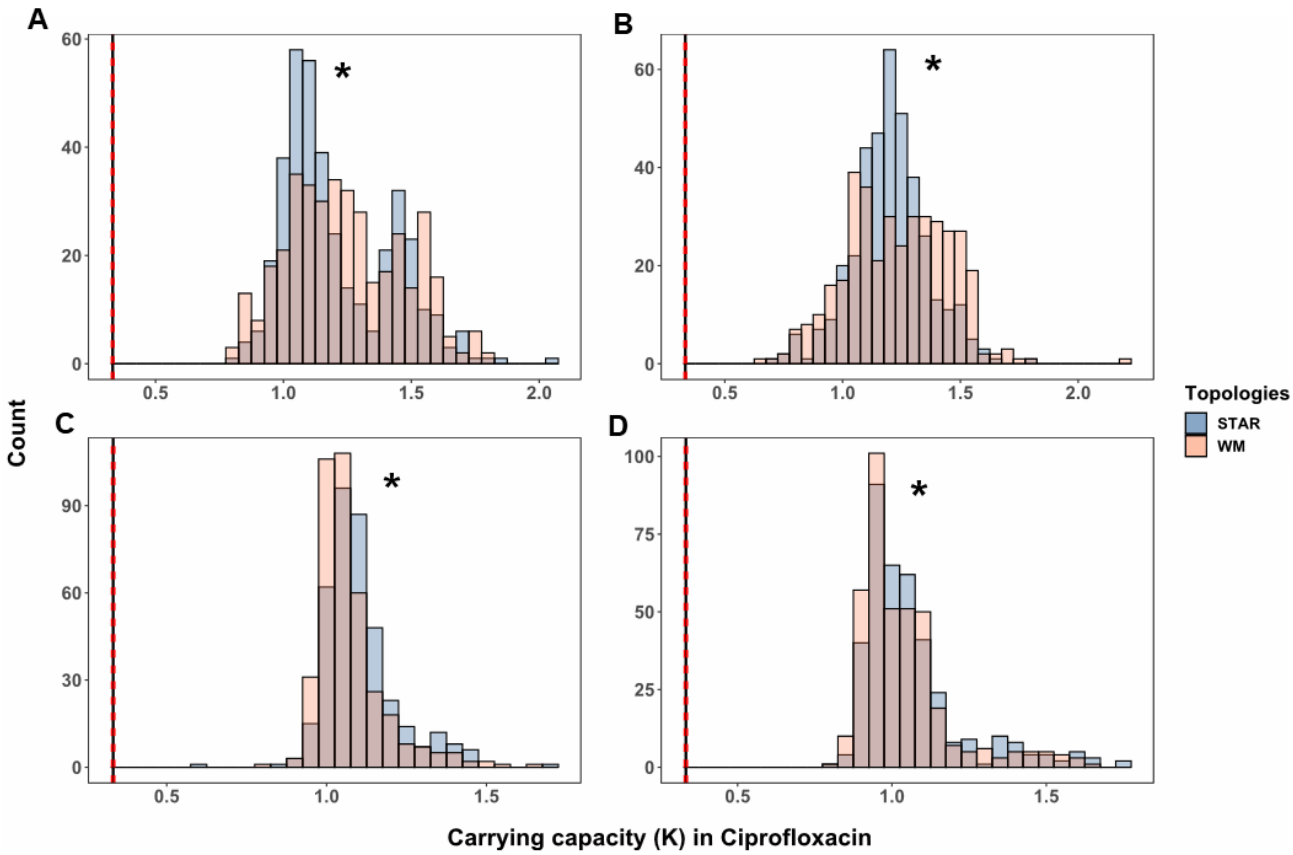

Figure 4.4 Distribution of fitness effects of isolates in the selection medium. Absolute fitness of evolved end-point isolates in the selection medium (LB supplemented with subinhibitory concentration of ciprofloxacin). Fitness effect distributions are shown as histograms of absolute fitness for all mutants isolated from the large (LPHM and LPLM) metapopulations (A and B, respectively) or the small (SPHM and SPLM) metapopulations (C and D, respectively). Blue and red bars denote isolates collected from metapopulations propagated either by the star or the well-mixed topologies, respectively. The asterisk (*) indicates significance at $P<0.05$ for permutation K-S test (10000 permutations). The vertical line on the left hand side of each histogram is the mean absolute fitness of the ancestor in the selection medium and the red dotted vertical lines are one standard error (SE) to the mean.

Next, we investigated whether the distribution of fitness effects of the substituted mutations were different depending on the topologies they were evolved in. This was inspired from the observation that at the endpoint of the evolution experiment we did not see a significant difference in the extent of adaptation between the network topologies for any of the mutation supply rates despite the observed difference for the rate of adaptation. To do this, we measured absolute fitness of the evolved isolates (in terms of their carrying capacity in the selection environment) collected from the metapopulations at the end time-point of the evolution experiment. The expected distribution of fitness effects of substituted beneficial mutants is not immediately clear from the population level fitness predictions derived in EGT. However, we can hypothesize that since fixation times are longer in the star topology when more mutations are competing for fixation, well-mixed topology will fix mutations with larger beneficial effects faster. In contrast, when there is lower mutation supply, star topologies will avoid the drift-loss of large effect beneficial mutations, subsequently fixing them in the metapopulations.

Consistent with our hypotheses, we find that network topology impacts the fitness effects of the beneficial mutants differentially depending on the mutation supply rates in the metapopulations. Specifically, we find that in large metapopulations, a higher frequency of large effect beneficial mutants segregate in the well-mixed metapopulations than the star metapopulations and this effect is consistent for both the high and the low migration rate (Fig 4.4 panel A-B, permutation Kolmogorov Smirnov test to determine the exclusivity of the frequency distributions, $p<10^{-3}$ and $p<10^{-3}$, for high and low migration rates, respectively for 10000 permutations). In contrast, star metapopulations harbor more large

effect beneficial mutants compared to the well-mixed metapopulations when the effective population size is low, for both high and low migration rates (Fig 4.4 panel C-D, permutation Kolmogorov Smirnov test, $p<10^{-4}$ and $p < 0.05$, for high and low migration rates, respectively for 10000 permutations). Interestingly, we find that the mean fitness of isolates evolved in either star or the well-mixed metapopulation is not significantly different (main effect of network, 3 way ANOVA with interactions, Chisq = 0.0177, p=0.89) for either of the mutation supply rate studied in our experiment. Furthermore, keeping consistent with the expected effect of population size and migration rate (both contributing to mutation supply rate) on the fitness distribution of beneficial mutants, we find that the mean fitness of isolates is significantly higher in larger effective population size (main effect of population size, 3 way ANOVA with interactions, Chisq = 49.1291, $P<10^{-11}$) and high migration rate (main effect of migration rate, 3 way ANOVA with interactions, Chisq = 7.0562, p<0.01). Thus, our results illuminate how the shape of the fitness distribution of substituted beneficial mutations can change in metapopulations differing in topological connections and emphasize the importance of inclusion of this factor in the further developments in EGT.

The fitness cost of antibiotic resistant mutations depends on the effective population size and network topology of the metapopulations

During the evolution of resistance to an antibiotic, populations often tend to substitute mutations that are beneficial in the growth medium containing the antibiotic but those can become costly and lead to a decrease in fitness in the absence of the antibiotic.

Populations that substitute larger effect beneficial mutations might pay less to no cost or they can also compensate for the cost by substituting second site mutations somewhere else in their genome (Melnyk et al. 2017). These cost-free or compensatory mutations are rare and logically only populations with a high mutation supply will have access to them. We assessed these possibilities by measuring the absolute fitness (in terms of carrying capacity) of the same beneficial mutants used in the previous section but in the absence of ciprofloxacin in the growth medium. We hypothesized that mutants evolved in large metapopulations will bear less-to-no cost and mutants from small metapopulations will be costly. We can extend these predictions for the network topologies studied as well. Since, we observed a higher number of large effect antibiotic resistance mutations in large well-mixed and small star metapopulations, we expect mutations substituted in these topologies to be less-costly.

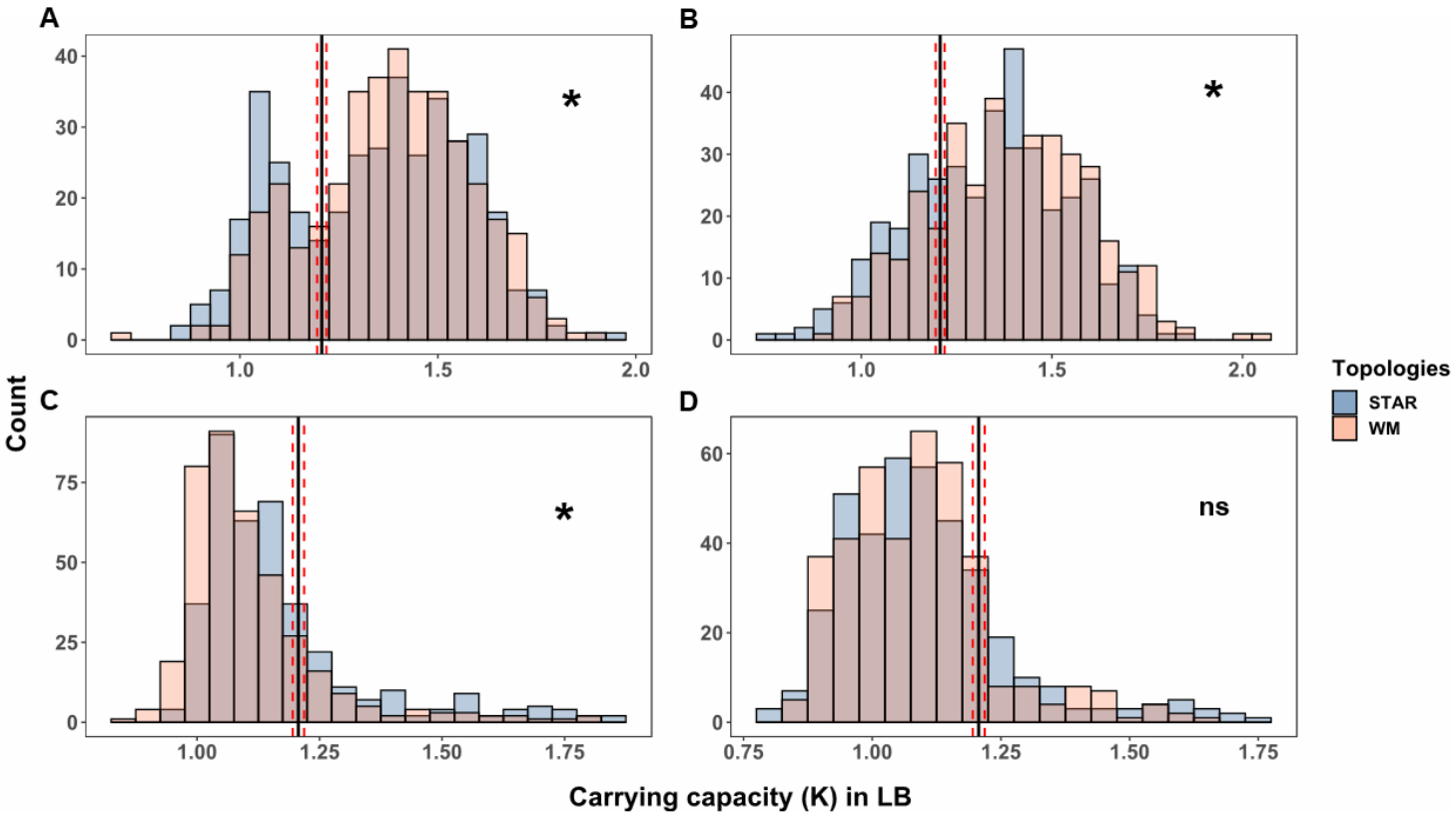

Figure 4.5 Distribution of fitness effects of isolates in in the permissive medium. Absolute fitness of evolved end-point isolates in the permissive medium (LB without ciprofloxacin). Fitness effect distributions are shown as histograms of absolute fitness for all mutants isolated from the large (LPHM and LPLM) metapopulations (A and B, respectively) or the small (SPHM and SPLM) metapopulations (C and D, respectively). Blue and red bars denote isolates collected from metapopulations propagated either by the star or the well-mixed topologies, respectively. The asterisk (*) indicates significance at $P<0.05$ for permutation K-S test (10000 permutations), 'ns' denotes insignificant statistical result in K-S test. The vertical line in each histogram is the mean absolute fitness of the ancestor in the permissive medium and the red dotted vertical lines are one standard error (SE) to the mean. Isolates on the left hand side of the vertical line are costly.

Our findings match our expectations. We observe a significantly higher enrichment of cost-free mutations in large metapopulations (Fig 4.5 panel A-B, one-sample t-test, $p<10^{-11}$, irrespective of network topology). We observe the same trend for large metapopulations propagated by the well-mixed topology, an effect consistent with both high and low migration rates (Fig 4.5 panel A-B, permutation Kolmogorov Smirnov test, $p<0.05$ and $p<0.05$, for high and low migration rates, respectively for 10000 permutations). Contrastingly, the small metapopulations primarily substitute costly resistance mutations (Fig 4.5 panel C-D, one sample t-test, $p<10^{-5}$) but small star metapopulations harbor a higher number of less costly mutations compared to the well-mixed metapopulations (Fig 4.5 panel C-D, permutation Kolmogorov Smirnov test, $p<10^{-3}$ and $p>0.05$, for high and low migration rates, respectively for 10000 permutations). In addition to this, evolved isolates collected from large metapopulations show higher fold-increase in their minimum inhibitory concentrations to ciprofloxacin compared to small metapopulations, for both migration rates (main effect of population size, 3 way ANOVA with interactions, $p<10^{-15}$) but we observe no difference between the two topologies (main effect of network topology, 3 way ANOVA with interactions, $p = 0.44$, Fig 4.6). Our results uncover a novel relationship between the cost of resistance, the mutation supply rate and the network topology of spatially structured metapopulations - an effect previously unseen in any other microbial evolution studies.

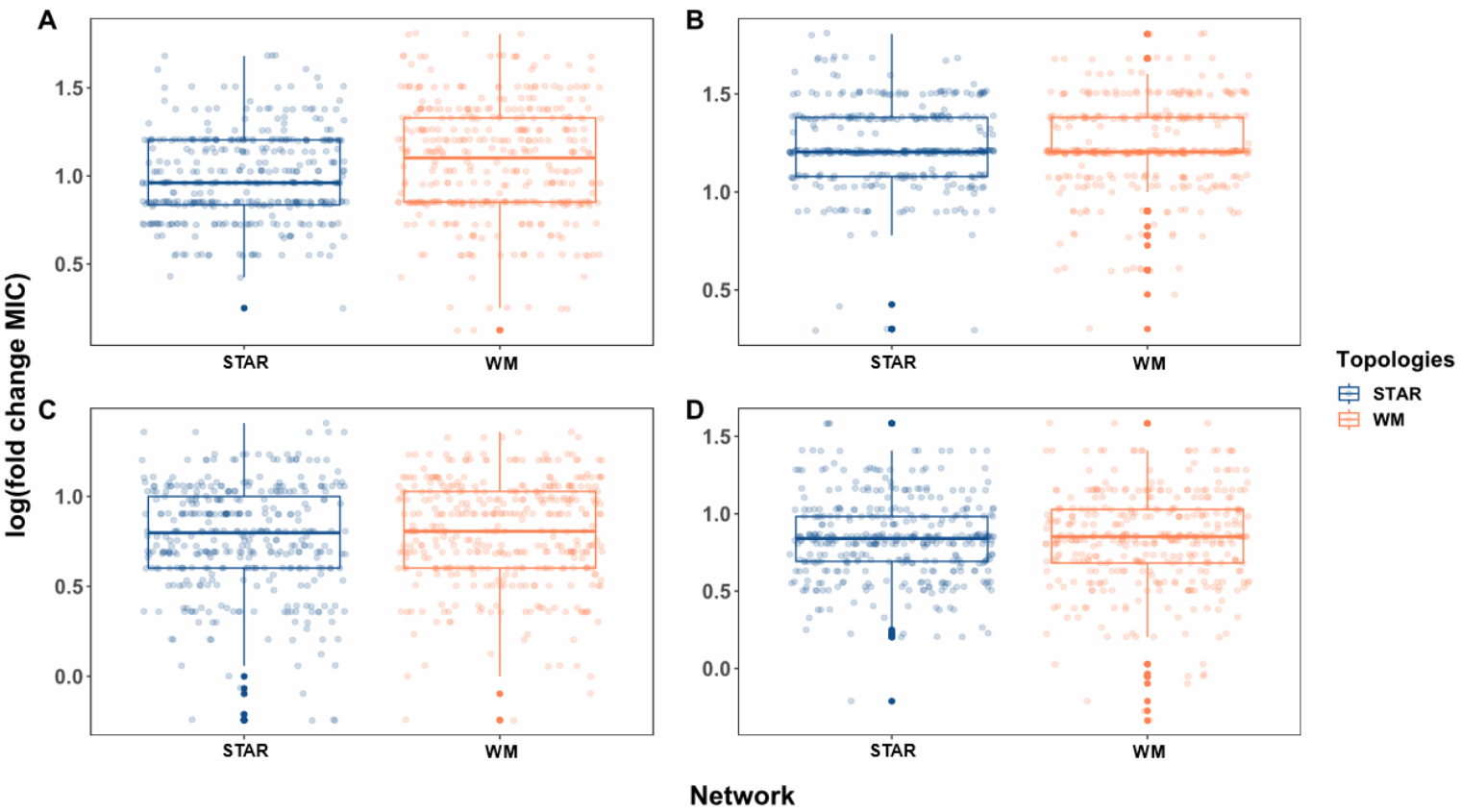

Figure 4.6 Ciprofloxacin resistance of evolved isolates. Ciprofloxacin resistance measured as the log fold change in minimum inhibitory concentration (log_{10}(MIC), with MIC measured in μg/mL) of each of forty-eight isolates from each evolved metapopulation after ~ 100 generations of evolution in subinhibitory concentration of ciprofloxacin. Large metapopulations: (A) LPHM, (B) LPLM and small metapopulations: (C) SPHM, and (D) SPLM. MIC calculations are normalized by ancestral MIC of PA14 or PA14-LacZ isolates measured on the same day of assay. Each data point represents a single isolate. Boxplots show the quantile distribution of the data.

Discussion

By impacting the amount of genetic variation available for selection, spatial structure can influence the dynamics of adaptation. In classical population genetic theory, the extent of adaptive evolution has been shown to not change in spatially structured populations compared to well-mixed populations (Maruyama 1970; Slatkin 1981). In contrast, Evolutionary Graph Theory (EGT) posits that the specific arrangements of populations in space or network topologies can “amplify” adaptation in comparison to well-mixed populations (Lieberman et al. 2005). However, these predictions of EGT are only valid when the populations adapt by substituting beneficial alleles periodically and not when multiple mutations are contending for fixation (Gerrish and Lenski 1998; Desai and Fisher 2007; Sniegowski and Gerrish 2010; Sharma et al. 2023). Additionally, extant models of EGT do not predict the distribution of fitness effects of beneficial mutations that are ultimately substituted (Lieberman et al. 2005; Pavlogiannis et al. 2018; Marrec et al. 2021; Tkadlec et al. 2021; Sharma et al. 2023). However, these predictions are not empirically tested. To address these issues, here we have studied the effect of mutation supply rate and network topology on the dynamics of adaptation in experimental metapopulations of *P. aeruginosa* evolving under mild antibiotic stress.

Our study provides novel insight into the previously unexplored effect of network topology of metapopulations on the adaptive substitution of multiple beneficial mutations and also the dynamics of increment in fitness. Briefly, we find that the certain topologies of metapopulations can impact the extent of adaptive evolution, an effect that is critically dependent on the amount of genetic variation available for selection. In our study, star

topology sped up adaptation in metapopulations evolving with small effective population size compared to their well-mixed counterparts. However, this “amplifying” effect was not seen in the large metapopulations. Furthermore, we find beneficial mutants providing a large fitness increase are more frequently present in well-mixed metapopulations of large size and star metapopulations of small size. We see a similar pattern when measuring the fitness of these beneficial antibiotic resistant mutants in an “away” or drug-free environment, reiterating that adaptation has happened faster in the small star networks and the large well-mixed network compared with their respective counterparts. Interestingly, the mean effect of beneficial mutations substituted in each network topology did not differ significantly under any of the tested mutation supply rates.

Our results are remarkable because it provides the first experimental support for the newer models of Evolutionary Graph Theory (EGT) that track the fixation dynamics of multiple mutations segregating in graph-structured populations. These theoretical extensions of EGT predict that the fixation dynamics of beneficial mutation is slower in the star network compared to a well-mixed network when another mutation is contending for fixation in the same population. This is because the time it takes for a beneficial mutation to fix is longer in the star topology and the appearance of another beneficial mutation will further slow down the fixation process (Frean Marcus et al. 2013). However, in these same models the steady state fitness in populations inhabiting a star graph was found to be higher when the mutation rate was low (Sharma et al. 2023). Resoundingly, we have shown here that star metapopulations attained a higher rate and extent of adaptation than well-mixed metapopulations when supply of beneficial mutation was low.

This effect can be attributed to higher number of large effect beneficial mutations in the star network at low mutation supply rates. This result fits perfectly well with a previous study where under low levels of migration rate and increasing random drift a focal beneficial mutation reached significantly higher proportions in the star networks, an “amplification” effect of the star networks due to it minimizing the loss of the beneficial mutant to random drift compared to the well-mixed networks (Chakraborty et al. 2023). In the current study, we emphasize the generalizability of this result by monitoring not just one but several substitutions of *de novo* beneficial mutations while *P. aeruginosa* rapidly adapts to the antibiotic stress. By assessing the underlying distribution of fitness effects of the substituted beneficial mutations, we reiterate that this “amplification” effect is due to the star topologies restricting the “drift-loss” of beneficial mutations when mutation supply is lower, not because of it enhancing the fixation probabilities of beneficial mutations of the same fitness effects over well-mixed topologies. This was concluded because the mean effect of the beneficial mutations did not change but their underlying distributions were found to be significantly different. This overall pattern did not change when the fitness distributions were measured in a drug-free environment, indicating the importance of plausible pleiotropy and epistasis defining the underlying adaptive dynamics, and their cumulative dependence on mutational supply rate and spatial structure of the metapopulations. Teasing apart the role of pleiotropy and epistasis on the adaptive dynamics of populations evolving in a spatially structured environment is a massive undertaking and is out of scope for this current study. We hope that future theoretical and experimental endeavors will take up this challenge and integrate these

factors into their frameworks for correctly predicting the effect of spatial structure on evolutionary trajectories of microorganisms.

Our work has clear implications for understanding the evolutionary dynamics of microbial populations in their natural habitats, which are often spatially structured, such as soil metacommunities, host associated microbial communities and biofilms in industrial and clinical settings (Werner et al. 2014; Dang and Lovell 2015; Stacy et al. 2016; Kraemer and Boynton 2017; García-Bayona and Comstock 2018; Yanni et al. 2019; Shi et al. 2020; Coenye et al. 2022; Hajishengallis et al. 2023). Furthermore, our study shows that living in spatially structured conditions can be advantageous for microbes in the face of constant environmental insults and this can in turn determine their evolutionary trajectories (Hansen et al. 2007; Zhang et al. 2011; Kim et al. 2014; Baym et al. 2016; Fusco et al. 2016; France et al. 2019b; Durão et al. 2020; Aif et al. 2022). We also emphasize that the maintenance of genetic variation in microbial populations following harsh bottlenecks imposed during host dissociation or biofilm dispersal can have profoundly different outcomes depending on the spatial structure of the population (Abel et al. 2015; Nadell et al. 2016; Steenackers et al. 2016). Our work illuminates the plausible mechanisms behind the acquisition and maintenance of *de novo* antibiotic resistant mutations in spatially structured natural microbial populations such as in biofilms associated with human infections (Levin et al. 2000; Andersson and Hughes 2010; Hughes and Andersson 2017; France et al. 2019b; Durão et al. 2020). Finally, the current study demonstrates the importance of microbial interaction networks in dictating the spread of invasive microbial species and their associated pathogenicity (Donker et al. 2014;

Martínez and Baquero 2014; Krieger et al. 2020; Shapiro et al. 2020), the evolution of the microbial community composition in nature (Estrela and Brown 2013, 2018; Borer et al. 2020; Ciccarese et al. 2020; Denk-Lobnig and Wood 2023), and their impact on human health.

Materials and methods

Microbial strains and conditions:

For all experiments, clonal populations of *Pseudomonas aeruginosa* strain 14 (PA14) and PA14:lacZ, isogenic to PA14 except with an insertion in the lacZ gene respectively, were used. Colonies possessing the lacZ insertion appear blue when cultured on agar plates supplemented with 40 mg/L of 5-bromo-4-chloro-3-indolyl-beta-D-galactopyranoside (X-Gal), and are visually distinct from the PA14 white colouration. The neutrality of the lacZ marker was confirmed in our experimental environments by measuring the fitness of the marked strain relative to the unmarked strain. Populations were cultured in 24-well plates with 1.5 mL of media in each well, in an orbital shaker (150 RPM) at 37°C. The culture media consisted of Luria Bertani broth (LB: bacto-tryptone 10 g/L, yeast extract 5 g/L, NaCl 10 g/L) supplemented with 40 ng/mL of the fluoroquinolone antibiotic, ciprofloxacin. This particular subinhibitory concentration of ciprofloxacin was chosen to exert only a moderate level of selection pressure that would slow down the dynamics of fixation of resistant mutations compared to a lethal dose above MIC concentration. This let us discern the effect of network topology on the process of adaptive substitution with weakened interference of strong selection (Appendix A Fig A.7). Ciprofloxacin concentration lower than this did not enrich resistant mutations to high levels in the populations within the experimental time period tested (Appendix A Fig A.8). All strains and evolving populations were cryopreserved at −80°C in 20% (v/v) glycerol.

Evolution experiment:

A single metapopulation consisted of four subpopulations, one subpopulation being located on each of four different 24-well plates. Plate 2 was always assigned as the hub, and plates 1, 3, and 4 were treated as the leaves. Half of the metapopulations (every odd numbered replicate) in this experiment was inoculated with clonal PA14 and the other half (every even numbered replicate) with clonal PA14:LacZ. This was necessary in order to track any cross-contamination between metapopulations inhabiting adjacent wells in the 24 well plate. Metapopulations were propagated under two effective population sizes of the constitutive subpopulations (large and small) and two migration rates (high and low) between the subpopulations connected by two network topologies (star and well-mixed). This design allowed us to track a total of 64 replicate metapopulations (8 replicate metapopulations per topology(2) X population size(2) X migration rate (2) combinations). Each metapopulation was initiated by inoculating each subpopulation with ~10^7 (large) or ~10^5 (small) colony forming units (CFU) per ml of either PA14 or PA14:lacZ that descended from a single colony picked from an agar plate and grown overnight in liquid LB at 37°C with vigorous shaking (150 RPM). Metapopulations were transferred daily following dispersal among subpopulations (see below) by taking an aliquot corresponding to ~10^7 (large) or ~10^5 (small) CFUs per mL and inoculating into fresh medium supplemented with ciprofloxacin. The population density in each subpopulation reached ~10^9 CFUs after every 24 hours of growth, so this transfer regime corresponds to ~6.67 (large) or ~13.28 (small) daily generations of growth ($N_t = N_0 \times 2^g$, Nt = 10^9, N0 = 10^7 or 10^5, g = number of generations).

We constructed distinct network topologies by mixing subpopulations prior to serial transfer following the schematic shown in Appendix A Fig. A.4. Briefly, well-mixed networks were created by combining equal volume aliquots from all subpopulations into a common dispersal pool, diluting this mixture to the appropriate density to achieve the desired migration rate, and then mixing the dispersal pool with aliquots from each subpopulation (so-called 'self-inoculation') before transfer. Star networks, which involve bidirectional dispersal between the hub and leaves, were constructed in a similar way to the well-mixed situation only now the dispersal pool consisted of aliquots from just the leaves and aliquots from the hub (plate 2) were mixed with 'self-inoculation' samples from each leaf prior to serial transfer. For LPHM, LPLM, SPHM and SPLM ~10^5 , ~10^3 , ~10^3 , ~10 CFU/ml migrants were used in addition to the "self-inoculations", respectively. Further details on how each network topology and migration rate were achieved are same as chapter 3 and the schematics are provided in the appendix A.

This daily transfer protocol was continued until the metapopulations reached ~100 generations in their evolutionary time that is equivalent to 15 transfers ("days") for the large metapopulations and 7 transfers ("days") for the small metapopulations.

Phenotypic analyses:

Measurement of fitness of the metapopulations:

We measured the fitness of each evolved metapopulation every ~25 generations throughout the evolution experiment. Fitness was determined in terms of their growth rate (r) and carrying capacity (k) in the selective medium. During the evolution experiment, a mixture of the whole metapopulation was archived daily. We revived these metapopulation mixes saved on Day 1,3,7,11 and 15 for the large metapopulations, and Day 1,3,5 and 7 for the small metapopulations in the selection medium by overnight growth in 1.5 mL of media in each well, in an orbital shaker (150 RPM) at 37°C along with the PA14 and PA14:LacZ ancestors. On the next day, the overnight cultures were diluted 1:1000 in fresh 200µl selection medium in a 96 well plate and a growth curve experiment was started in a BioTek PowerWave spectrophotometer (BioTek Instruments Inc., Winooski, VT) that was incubated at 37°C with linear shaking for 20 seconds in every 5 minutes. The optical density(OD) of each sample was measured at 600 nm after every 20 minutes for 24 hours until the sample reached the stationary phase of growth. Carrying capacity was measured as the highest optical density reached during the 24 hour growth and maximum growth rate was estimated as the maximum slope of the growth curve over a running window of eight OD readings using a custom script in R. Each measurement was carried out with five biological replicates. We only revived cryo-stocks belonging to the same day together and the measured carrying capacity and growth rate was normalized by the appropriate ancestors growth on the same day of experiment, hence

minimizing any measurement bias. Also, the wells in the periphery of the 96 well plate were not inoculated with any samples to control for sample loss due to evaporation.

Measurement of fitness of the evolved isolates collected from the metapopulations:

We collected 12 single isolates from each subpopulation from all the evolved metapopulations (12 isolates X 4 subpopulations X 64 metapopulations = 3072 single isolates in total). The evolved subpopulations from the last time-point in the experiment were diluted $1:10^6$ and plated on LB-agar plates for overnight growth and inoculated at 37°C. Twelve single isolates from pre-marked positions were collected to avoid bias and were grown overnight in growth medium devoid of any ciprofloxacin to restrict any further genetic changes and were archived. For the fitness assay in the selection medium, the cryo-stocks for each isolate was streaked on a LB-Agar plate and a single colony was grown in the selective growth medium in 24 well plates overnight at 37°C with vigorous shaking (150 RPM). The optical density (OD) was measured at 600 nm in a BioTek PowerWave spectrophotometer after thoroughly mixing the overnight culture. Same protocol was used to measure the carrying capacity of the single isolate in the absence of ciprofloxacin, except that they were grown in the liquid LB media devoid of ciprofloxacin for 24 hours before the OD measurement. For each isolate, carrying capacity was measured only once given the large number of total isolates for measurement. However, PA14 and PA14-LacZ ancestors grown 64 times each for CIP and NO-CIP environments suggests there was negligible day to day variation in carrying capacity measurements even for biological replicates (vertical red dashed lines in Figure 4.4 and 4.5).

Minimum inhibitory concentration of isolates collected from the metapopulations:

For each isolate, we assayed resistance as their MIC to ciprofloxacin by first growing them overnight in LB media and then diluting the overnight culture 1:1000 into 96-well plates containing LB supplemented with 0.0, 0.125, 0.25, 0.5, 1.0, 2.0, 4.0, 8.0, 16.0 µg/mL ciprofloxacin, respectively, and incubating on an orbital shaker at 37°C. Growth was estimated by reading optical density (OD) at 600 nm after 48 hours of growth. If OD was more than 10% of the OD in permissive (without antibiotic i.e. 0.0 µg/mL CIP) media it was scored as growth. Log_{10}-transformed MICs were used for all analyses. MIC measurements for each isolate were performed with two biological replicates.

Statistical analyses:

All statistical analyses were performed in R (version 4.2.2) (R Core Team 2022). We modeled the rate of change in fitness change (both relative growth rate and carrying capacity) through time separately for each population size treatment using a linear mixed model (lmer) with time (Bates et al. 2015), migration rate and network topology as fixed factors, and a random intercept of individual replicate population to account for resampling across time (repeated measures). Time was considered to be a polynomial regressor in our model since the trajectories were not linear themselves. The distribution of fitness effects of the beneficial mutants isolated from the end-point metapopulations in selective and permissive media were compared between the network topologies using a Kolmogorov-Smirnov (K-S) test paired with a resampling procedure (10000

permutations). The impact of effective population size (two levels: large and small), migration rate (two levels: high and low) and network topology (two levels: Star and WM) on the mean fitness effects and the change in MIC of the isolated beneficial mutants were determined by treating these three explanatory variables as fixed categorical factors and running a 3-way ANOVA with interactions between these three factors. Model assumptions were subsequently checked to ensure the validity of statistical analyses.

Chapter 5:

Network topology increases genetic parallelism during de novo evolution of antibiotic resistance in Pseudomonas aeruginosa metapopulations

Partha Pratim Chakraborty & Rees Kassen

This chapter will be communicated along with Chapter 4 (manuscript under preparation).

Abstract

Evolutionary graph theory (EGT) predicts that certain metapopulation network topologies can accelerate adaptation over well-mixed topologies. Although the predictions are based on the increase in fitness, the underlying genetics of adaptation has not been theoretically or experimentally explored. Here we empirically assess the genetics behind the "amplification" process using evolve and resequence (ER) experiments. We propagate multiple replicate *Pseudomonas aeruginosa* metapopulations receiving differential mutational supplies and connected by varying network topologies under antibiotic stress for ~100 generations and perform whole genome sequencing of the evolved metapopulations. As predicted by EGT, metapopulations connected by star topologies where migration happens only through a central hub accelerate evolution but only at low mutation supply rates. Our genomic analyses show that star networks can achieve this acceleration by substituting beneficial mutations in the same gene with high repeatability. Additionally, we show that spectra of *de novo* antibiotic resistant mutations are highly divergent in their types and identities depending on mutation supply rates in the evolved metapopulations. Overall, our work provides the first experimental account for the genetic basis of the "amplification" process, establishes a novel relationship among spatial structure, mutation supply rate and *de novo* antibiotic resistance evolution, and helps determine the predictability of evolution of microbial metapopulations in their spatially structured natural habitats.

Introduction

Whether the arrangement of populations in space can influence their adaptive dynamics is a much debated subject in evolutionary biology. Classical population genetic theory has found that fixation dynamics of a beneficial mutation in a spatially structured population is the same as an unstructured, well-mixed population (Maruyama 1970; Slatkin 1981). However, relatively newer mathematical theories such as the Evolutionary Graph Theory (EGT) posit certain network topologies either accelerate or decelerate adaptive evolution by increasing or decreasing the fixation probability of a beneficial mutation in comparison to a well-mixed topology (Lieberman et al. 2005). Despite these contrasting theoretical predictions, a clear understanding of the genetic basis of adaptation in spatially structured populations is largely absent from literature.

Natural populations are often spatially structured, meaning they are composed of a series of populations that are arranged in space and interconnected by dispersal – in that sense, they resemble metapopulations (Hanski and Gilpin 1997). Analytical solutions and simulation models do not find the fixation dynamics in a structured population to be any different from a well-mixed scenario when mutation supply is low (Strong Selection Weak Mutation or the SSWM regime)(Maruyama 1970; Gordo and Campos 2006). However, with the increase in mutation supply rate (Strong Selection Strong Mutation or the SSSM regime) fixation dynamics in structured populations slows down in comparison to well-mixed populations, decelerating the rate of their evolution (Gordo and Campos 2006). This is mainly because the fixation time of beneficial mutations increases in structured populations due to an increase in competition among beneficial mutations for fixation in

the absence of recombination('clonal interference') (Gerrish and Lenski 1998). Additionally, dispersal among the subpopulations in a spatially structured population can accentuate the effect of clonal interference by mimicking the role of mutation supply. However, these predictions are based on the fitness of entire metapopulations and we lack clear expectations regarding the magnitude of the fitness effects of substituted beneficial mutations or the underlying genetics of adaptations in spatially structured populations.

We can start building these expectations by thinking about the role of clonal interference on the fitness effects of beneficial mutations that are ultimately fixed in a population. As mutation supply rate increases, clonal interference increases the variation in adaptive potential in highly polymorphic asexual populations (Gerrish and Lenski 1998). In competition with beneficial mutants with larger fitness advantages, small effect beneficial mutants lose out and bias the fitness effects of mutations that ultimately fix to those with large fitness advantages (Rozen et al. 2002; Perfeito et al. 2007a; Schoustra et al. 2009; Kassen 2014). According to population genetic models and their experimental tests, beneficial mutations with large fitness advantage are rare and this constrains the choice of genetic loci that can provide such large fitness increments (Fisher 1930; Gillespie 1983, 1984, 1994; Orr 1998, 2002, 2003, 2005a; Kassen and Bataillon 2006; Eyre-Walker and Keightley 2007; MacLean and Buckling 2009; Chevin et al. 2010). Therefore, if multiple populations were adapting to a similar environmental challenge they would repeatedly substitute the mutations in the same gene given a high enough mutation supply rate. Such repeated and independent substitution of mutations in the same gene in multiple

populations exposed to similar environmental challenges is called parallel evolution and is taken to be a strong indicator of selection acting on that genetic locus (Orr 2005b).

Theory shows that spatially structured populations fix larger effect mutations due to heightened clonal interference as opposed to well-mixed populations (Gordo and Campos 2006). Logically, such high levels of clonal interference should increase genetic parallelism in spatially structured populations during their evolution (Bailey et al. 2017, 2021b). Testing this prediction, a recent empirical study looking at the effect of spatial structure on the genetic parallelism did not find a significantly higher genetic parallelism in spatially structured populations of *Pseudomonas fluorescens* evolving in xylose as the sole carbon source (Bailey et al. 2021b). Their results were supported by the fact that their experiment spatially structured populations evolved slower than well-mixed populations. In contrast, another experimental study where spatial structure accelerated the adaptation of *E. coli* metapopulations showed that the isolates derived from structured metapopulations fixed significantly more mutations and were genotypically more diverse than isolates from unstructured metapopulations (Nahum et al. 2015). The structured metapopulations of *E. coli* reached the furthest fitness optimum because they opted for alternate, longer genetic pathways of adaptation that the unstructured metapopulations could not access. However, since genetic parallelism was not formally quantified, the question whether spatially structured metapopulations achieved higher fitness because they fixed beneficial mutations with a high repeatability, was not answered.

According to Evolutionary Graph Theory (EGT) certain graphs or network topologies, such as the star topology with bidirectional dispersal through a central “hub”, can accelerate the speed of adaptive evolution as compared to a well-mixed topology (Lieberman et al. 2005). We have provided experimental support for this prediction previously by measuring the dynamics of spread of an initially rare beneficial mutant of known identity in a four-deme metapopulation connected by either the star or the well-mixed network topology. Mechanistically, the star topology achieves this “amplification” of selection by minimizing the loss of the initially rare beneficial mutation from genetic drift by concentrating them in the central “hub” (Chakraborty et al. 2023). We have extended this experimental framework beyond the dynamics of spread of a single beneficial mutation to a scenario involving more open-ended adaptation that allows for the fixation of multiple mutations (chapter 4). Similarly to the one-mutation case, star networks adapted faster and achieved higher average fitness than well-mixed networks when population sizes were small, largely due to the increased availability of rare, large effect mutations. This is a surprising result because the likelihood of drift loss is expected to be high when population sizes are small. Nevertheless, these results are in tune with the predictions of evolutionary graph theory where migration through a central hub in a star network serves to decrease the probability of drift loss, and so allows rare large effect mutations more chances of contributing to adaptation. This result suggests that genetic parallelism may be higher in small population star networks relative to well-mixed systems. The present work evaluates this prediction directly and provides insight into the variety of genetic routes to adaptation in evolving metapopulations.

We performed whole genome sequencing of a total of 24 metapopulations (out of 64) evolved for ~100 generations in ciprofloxacin in Chapter 4 spanning four mutation supply rate and network topology treatment combinations. Consequently, we identify the genes responsible for adaptation to the selection medium and quantify genetic parallelism at the (meta)population-level. There can be two alternate hypotheses as to why substituting a certain set of genes can lead to "amplification" of selection. First, star metapopulations achieve higher fitness because they explore more diverse genetic pathways of adaptation and sample more unique mutations as compared to the well-mixed metapopulations. This idea is inspired from a previous observation where structured metapopulations of *E. coli* traveled to higher fitness optimums by substituting unique variations while evolving on a "rugged" or epistatic fitness landscape whereas unstructured metapopulations fixed less number of mutations and achieved lower fitness (Nahum et al. 2015). Although it is hard, if not impossible, to predict the ruggedness of the fitness landscape in our current experiment in advance, this explanation for the genetic basis of "amplification" remains a plausibility. Another reasonable explanation is that star metapopulations are able to preserve the supplied genetic variation better than the well-mixed metapopulations until selection acts on them – through a mechanism that is akin to the avoidance of "drift-loss" of beneficial mutations. In the current study, we set the rate of supply for *de novo* genetic variation by externally controlling the mutation supply rate of each metapopulation so that the speed and extent of adaptation can only be influenced by their varying network topologies.

We find that the mutations substituted under each mutation supply rate are significantly different – insomuch as some mutations are exclusive to either mutation supply rate. We also find that network topology itself does not impact the genetic targets of adaptation. Finally, we show that genetic parallelism is indeed significantly higher in the star compared to well-mixed metapopulations when mutation supply rate is low indicating that star metapopulations can sample genetic routes to higher fitness with higher certainty even when genetic drift is high.

Results

Genomics of adaptation reveal distinct mutational spectra in metapopulations with high and low mutation supply

To determine whether the mutation supply rate and the topology of the metapopulations can define the genetic targets of adaptation to ciprofloxacin we conducted whole genome sequencing of twenty four replicate metapopulations evolved under either large or small effective population size, and propagated either by the star or the well-mixed topology. Comparing whole-genome sequence data from the 24 evolved metapopulations against the ancestral Pa14 genome (PA14 and PA14-LacZ, sequenced alongside the evolved metapopulations) revealed a total of 187 unique genetic variants above a detection threshold of 5%. The mutational spectrum of the evolved metapopulations are shown in table 5.1. Additionally, the identity and genomic location of all mutations recovered in our analysis (single-nucleotide polymorphisms [SNPs], small insertions and deletions [small

indels], large deletions and large amplifications and intergenic mutations) are provided as Table B.1 - B.13 in Appendix B. As expected from the short time span of our evolution experiment, the majority of variants were present at low frequencies (mean frequency in large metapopulations= 0.137 and median frequency in large metapopulations= 0.129, mean frequency in small metapopulations= 0.102 and median frequency in small metapopulations= 0.0988), with only 6 variants fixed in large metapopulations (i.e., variant frequency = 1) whereas no fixation events occurred in the small metapopulations. This is on par with theoretical expectations as small populations are supposed to lose genetic variation due to random genetic drift applied by harsh population bottlenecks, taking longer time for the mutations to fix. As an indicator of strong positive selection, we observe high non-synonymous to synonymous mutation ratios in both mutation supply rates (8.38 in large and 10.33 in small), significantly higher than would be expected under neutrality (χ^2=18.481, $p<10^{-4}$). Additionally, we identify on average 34.5 genetic changes in metapopulations with large effective population size compared to an average of 29.4 genetic changes in small metapopulations, values that are not significantly different (two way ANOVA with interactions, main effect of population size, p=0.09). Although well-mixed metapopulations harbored more genetic changes on average (mean for large metapopulations, WM = 37, Star = 32 and for small metapopulations, WM = 31.7, Star = 27.2), it was not significantly higher than that of star metapopulations for either of the population size (p=0.23 for large and p=0.28 for small metapopulations, respectively). 29.72% of all mutations discovered were intergenic. In experimental evolution studies with *P. aeruginosa* and other bacteria, often intergenic SNPs have been shown to be present in medium to high frequencies - sometimes with adaptive consequences (Thorpe

et al. 2017; Khademi et al. 2019; Santos-Lopez et al. 2019; Harris et al. 2021). However, the validation of this hypothesis is out of scope for our current study.

	Mutation supply rate			
	High		Low	
Network topologies	**Star**	**WM**	**Star**	**WM**
Small indel	42	43	22	36
SNP intergenic	51	64	54	59
SNP nonsense	4	3	7	2
SNP nonsynonymous	85	91	74	81
Large deletion	3	7	1	0
SNP synonymous	7	14	5	10
Large amplification	0	0	0	2
Total	192	222	163	190

Table 5.1 Mutational spectrum of the evolved metapopulations. Total number of different mutational types detected for different combinations of mutational supply rate and network topology. Each cell represents the number of a certain type of mutation class pooled over all replicate metapopulations.

As expected from the strong selection pressure exerted by ciprofloxacin, we detect many known resistance mutations circulating in moderate to high frequencies in these metapopulations (Figure 5.1). The mechanisms by which *P. aeruginosa* evolves resistance to fluoroquinolones such as ciprofloxacin are very well-studied (Ruiz 2003; Jacoby 2005; Rehman et al. 2019). Specifically, we identify frequent mutations (indels and nonsynonymous SNPs) in the negative regulators and components of efflux pumps such as *mexA* and *mexR* (mexAB-oprM), *mexS* (MexEF-OprN) and *nfxB* (MexCD-OprJ)

that are constitutively expressed when it is necessary to decrease intracellular concentration of ciprofloxacin (Poole 2005; Richardot et al. 2016). We also uncover mutations that prevent ciprofloxacin from binding to the DNA-modifying subunits of DNA gyrases (*gyrA*, *gyrB*) (Yoshida et al. 1990a,b; Barnard and Maxwell 2001). Not unexpectedly, our metapopulations also harbor mutations in genes that do not confer resistance to ciprofloxacin but are global regulators of quorum sensing, c-di-GMP signaling, virulence, twitching motility and biofilm formation. These mutations typically increase fitness of *P. aeruginosa* in the laboratory growth medium by saving synthesis cost of these factors (Schick et al. 2022). Among them, we notice *lasR* (a global regulator of quorum sensing) (Rumbaugh et al. 2000; Schuster and Peter Greenberg 2006; Williams and Cámara 2009; Moradali et al. 2017; Chadha et al. 2022), *morA* (an enzyme with both diguanylate cyclase and phosphodiesterase domains that can increase or decrease c-di-GMP levels, leading to biofilm formation and/or dispersal) (Choy et al. 2004; Ha et al. 2014; Harrison et al. 2020; Katharios-Lanwermeyer et al. 2021), *wspA*, *wspR* and *wspF* (substrate sensing, biofilm formation and maintenance by increasing c-di-GMP levels) (Ryder et al. 2007; Römling et al. 2013; Ha and O'Toole 2015; Jenal et al. 2017; Ma et al. 2022) to be repeatedly mutated in multiple replicate metapopulations.

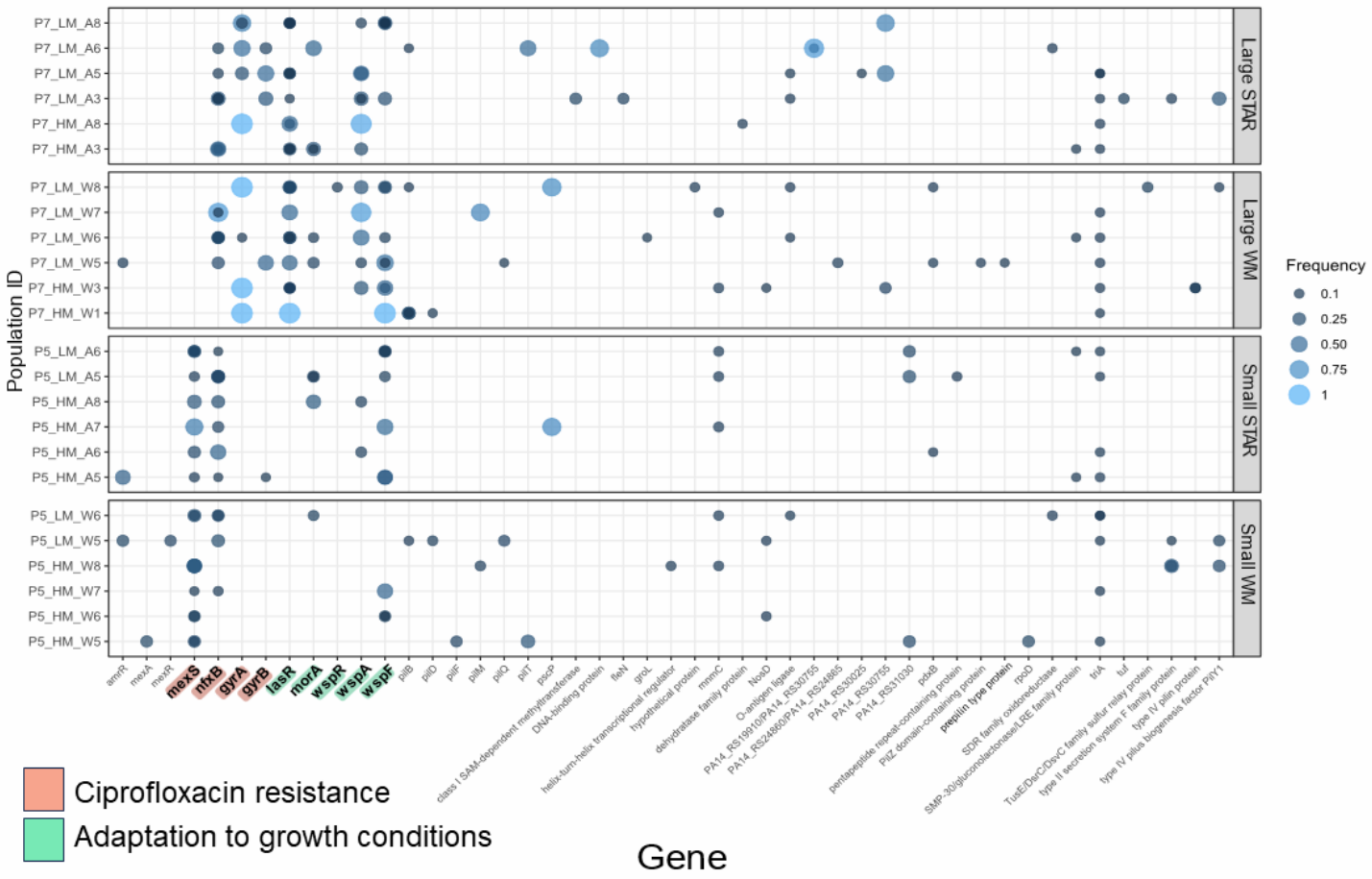

Figure 5.1 Genetic changes detected in the metapopulations (not showing intergenic mutations, file with the intergenic mutations is available in Appendix B Figure B.2) after ~ 100 generations of evolution in the selection media (LB supplemented with subinhibitory concentration of ciprofloxacin). From the top, the first and the second panel show large star and large well-mixed metapopulations, respectively. Similarly, the third and the fourth panel show small star and small well-mixed metapopulations, respectively. Mutation in genes highlighted with either red or green background denote recurring canonical ciprofloxacin resistance genes and genes that are relevant for adaptation of *P. aeruginosa* to laboratory conditions, respectively. Size of the circles depict observed frequencies of mutants in the metapopulations. More than one circle for a gene represents the presence of its different genetic variants (alleles) in the same metapopulation.

One of the most striking result from our genomic analyses is that metapopulations evolved under high and low mutation supply diverge in the repertoire of resistance mutations they accumulate over the evolutionary period. Notable examples include enrichment of *mexS* mutations in small metapopulations (binomial test, $p<0.005$) and *gyrA* mutations exclusively in large metapopulations (binomial test, $p<0.05$). We see the same pattern for non-resistance mutations as well: *lasR* and *wspA* being specifically mutated in the large (binomial test, $p<0.005$ and $p<0.05$, for *lasR* and *wspA,* respectively) but not in the small metapopulations. Although we do not uncover any mutations that are network specific in the large metapopulations there is a marginally significant enrichment of mutations in the *wspA* and *wspF* specific to the small star metapopulations (*wspA* and *wspF* mutations in 6 star compared to *wspF* mutations in 2 well-mixed metapopulations). Additionally, it is notable that mutations in *nfxB* are present in all (6 out of 6) small star but only 50% (3 out of 6) in the small well-mixed metapopulations sequenced, although the difference is not statistically significant (binomial test, $p=0.08$). Taken together, our genomic data demonstrates that the identity of substituted beneficial alleles under varying mutation supply rates could be distinctly divergent and network topology does not determine the genetic targets of adaptation, at least not in the current experiment.

High population-level parallelism in small star metapopulations indicate stronger levels of selection

Parallel evolution, or repeatability of the same phenotypic or genotypic changes in independent populations as a response to similar ecological pressures, is widely taken to

be a strong indicator that evolution has happened through natural selection and not by random chance. Among many possible genetic routes that reach an adaptive peak, more often than not populations follow the paths where selection is strong because of ample genetic variation available for increment in fitness. This is specifically the case for microbial populations that attain very large population sizes during growth and as a result, generate ample genetic variations for adaptation. Effective population size and spatial arrangement of populations can both influence the probability of parallel evolution as these factors modulate the strength of selection or the amount of genetic variation for fitness in that particular environment. In large metapopulations, the strength of selection is the predominant force determining the probability of parallel evolution but in small metapopulations random genetic drift will create uncertainty around the choice of genetic routes for adaptation (Bailey et al. 2017). We hypothesized that, as the high efficacy of selection will already select for highest effect beneficial mutations in the large metapopulations the effect of star topology in enhancing the strength of selection will be minimal. In contrast, in the small metapopulations star topology will minimize the drift-loss of rare beneficial mutations that would otherwise be lost in the well-mixed topology, increasing the extent of parallel genetic changes in replicate lineages.

We examine these possibilities by quantifying population-level parallelism in the replicate metapopulations sequenced for each population size and network topology treatment combination. As 99% synonymous mutations reach the frequency ~8% or lower in our experiment (Appendix B Figure B.1), we assume that mutations present beyond this frequency might be drivers of adaptation. Therefore, we only include genes which are

found in more than 8% frequency in the metapopulation in the calculation of population-level genetic parallelism and do not include synonymous mutations that are generally thought to not contribute to adaptation, although evidence to the contrary exists(Bailey et al. 2014, 2021a). Also, as we did not see any effect of migration rate on the fitness trajectories in either large or small metapopulations, we pooled the observations from both the migration rates together under each effective population size treatment (large and small) for calculating the population-level parallelism statistics.

Since there is no broadly accepted metric for quantifying gene-level parallelism, we use three distinct measures: variance in dispersion of Euclidean distances between populations, Jaccard distance (Jdist = 1 - Jaccard Index, which describes the likelihood that the same gene is mutated in two independent populations) and observed repeatability relative to expectation under randomness using the hypergeometric distribution (C-score) (Schick et al. 2022). Briefly, a low value for dispersion, a low Jaccard distance and a high C-score indicates a high degree of parallelism and vice versa (see materials and methods). For all of the metrics calculated, we detect no significant effect of population size but a significant effect of network topology and a significant interaction between these two factors. We followed up our analyses by calculating the difference in the degree of parallelism between the two topologies for each effective population size. Our results are shown in table 5.2 and they are striking.

	Estimate = (star - well-mixed)					
Population size	Dispersion		Jaccard Distance		C-score	
	estimate	significance	estimate	significance	estimate	significance
Large	0.0167	0.7153	0.0165	0.6569	0.0219	0.5356
Small	-0.1265	**0.0108**	-0.1514	**0.0009**	2.0156	**0.0029**

Table 5.2 Population-level parallelism. Difference in population-level parallelism between the two topologies for each effective population size. Differences between the mean values for each metric (estimate) in the star and the well-mixed topologies are presented. A positive value denotes the calculated metric for the star topology is higher than the well-mixed topology and *vice versa*. Significance ($P<0.05$) is determined by a 2-way ANOVA for dispersion and a 2-way ANOVA followed by a permutation test (10,000 permutations) for Jaccard distance and C-score (materials and methods).

Consistent with our predictions, we do not find any significant difference in degree of genetic parallelism between the two topologies in large metapopulations but small star metapopulations are found to have significantly higher population-level parallelism than their well-mixed counterparts. However, we do not see any significant effect of effective population size (in modulating mutation supply rate) on the extent of parallelism in contrast to what is expected from theoretical predictions (Bailey et al. 2017). In sum, our results show that certain network topologies, such as the star, can attain higher fitness by minimizing drift-loss of adaptive genetic variations when the chance for stochastic loss is high, an effect previously not described by the EGT literature. These results are also the first in demonstrating that adaptation in spatially structured populations can lead to a high

degree of population-level genetic parallelism in comparison to well-mixed populations, an effect that is contingent on the underlying mutation supply rate.

Discussion

Parallel evolution is so unlikely to occur by chance alone that, when it does happen, it is taken to be a strong signature of selection (Conte et al. 2012; Kassen 2014; Lenormand et al. 2016). The probability of parallel evolution depends on the strength of selection and availability of genetic variation for fitness (Orr 2005b; Bailey et al. 2017, 2018). The current study provides novel insights into the role of mutation supply rate and spatial structure on the extent of genetic parallelism. Both of these factors are expected to increase the probability of genetic parallelism. This is because both of them increase the amount of clonal interference in a population and enhance the probability with which rare, large effect beneficial mutants fix repeatedly in independent populations. In addition, spatial structures such as the star can “amplify” selection over their well-mixed counterparts when the probability of losing beneficial mutants to drift is high, allowing more opportunity for rare, large effect beneficial mutations to contribute to adaptation. Our results in Chapter 4 provided direct evidence for this effect, small star metapopulations achieving higher fitness than well-mixed ones due to an enrichment of large effect beneficial mutations. The genomic analyses presented here further bolster this conclusion: parallelism was higher in small star metapopulations than well-mixed ones in the face of high genetic drift, as expected if amplification leads to the preferential substitution of rare large effect beneficial mutations. Below we highlight some other significant observations.

We saw that the spectra of beneficial mutations substituted were significantly different between the two mutation supply rates studied, with certain mutations specific to either mutation supply rate. This effect has been empirically demonstrated in microbial evolution studies where easily available beneficial mutations providing smaller fitness increase ("high rate low effect") were substituted in small populations whereas rare beneficial mutations with large fitness effects ("low rate high effect") were predominantly acquired by large populations (Schenk et al. 2022). Same was also observed for *E. coli* evolving to ciprofloxacin - mutations that change the target site of drug binding were preferentially substituted in large populations but genetic changes in efflux pumps upregulation, transcription and translation factors occurred routinely in small populations (Garoff et al. 2020). In our experiment, we observe that large metapopulations substitute presumably large effect *gyrA* and *gyrB* mutations modulating the ciprofloxacin binding site in DNA gyrase subunits A (*gyrA*) and B (*gyrB*) that reduce their susceptibility to ciprofloxacin (Melnyk et al. 2017). Along with these canonical resistance mutations, additional mutations that increase fitness in the laboratory growth conditions such as *lasR* and *wspA* reach substantially higher frequencies exclusively in large metapopulations. This is probably because these mutations are lost to genetic drift in the small but not in the large metapopulations.

In contrast to large metapopulations, we find presumably loss-of-functions mutations in the repressors of efflux pump expression such as *mexS* and *nfxB* to be repeatedly substituted in small metapopulations. Decreasing intracellular drug concentration by

increasing the production of efflux pumps is one of the most frequent mechanisms of resistance acquired in the presence of ciprofloxacin and many other antibiotics (Poole 2004, 2005, 2007). Therefore, it is not surprising that we observe efflux pumps to be upregulated in the paucity of other target site mutations in small metapopulations. Other studies evolving *P. aeruginosa* in the presence of ciprofloxacin in the laboratory have reported that, large effect mutations such as *gyrA* and *gyrB* were cost-free, i.e., they do not decrease fitness in the absence of ciprofloxacin whereas mutations upregulating efflux pump expression such as *mexS* and *nfxB* were found to exert fitness costs (Melnyk et al. 2017). This helps explain our observation in Chapter 4 (Figure 4.5) that most mutations in large metapopulations were cost-free compared with mutants isolated from the small metapopulations that were costly.

However, the spectra of substituted beneficial mutations were not significantly different between the metapopulation topologies studied. This is in contrast with another experiment that investigated the choice of biofilm or planktonic growth lifestyle - as a form of spatially structured environment - on the antibiotic resistance evolution in *Acinetobacter baumannii* populations (Santos-Lopez et al. 2019). Here, biofilm populations primarily substituted efflux pump mutations but unstructured planktonic populations substituted target-site mutations, while evolving to ciprofloxacin. It could be due to the strong divergent selection pressures applied by strictly biofilm or planktonic lifestyle of these populations. However, that is not the case in our experimental system where biofilm only forms on the surface of planktonic liquid cultures, and any biofilm is thoroughly mixed with rest of the planktonic culture in each subpopulation during daily serial transfer. Therefore,

our results implicate different roles for mutation supply and network topology in dictating the genetic routes for adaptation. Mutation supply controls the availability of beneficial mutations to selection and spatial structure - in terms of network topology - influences the likelihood that each beneficial mutation will be substituted.

Parallel evolution is often taken to be an indicator of strong selection for a particular genetic locus in a given environment. While many factors can modulate the likelihood of genetic parallelism, population size has emerged as the most reliable predictor in evolve-and-resequence experiments such as ours (Bailey et al. 2017). Increased population sizes means a higher supply of mutations and more clonal interference, the latter acting to bias the spectrum of beneficial mutations contributing to adaptation towards those rare mutations with the largest fitness effect and leading to increased probability of genetic parallelism. However, we did not see higher levels of genetic parallelism in large compared to small metapopulations in our study. This might be due to exaggerated clonal interference in large metapopulations keeping the segregating genetic variation around for longer. These slower selective sweeps might have increased inter-metapopulation variation in the identity of all substituted mutations and decreased population-level genetic parallelism than expected.

Interestingly, we observe a significantly higher average population-level parallelism in small star compared to small well-mixed metapopulations. This effect is probably due to the star topology minimizing the loss of rare large effect beneficial mutations to genetic drift in small metapopulations, hence accumulating more genetic variation available for

selection to act upon. Our results are novel because we show for the first time that a form of spatial structure, specifically a bi-directional star network topology, can produce higher genetic parallelism when populations are critically constrained by the availability of genetic variation for fitness. This result has not been demonstrated before either by theory or experiments. We speculate this high level of parallelism in the small but not in the large star metapopulations is a cumulative effect of mutational heterogeneity i.e., efflux upregulating mutants being produced at a high rate, and star topology increasing the efficacy of selection by minimizing the loss of these mutants - an exciting hypothesis that awaits further evaluation in the future.

Our results provide a clear perspective for understanding whether the spatial structure of microbial populations can modulate their genetic targets of adaptation. This is particularly important because microbial populations in nature often live spatially arranged on structured surfaces, like in a biofilm (Hall-Stoodley et al. 2004; Werner et al. 2014; Dang and Lovell 2015; Nadell et al. 2016; Hajishengallis et al. 2023). Our results are specifically relevant to the evolution of antibiotic resistance or virulence in microbes in scenarios where they repeatedly face harsh population bottlenecks, such as in host-associated infections (Levin 1981; Levin et al. 2000; Handel and Bennett 2008; Andersson and Hughes 2010; Hannan et al. 2012; Abel et al. 2015; Papkou et al. 2016; Hughes and Andersson 2017). Our work also adds to the growing literature on whether microbial lifestyle (structured vs. unstructured environment) and effective population size can impact their genetics of adaptation (Poltak and Cooper 2011; Vogwill et al. 2016; Santos-Lopez et al. 2019; Wein and Dagan 2019; Garoff et al. 2020; Bailey et al. 2021b; Harris

et al. 2021; Mahrt et al. 2021; Schenk et al. 2022; Scribner et al. 2022). Only by fully understanding how ecological complexities drive evolutionary dynamics in microbial populations can we predict the spread of pathogenic microbes, design evolution-proof treatments for their control or enhance production of biomolecules of interest for industrial purposes.

Methods

Microbial strains, culture conditions and experimental evolution:

Same as chapter 4.

Genomic analyses:

Whole-Genome Sequencing:

We randomly selected 6 replicate end-point metapopulations from each the effective population size and the network topology treatment combinations (2 effective population size (large or small) X 2 topologies (star or well-mixed) X 6 replicates = a total of 24 metapopulations). Among the selected metapopulations, for each topology 2 were from LPHM, 4 from LPLM, 4 from SPHM and finally 2 were from SPLM (Figure 4.1). The rationale behind this selection was two-fold: (a) LPLM and SPHM were seen to have the biggest differences between the topologies in the phenotypic analyses; and (b) the different migration rates did not influence the fitness trajectories of the metapopulations in Chapter 4.

Two ancestral strains of *P. aeruginosa*, PA14 and PA14-LacZ, were also sequenced to facilitate genome assembly and to further identify genetic variants. The four constituent subpopulations of each selected metapopulation were revived overnight from frozen stock. Following overnight growth, each metapopulation mix was reconstructed by mixing the revived subpopulations by equal volume. This was done to capture the diverse genetic

changes that might have happened in the metapopulations as a result of evolution. Genomic DNA was then extracted from each metapopulation mix for whole-genome sequencing using the QIAGEN DNeasy UltraClean 96 Microbial kit, following the manufacturer's recommended protocol. Library preparation and sequencing were performed by Genome Quebec at McGill University on the Illumina NovaSeq 6000 platform, using paired-end sequencing of 2 × 150 base-pair reads.

Processing of genomic data and variant calling:

Whole-genome sequencing of 24 metapopulations yielded a total of ~750 Gb of raw data, with a median coverage of 3622.3-fold and an average of 98.5% genome coverage. Sequencing reads were first quality checked by generating FastQC reports using FastQC version 0.11.9 and quality trimmed using Trimmomatic version 0.39 (Bolger et al. 2014), with the command SLIDINGWINDOW:5:20 MINLEN:20 LEADING:5 TRAILING:5 CROP:140 HEADCROP:10. Variants were called using Breseq version 0.36.1 (Deatherage and Barrick 2014) - a tool specifically designed for detecting mutations in microbial genomes, with default parameters (detection limit of 5%) and -p flag for detecting polymorphisms in the sequenced metapopulations. Reads were aligned to the *P. aeruginosa* reference genome UCBPP-PA14 - assembly GCF_000014625.1 (Winsor et al. 2016). We subsequently discarded variants common across both ancestral strains (PA14 and PA14-LacZ) and all evolved populations using the *gdtools* module of breseq to identify only the mutations that arose over the course of the selection experiment. We found no evidence of cross-contamination in our sequenced metapopulations (each even

numbered replicate had the LacZ insertion which was absent in the odd numbered replicates). Also, none of the metapopulations harbored any mutations in the genes that have been linked to increased mutation rates(Sanders et al. 2006; Wiegand et al. 2008; Oliver and Mena 2010) in *P. aeruginosa*, so we did not have to discard any sequenced genomes for from further downstream analyses. All genomic analyses were performed on Compute Canada high performance computing platform using a custom bash script for bioinformatic workflow. Breseq output files with information on genetic changes were processed further for performing statistical tests and generating plots in R statistical computing software.

Statistical analyses

All statistical analyses were performed in R (version 4.2.2) (R Core Team 2022). We quantified population level of parallelism using three different metrics: dispersion, Jaccard distance, and C-scores (Schick et al. 2022). All three metrics were calculated with the same set of data only using mutations that reached at least 8 percent in frequency in the metapopulation and, after excluding synonymous variants.

For dispersion, we calculated the mean distance between a population and the corresponding population or network topology treatment centroid, following a PCoA on a Euclidean distance matrix using the vegdist function from the vegan package in R (Oksanen et al. 2022). The distance is measured as the population and network topology level genetic variance with larger mean dispersion signifying more divergent genetic

changes and therefore less parallelism. To determine the significance, we performed an 2-way ANOVA with Euclidean distance as the response variable and effective population size and network topology and their interactions as explanatory variables. Following the assessment of the assumptions of ANOVA we subsequently analyzed the mean difference between the large and small populations or, star and well-mixed topologies using the emmeans package from R (Lenth 2020).

For the Jaccard distance measure, we calculated the Jaccard measure from the vegdist function from the vegan package in R as the dissimilarity between all pairs of populations within a treatment (effective population size or network topology). Jaccard distance is the complement to Jaccard index which describes the likelihood that the same gene is mutated in two independent populations (here metapopulations). Jaccard distance can range 0 to 1: zero being two samples are exactly alike and one being two samples are completely different. We reported the difference between the network topology means (estimated difference = star - well-mixed, averaged over samples) for each effective population size treatment. For the J-distance, a positive difference denotes higher parallelism for well-mixed and negative difference means higher parallelism for the star topology.

We extended our analyses by measuring C-score, which is a metric for repeatability. It uses the hypergeometric distribution to calculate the deviation between the observed amount of parallelism and the expectation under random gene use (Yeaman et al. 2018). The magnitude of the C-score represents the magnitude of the deviation with larger C-

scores signifying higher repeatability and therefore more parallelism. Same as Jaccard distance we reported the differences between the C-score means for each network topology, for each population size. For C-score, a positive difference denotes higher parallelism for a star and negative difference means higher parallelism for the well-mixed topology. To determine the significance of both Jaccard and C-score metrics, we performed a permutation test by randomizing population size and network topology treatment labels (number of permutations = 10,000) and calculating a null distribution of F-values. We complemented this analysis by calculating the probability (out of total number of permutations) of the observed difference between the star and the well-mixed topologies being higher (C-score) or lower (J-distance) than the randomized estimated difference between the topologies, for each effective population size.

Parallelism at the gene level was defined as the proportion of populations with mutations in that gene, both globally for effective population size and network topology and within all of the four treatment combinations. To test for significance, we calculated the probability of our observed results against the null hypothesis that gene use was random, using the binomial distribution with the number of metapopulations as the number of trials, number of times a gene was mutated as the number of successes, and proportion of total metapopulations across all treatments with a mutation in that gene as the probability of success. From this, if the probability of an observation was <0.05, we considered that gene to be either effective population size or network topology treatment specific.

Chapter 6:

General conclusions:

Whether spatial structure of metapopulations, in terms of their network topologies, can alter the pace of adaptive evolution - remains a much debated topic in evolutionary biology. Evolutionary Graph Theory (EGT) predicts that certain network topologies can accelerate the rate of adaptive substitution. In this thesis, I experimentally test this prediction using laboratory metapopulations of *Pseudomonas aeruginosa* propagated by different network topologies as they adapt to the fluoroquinolone antibiotic ciprofloxacin.

By summarizing the empirical patterns observed in past microbial evolution experiments, I showed that spatial structure of populations, in terms of restricted migration between the subpopulations, mostly slowed down the dynamics of adaptation. In stark contrast to previous trends, I found that certain metapopulation structures - such as the star networks - can accelerate the spread of an initially rare beneficial mutation compared to a well-mixed network. Star networks achieved this acceleration by concentrating the beneficial mutant in the central “hub” and thus minimizing its loss due to genetic drift. Furthermore, when the metapopulations were supplied with different amounts of beneficial mutations, the star network accelerated the dynamics of adaptation in metapopulations with low mutation supply. This was because in small metapopulations large fitness effect beneficial mutations were substituted more frequently in the star compared to well-mixed

metapopulations. In contrast, when mutation supply was high, the dynamics of adaptation was not different between star and well-mixed metapopulations. Finally, I found that star metapopulations with low mutation supply accelerated adaptive evolution by substituting the beneficial mutations in identical genes with high repeatability.

The work performed in this thesis certainly has some limitations that can be addressed in future experiments. Due to logistic reasons, it was not possible to test another class of network topologies, called the 'suppressor', that decelerate adaptation or larger topologies that have more nodes and substantially complicated migration networks. Using robotic liquid handling setups or microfabrication technologies these logistic limitations can be alleviated and longer term evolution experiments can be performed on these networks. Whole genome sequencing of evolved isolates collected from different evolutionary time-points can help reconstruct the evolutionary history better. Also, I only investigated the spread of chromosomal antibiotic resistant mutations. However, similar experiments with resistant genes that can be transferred horizontally among bacteria could yield exciting results. Finally, I have not assessed the efficacy of selection in star networks under conditions of spatial heterogeneity. Spatially heterogeneous environmental conditions in a connected metapopulation where growth conditions vary in each subpopulation - can have profound impact on the dynamics of adaptation and the evolution and maintenance of diversity. Therefore, including spatial heterogeneity in the current experimental framework would definitely be an important next step.

My work serves two broader purposes. First, it contributes to a better understanding of the rate of adaptive evolution in spatially structured metapopulations. It identifies an empirically under-studied aspect of spatial structure, the network topologies of metapopulations, to be able to accelerate adaptation under realistic conditions in the laboratory. Furthermore, it also provides a general evolutionary mechanism behind the observed “amplification” phenomenon. Second, my work has direct implications for understanding the spread of antibiotic resistance in microbial populations. In nature, microbes live as sessile assemblages - such as biofilms - which are spatially structured. Biofilms aid in the evolution and persistence of antibiotic resistant pathogens(Høiby et al. 2010; Coenye et al. 2022). Biofilms are also dynamic dwelling for microbes as they constantly go through cycles of establishment and dispersal (McDougald et al. 2012; Wood 2014; Rumbaugh and Sauer 2020). My work indicates that particular spatial conformations of microbial populations in biofilms may increase their pathogenicity by speeding up antibiotic resistance evolution. In other applications, star network topologies may be customized to be used as ‘incubators’ for directed evolution of desired traits or biomolecules of interest in industrial applications. In sum, this work extends our understanding of the impact of spatial structure on the dynamics of adaptive evolution, and illustrates the significance of this knowledge for predicting and controlling the spread of pathogenic microbial populations in nature. I conclude that my thesis represents a valuable contribution to this growing body of work.

Appendix A:

Appendix to Chapter 3

Supplemental Figures, Tables and Text

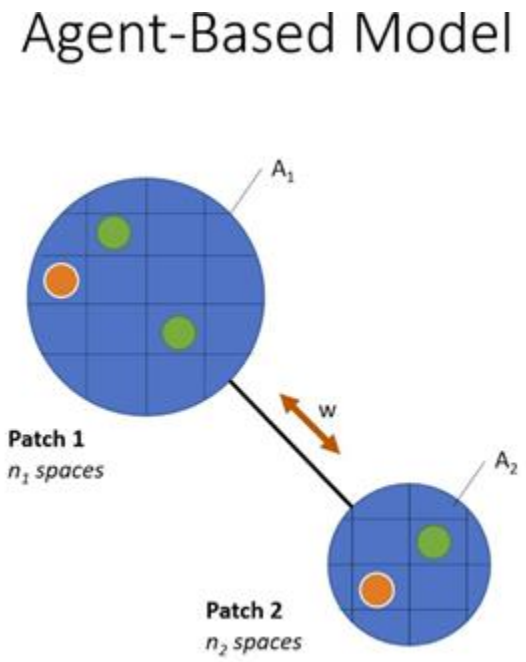

Figure A.1 : Schematic depiction of the algorithm used in the SANCTUM model. See methods section for details.

Modified Agent Based Model with daily bottleneck and sensitive-specific killing (developed by Partha Pratim Chakraborty):

The original SANCTUM model incorporates selection as antibiotic dependent killing of either the wild type or the mutant. This approach means the uncertainty in selection was introduced in the antibiotic mediated killing step. However, in our experimental model, antibiotics can only kill the sensitive wild-type, not the resistant mutant. To account for this fact and to adhere to the experimental methods better, we modified the original SANCTUM model as described below for a replicate run:

For each Day -

1. The resistant mutant is inoculated in one of the patches in a 1:1000 ratio. All the other patches are inoculated with 1000 wild type agents.
2. Only the wild-type bacteria is killed in the antibiotic mediated killing step according to the antibiotic concentration.
3. Agents grow until they reach the carrying capacity of each patch (in a density dependent fashion that is proportional to the empty spaces remaining at each step).
4. A drift / bottleneck event happens where only 15% of a fully grown patch is carried forward to the next day again for growth.
5. Migration in between the patches happens according to the simulated migration rate and network.
6. Steps 1-5 repeats until the simulation reaches the time limit.

In the modified model, all the parameters remain the same as in the original model except for the introduction of the drift (bottleneck) step. 100 replicates were run for each of the network (STAR or WM) and the frequency of resistant mutants in the metapopulation were recorded at each time step. The simulations were coded in Python.

The results are shown in Supplementary Fig 2 and 3 for the unweighted and weighted migration, respectively. Briefly, and in tune with the original model, we find a close correspondence between the dynamics of spread of the resistant mutant between our experiments and the modified model. Specifically, the modified model closely mirrors the distinct dynamics of spread of resistant mutants in the two topologies, showing a clear advantage to the star topology over the well-mixed topology at the lowest migration rates. Moreover, the dynamics of spread in the modified model also closely matches those observed for the probability of fixation in the original model (compare figures 2b and 3b in the main text with Supplementary figures 2b and 3b, respectively). This last result reassures us that the dynamics of spread is a good proxy for the probability of fixation.

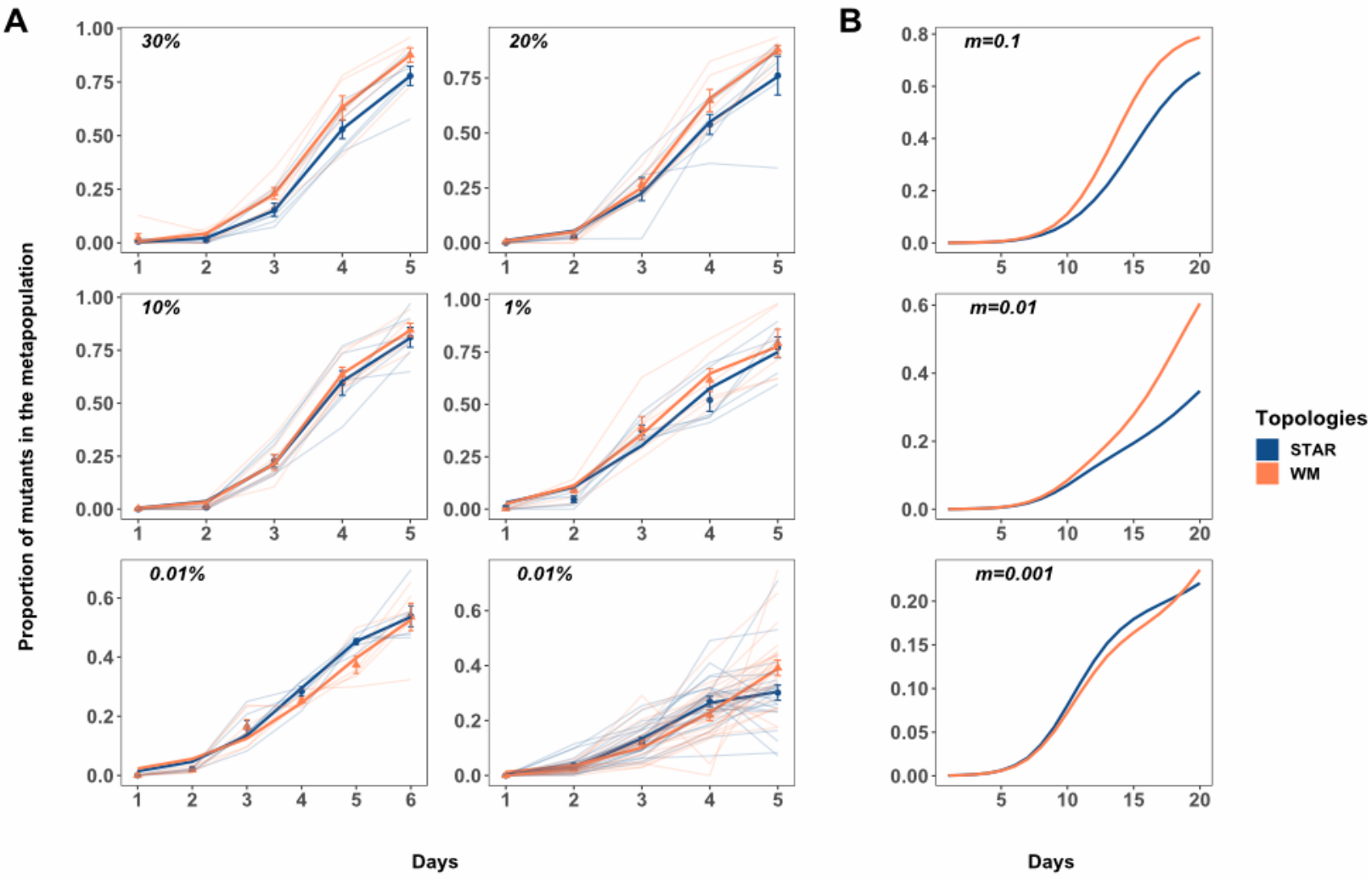

Figure A.2 : The proportion of cip^R mutant in replicate metapopulations propagated by either star (blue) or well-mixed (red) networks with unweighted migration. Panel A shows experimental results (Fig 3.2: main text); simulation results (modified) are shown in Panel B. Migration rates are noted in the inset of each plot.

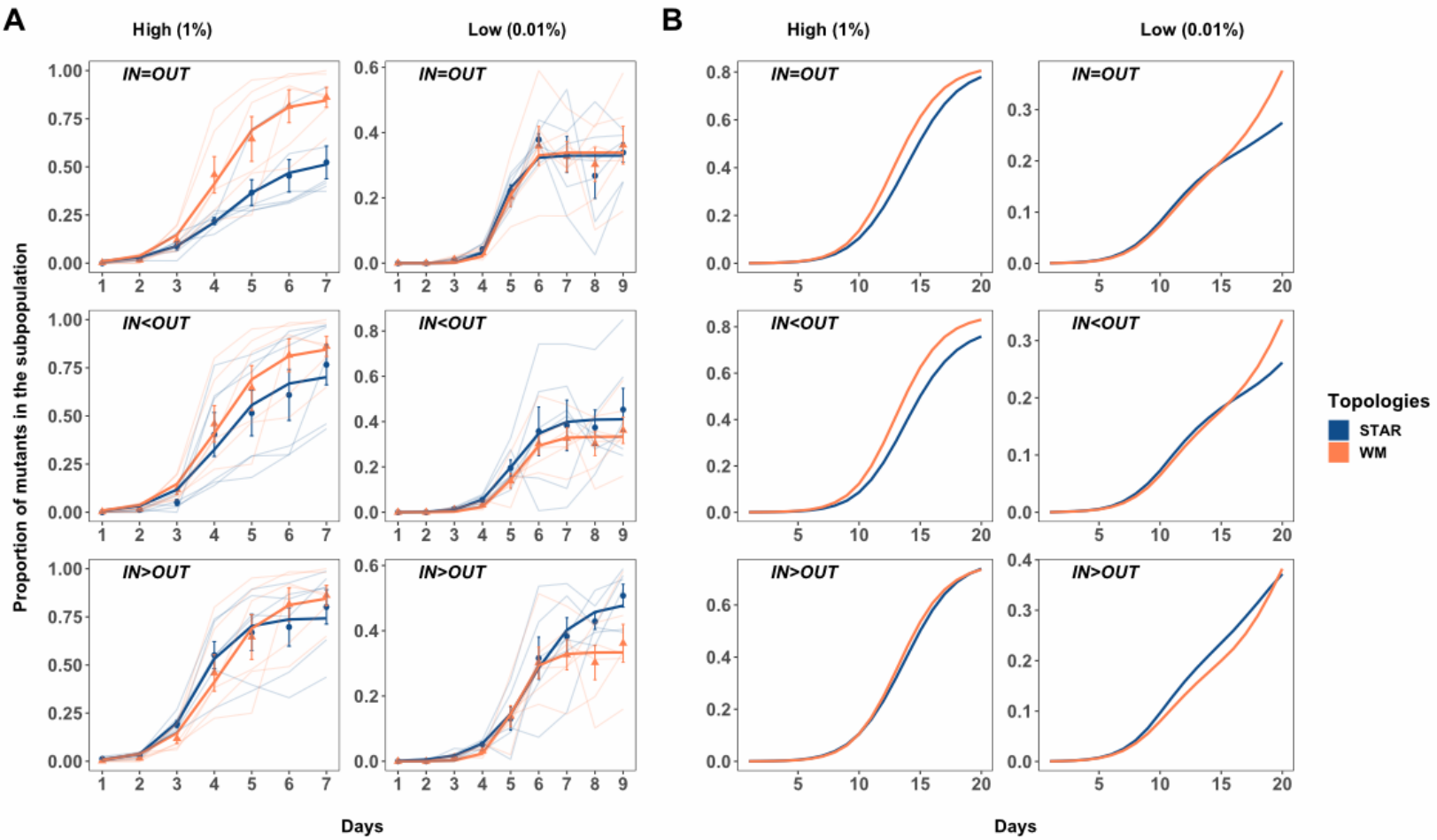

Figure A.3 : The proportion of cip^{R} mutant in replicate metapopulations propagated by either star (blue) or well-mixed (red) networks with weighted migration. Panel A shows experimental results (Fig 3.3: main text); simulation results (modified) are shown in Panel B. Migration rates are noted in the inset of each plot.

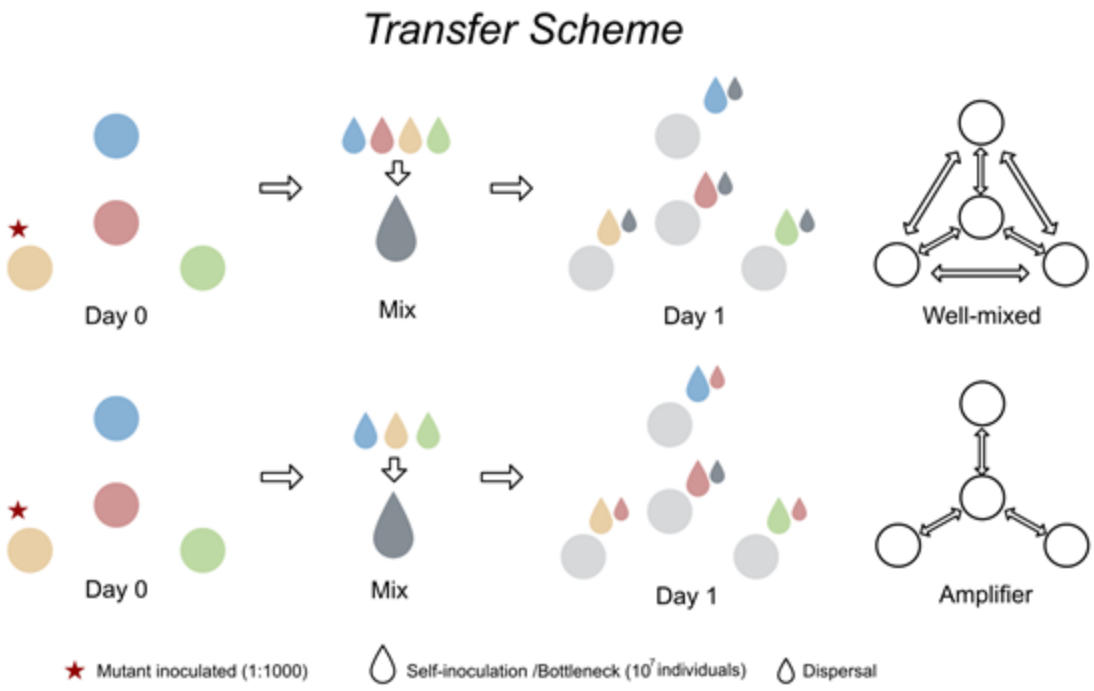

Figure A.4: Transfer scheme to experimentally create star and well-mixed network structures. The red star indicates the patch (P3) where the mutant (PA14-*gyrA*) was inoculated 1:1000 ratio to the wild type (PA14-*LacZ*). Big droplets of the four colors indicate self-inoculation from respective patches whereas big and small gray droplets indicate dispersal mix and dispersal volume, respectively.

Detailed methods used to construct network topologies:

Unweighted migration:

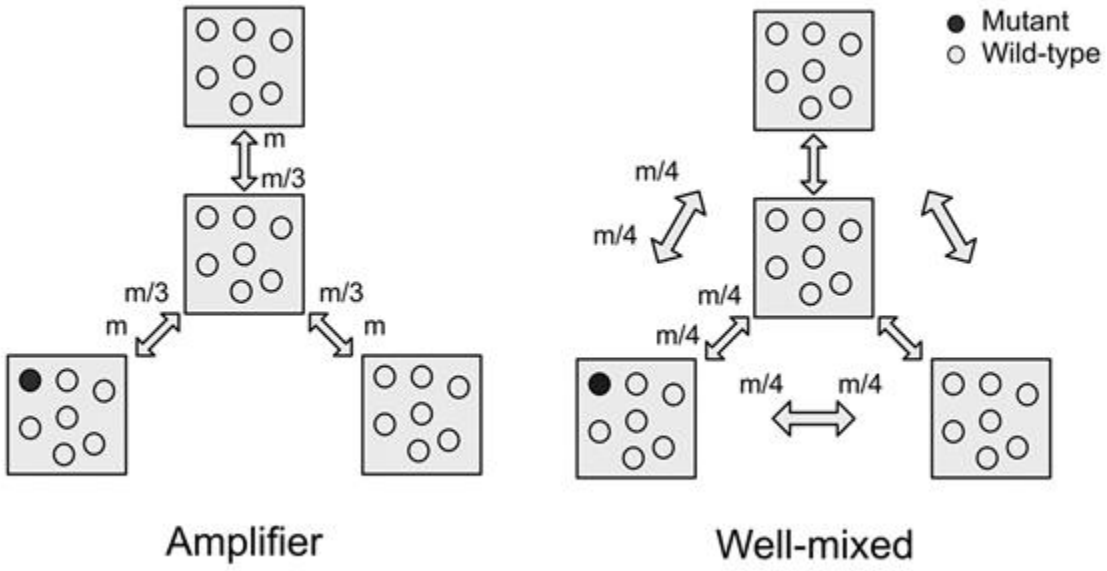

Figure A.5: Schematics depicting the number of transferred migrants per edge connection in the cases of unweighted migration regime for star and well-mixed networks. The value of *m* shows the total number of migrants for each migration treatment, and the fractions are calculated as the contributions from each patch. Filled circles (black) indicate the mutants (PA14-*gyrA*) while initializing the experiment and open circles (clear) are the predominant wild type (PA14-*LacZ*).

Well-mixed: 35 µL of subpopulations 1, 2, 3, and 4 were mixed together, and 20 µL from this resulting pool of migrants (MIX) was serially diluted in fresh media supplemented with 20 ng/mL Ciprofloxacin to achieve ~10^8, ~10^7, ~10^5 and ~10^4 CFU/mL. Then, 15 µL of the diluted MIX was added to 1.5 mL of fresh media along with 15 µL of the previous day's culture to achieve desired migration levels of ~10^6, ~10^5, ~10^3 and ~10^2 CFU/mL. For

20% and 30% migration, 30 µL and 45 µL of the diluted MIX were added with the culture from the previous day.

Amplifier: 35 µL of subpopulations 1, 3, and 4 were mixed together, and 20 µL from this resulting pool of migrants (MIX) was serially diluted in fresh media and 20 ng/mL antibiotic to reach ~10^8, ~10^7, ~10^5 and ~10^4 CFU/mL. Also, 20 µL of subpopulation 2 (HUB) was serially diluted in fresh media and 20 ng/mL Ciprofloxacin to reach ~10^8, ~10^7, ~10^5 and ~10^4 CFU/mL. Then, 15 µL of the diluted MIX was added to 1.5 mL fresh media along with 15 µL of the previous day's subpopulation 2 culture to achieve the desired migration levels of ~10^6, ~10^5, ~10^3 and ~10^2 CFU/mL. Also, 15 µL of the diluted HUB was added to 1.5 mL fresh media along with the previous day's culture to achieve desired migration levels of ~10^6, ~10^5, ~10^3 and ~10^2 CFU/mL in subpopulations 1, 3, and 4. For 20% and 30% migration, 30 µL and 45 µL of the diluted MIX were added after the bottleneck ("self-inoculation").

Asymmetric migration:

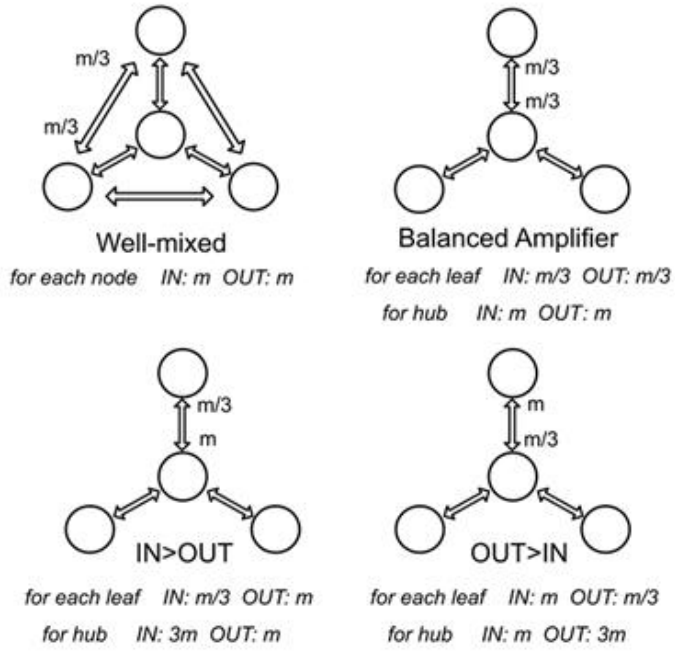

Figure A.6: Schematics depicting the transferred migrants per edge connection in the case of the weighted migration regimes for three asymmetric star networks and the well-mixed network. Each double-sided arrow indicates the number of migrants received and contributed by each patch.

Well-Mixed: 20 µL of subpopulations 1, 2, 3, and 4 (MIX) were mixed in 120 µL of fresh culture media with 20 ng/mL Ciprofloxacin and serially diluted to reach ~4 x 10^7 or ~4 x 10^4 CFU/mL. Then, 15 µL of the diluted MIX was added to 1.5 mL fresh media along with 15 µL of the previous day's culture. This resulted in the transfer of 4 x 10^5 for the high migration rate experiments, or 4 x 10^2 CFU/mL for the low migration rate.

Balanced star (IN = OUT): 20 µL of subpopulations 1, 3, and 4 (MIX) were mixed in 140 µL of fresh culture media with 20 ng/mL Ciprofloxacin and serially diluted to reach ~3 x 10^7 or ~3 x 10^4 CFU/mL. Also, 20 µL of subpopulation 2 (HUB) was mixed in 180 µL of fresh culture media with 20 ng/mL Ciprofloxacin and serially diluted to reach ~10^7 or ~10^4 CFU/mL. This resulted in the transfer of ~3 x 10^5 and ~3 x 10^2 CFU/mL to the hub, and

~10^5 and ~10^2 CFU/mL to the peripheral leaves, for the high and low migration rates, respectively.

OUT>IN regime: 20 µL of subpopulations 1, 3, and 4 (MIX) were mixed in 140 µL of fresh culture media with 20 ng/mL Ciprofloxacin and serially diluted to reach ~3 x 10^7 or ~3 x 10^4 CFU/mL. Also, 60 µL of subpopulation 2 (HUB) were mixed in 140 µL in fresh culture media with 20 ng/mL Ciprofloxacin and serially diluted to reach ~3 x 10^7 or ~3 x 10^4 CFU/mL. This resulted in the transfer of ~3 x 10^5 or ~3 x 10^2 CFU/mL to the hub and ~3 x 10^5 or ~3 x 10^2 CFU/mL to the peripheral leaves, for the high and low migration rates, respectively.

IN>OUT regime: 60 µL of subpopulation 1, 3, and 4 (MIX) were mixed in 20 µL of fresh culture media with 20 ng/mL Ciprofloxacin and serially diluted to reach ~9 x 10^7 or ~9 x 10^4 CFU/mL. Also, 20µL of subpopulation 2 (HUB) was mixed in 180 µL of fresh culture media with 20 ng/mL Ciprofloxacin and serially diluted to reach ~10^7 or ~10^4 CFU/mL. This resulted in the transfer of ~9 x 10^5 or ~9 x 10^2 CFU/mL to the hub and ~10^5 or ~10^2 CFU/mL to the peripheral leaves, for the high and low migration rates, respectively.

Low population size:

Well-mixed: 20 µL of subpopulations 1, 2, 3, and 4 (MIX) were mixed in 120 µL of fresh culture media with 20 ng/mL Ciprofloxacin and serially diluted to reach ~4 x 10^5 CFU/mL. Then, 15 µL of the diluted MIX was added to 1.5 mL fresh media along with 15 µL of 1:100 diluted the previous day's culture. This resulted in the transfer of ~4 x 10^3 CFU/mL for the migrant and ~10^5 CFU/mL residents ("self-inoculation").

IN>OUT Star: 60 µL of subpopulations 1, 3, and 4 (MIX) were mixed in 20 µL of fresh culture media with 20 ng/mL Ciprofloxacin and serially diluted to reach ~9 x 10^5 CFU/mL. Also, 20 µL of subpopulation 2 (HUB) was mixed in 180 µL of fresh culture media with 20 ng/mL Ciprofloxacin and serially diluted to reach ~10^5 CFU/mL. This resulted in the transfer of ~9 x 10^3 CFU/mL to the hub and ~10^3 CFU/mL to the peripheral leaves, respectively. Every subpopulation also received 15 µL of 1:100 diluted the previous day's

culture from itself which resulted in the transfer of ~10^5 CFU/mL residents ("self-inoculation").

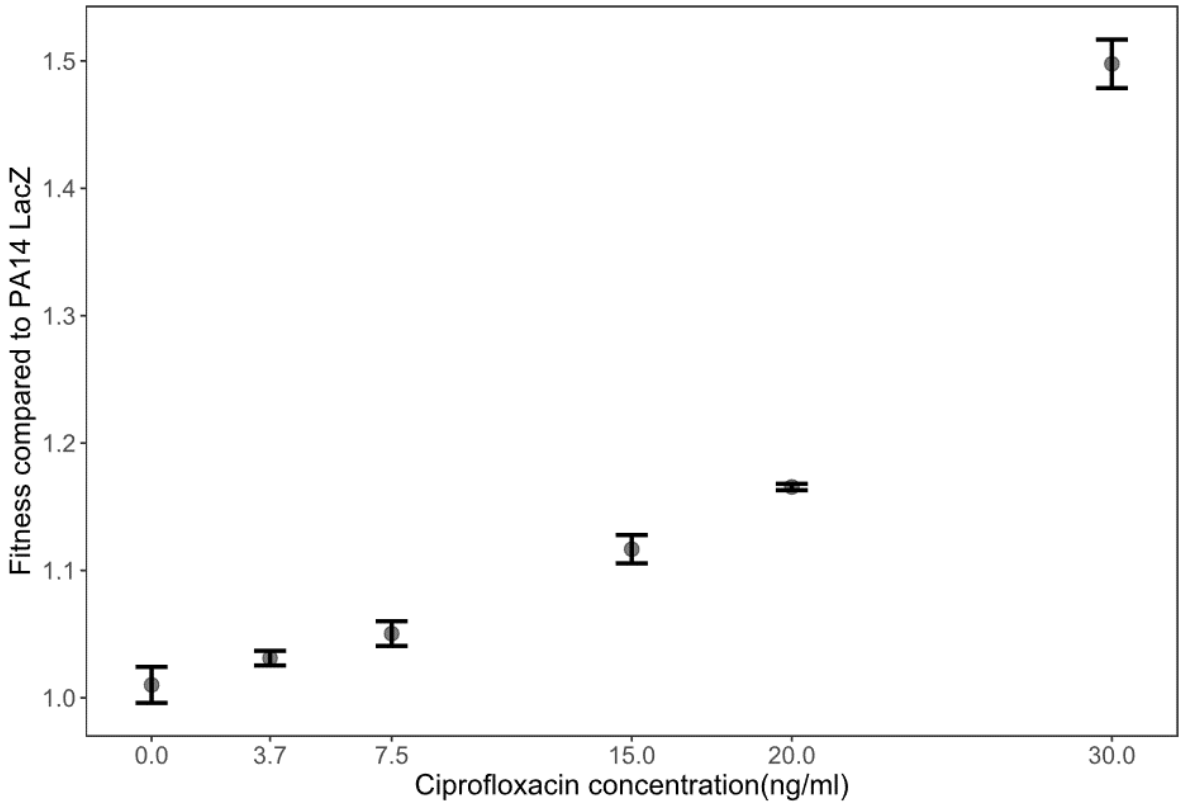

Figure A.7: Competitive advantage of *PA14-gyrA* in head-to-head competitions (~ 50:50) with *PA14-LacZ* at different sub-inhibitory Ciprofloxacin concentrations. Relative fitness of three biological replicate competitions are shown.

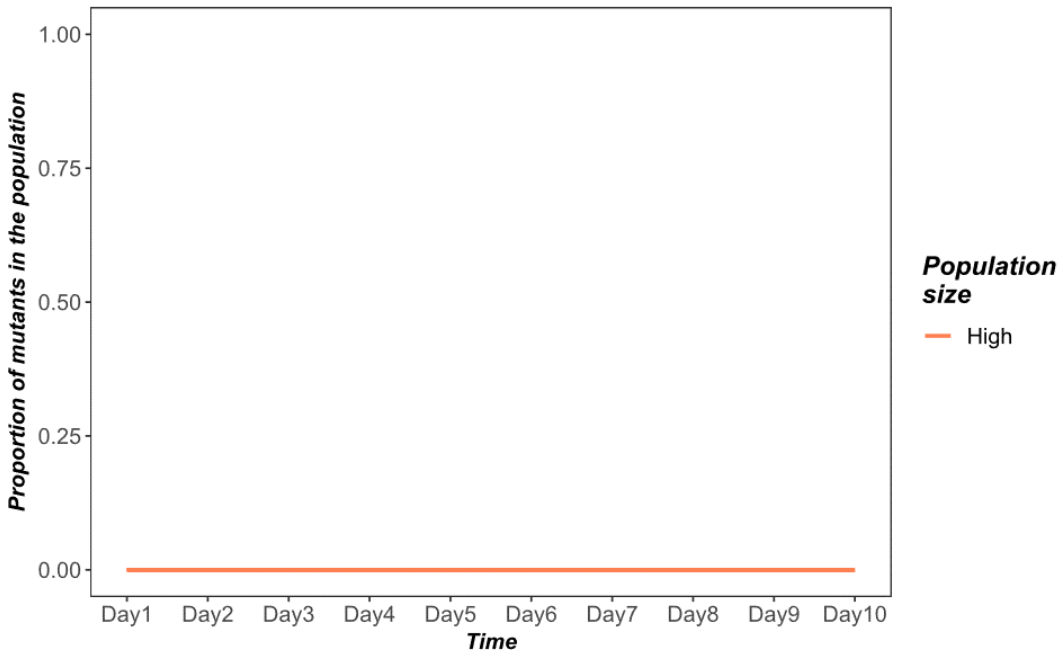

Figure A.8: Frequency of spontaneous ciprofloxacin resistant (≥ 1µg/ml) mutants derived from the sensitive wild type strain, PA14-*LacZ*, over 10 days of experimental evolution in 20ng/ml Ciprofloxacin. A proportion of zero means there were no detectable colonies capable of growing above the MIC of the cip^{R} strain *PA14-gyrA* (T83I) used in our experiments.

Statistical results for the full models and the nls:

Migration rate	Simple slope contrasts (Trt1 - Trt2)*time	Estimate	SE	DF	t ratio	p-value
30%	AMP - WM	-0.0212	0.156	51	-0.136	0.8923
20%	AMP - WM	-0.32	0.158	51	-2.023	0.0483
10%	AMP - WM	-0.0915	0.156	51	-0.585	0.5613
1%	AMP - WM	-0.0158	0.139	51	-0.114	0.9097
0.01%	AMP - WM	0.011	0.0834	63	0.132	0.8956
0.001%	AMP - WM	-0.198	0.0732	213	-2.708	0.0073

Table A.1: Statistical analyses of full models for experiments with unweighted migration. For each statistical analysis, the estimated analyzed slope contrast for the GLMM, standard error (SE), degrees of freedom, t-ratio, and p value are shown.

Migration rate	Simple slope contrasts (AMPx - WM)* Time	Estimate	SE	DF	t ratio	p-value
High	In = Out	-0.489	0.121	140	-4.032	0.0005
	In < Out	-0.111	0.134	140	-0.832	0.8392
	In > Out	-0.295	0.121	140	-2.432	0.0758
Low	In = Out	-0.0364	0.0743	188	-0.490	0.9612
	In < Out	0.0695	0.0766	188	0.907	0.8012
	In > Out	0.1376	0.0797	188	1.728	0.3123

Table A.2: Statistical analyses of full models for experiments with weighted (asymmetric) migration. For each statistical analysis, the estimated analyzed slope contrast for the GLMM, standard error (SE), degrees of freedom, t-ratio, and p value are shown.

Unweighted migration:

Migration rate	Rate of increase (analogous to R in a logistic growth model)	Final frequency (analogous to K in a logistic growth model)	Conclusion:
30%	F1,10 =1.623, p = 0.2315	$\chi2$ = 15.348, p = 8.94e-05 (EXPT 5th day) $\chi2$ = 8.4269, p = 0.003697 (NLS)	WM has a significantly higher K but R is not significantly different between AMP and WM
20%	F1,10 = 0.9149, p = 0.3614	$\chi2$ = 9.0148, p = 0.002678 (EXPT 5th day) $\chi2$ = 6.5309 , p = 0.0106 (NLS)	WM has a significantly higher K but R is not significantly different between AMP and WM
10%	F1,10 = 0.0515, p = 0.825	$\chi2$ = 0.7082, p = 0.4001 (EXPT 5th day) $\chi2$ = 0.1777, p = 0.6734 (NLS)	R and K is not significantly different between AMP and WM
1%	F1,10 = 0.0258, p = 0.8757	$\chi2$ = 0.2168, p = 0.6415 (EXPT 5th day) $\chi2$ = 1e-04, p = 0.9908 (NLS)	R and K is not significantly different between AMP and WM
0.01%	F1,10 = 0.1229, p = 0.7331	$\chi2$ = 0.0021, p = 0.963 (EXPT 6th day) $\chi2$ = 1.5471, p = 0.2136 (NLS)	R and K is not significantly different between AMP and WM
0.001%	F1,46 = 1.542, p = 0.2206	$\chi2$ = 5.4046, p = 0.02008 (EXPT 5th day) $\chi2$ = 9.2005, p= 0.00242 (NLS)	WM has a significantly higher K but R is not significantly different between AMP and WM

Table A.3: Statistical analyses of 3 parameter logistic growth model with nonlinear least squares (nls) for experiments with large population size and unweighted (and comparable well-mixed) migration. For each statistical analysis, rate of increase (r) and final frequency of the beneficial mutant (K) are shown. In the case of K, results from both the final day of experimental data and nls models are compared.

Weighted migration:

Comparisons	Migration	Rate of increase (analogous to R in a logistic growth model)	Final frequency (analogous to K in a logistic growth model)	Conclusion
In = Out vs. WM	High (1%)	F1,10 =4.8754, p = 0.05173	$\chi2$ = 12.234, p = 0.0004694 (EXPT 7th day) $\chi2$ = 13.19 , p = 0.0002815 (NLS)	WM has a significantly higher K but R is not significantly different between AMP and WM
	Low (0.001%)	F1,10 =0.6108, p = 0.4526	$\chi2$ = 0.1848, p = 0.6673 (EXPT 9th day) $\chi2$ = 0.8844, p = 0.347 (NLS)	R and K is not significantly different between AMP and WM
Out>In vs. WM	High(1%)	F1,10 =0.1022, p =0.7557	$\chi2$ = 1.1888, p = 0.2756 (EXPT 7th day) $\chi2$ = 0.6612, p = 0.4161 (NLS)	R and K is not significantly different between AMP and WM
	Low(0.001%)	F1,10 =0.2279, p = 0.6434	$\chi2$ = 0.5233, p = 0.4694 (EXPT 9th day) $\chi2$ = 2.1761, p = 0.1402 (NLS)	R and K is not significantly different between AMP and WM
In>Out vs. WM	High (1%)	F1,10 =0.7773, p = 0.3986	$\chi2$ = 0.4124, p = 0.5208 (EXPT 7th day) $\chi2$ = 1.1907, p = 0.2752 (NLS)	R and K is not significantly different between AMP and WM
	Low(0.001%)	F1,10 =0.9051, p = 0.3638	$\chi2$ = 5.2917, p = 0.02143 (EXPT 9th day) $\chi2$ = 5.7524, p = 0.01647 (NLS)	AMP has a significantly higher K but R is not significantly different between AMP and WM

Table A.4: Statistical analyses of 3 parameter logistic growth model with nonlinear least squares (nls) for experiments with large population size and weighted (asymmetric and comparable well-mixed) migration. For each statistical analysis, rate of increase (r) and final frequency of the beneficial mutant (K) are shown. In the case of K, results from both the final day of experimental data and nls models are compared.

Comparisons	Migration	Rate of increase (analogous to R in a logistic growth model)	Final frequency (analogous to K in a logistic growth model)	Conclusion
In>Out vs. WM Small population size	1000 cfu/ml	F1,10 =0.10674, p = 0.4059	$\chi 2$ = 3.562, p = 0.05912 (EXPT 9th day) $\chi 2$ = 5.2773 , p = 0.02161 (NLS)	R is not significantly different between AMP and WM. K is significantly higher in the NLS fit model but not significantly different from WM for the experimental data from the final day

Table A.5: Statistical analyses of 3 parameter logistic growth model with nonlinear least squares (nls) for experiments with small population sizes and weighted (asymmetric) (and comparable well-mixed) migration. For each statistical analysis, rate of increase (r) and final frequency of the beneficial mutant (K) are shown. In the case of K, results from both the final day of experimental data and nls models are compared.

Low population size:

Migration rate	Simple slope contrasts (AMPx - WM)* Time	Estimate	SE	DF	t-ratio	p-value
1000 cfu/ml	In>Out	-0.104	0.0367	99	-2.841	0.0055

Table A.6: Statistical analyses of full models for experiments with weighted (asymmetric) migration and small population size. For each statistical analysis, the estimated analyzed slope contrast for the GLMM, standard error (SE), degrees of freedom, t-ratio, and p value are shown.

Appendix B:

Appendix to Chapter 5

Supplemental Figures and Tables

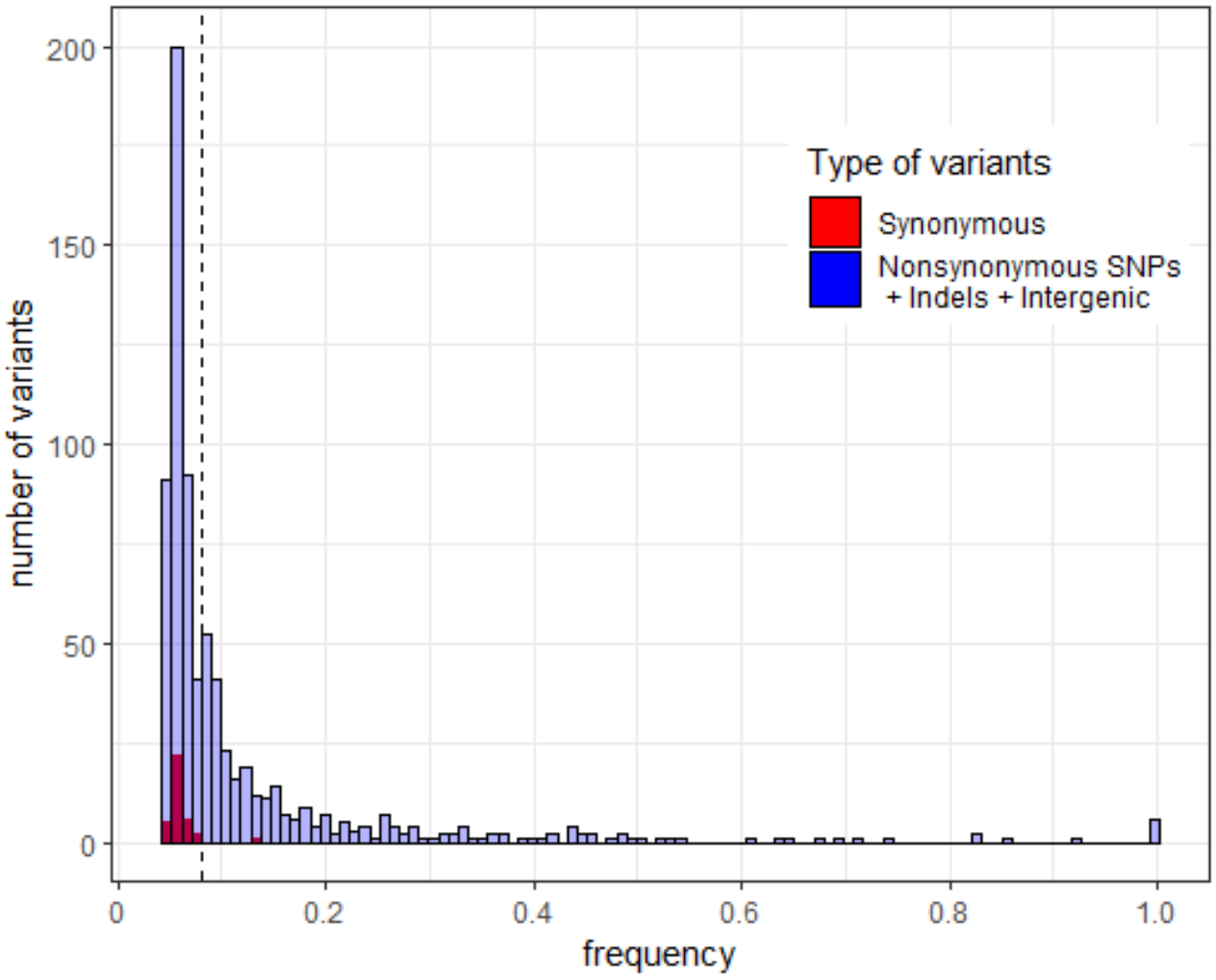

Figure B.1. Frequency spectra for all discovered genomic changes. Distribution of read frequencies for all SNPs found across all evolved populations: nonsynonymous SNPs, Indel and intergenic mutations (light blue) and synonymous SNPs (dark blue). The vertical dashed line (read frequency 8%) represents the threshold above all statistical analyses for parallelism were performed.

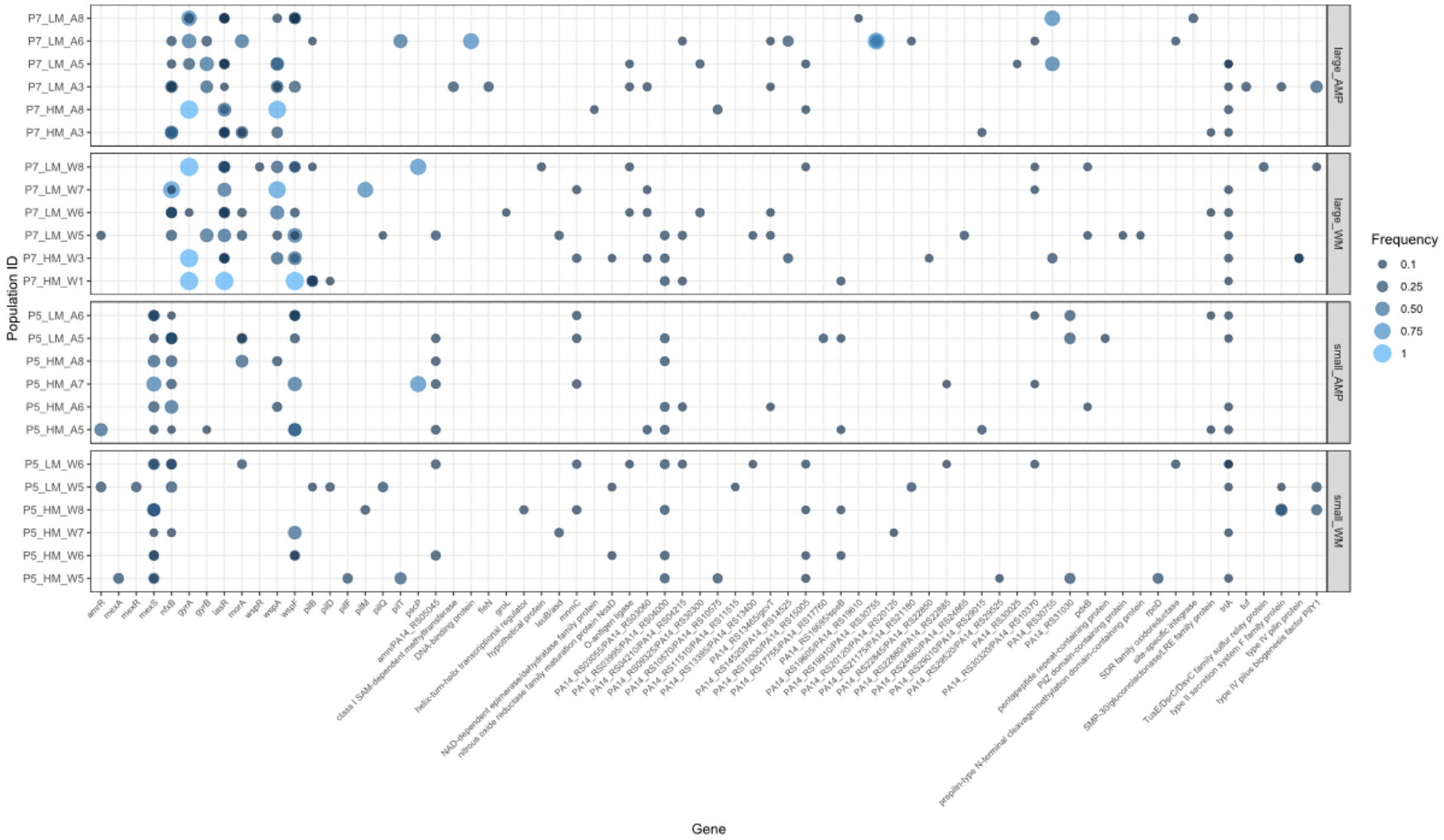

Figure B.2. All genetic changes detected in the metapopulations (including intergenic mutations). Abbreviations: AMP is Star and WM is well-mixed network. Size of the circles depict observed frequencies of mutants in the metapopulations. From the top, the first and the second panel show large star and large well-mixed metapopulations, respectively.

Treatment	sample	frequency	ref_seq	new_seq	codon_new_seq	codon_ref_seq	gene_position	Mutation_ID
Small_STAR	P5_HM_A5	0.111220611	GCCAGAGGTCCTCA				coding (36-49/1020 nt)	DEL(14bp)
	P5_HM_A6	0.228522223	AAGGCTCTCGGC				coding (499-510/1020 nt)	DEL(12bp)
	P5_HM_A7	0.60422341	G	GTC			coding (951/1020 nt)	INS
	P5_HM_A8	0.333916084	CTGCCGACCCCGGC				coding (61-74/1020 nt)	DEL(14bp)
	P5_LM_A5	0.119959532	AAT				coding (50-52/1020 nt)	DEL(3bp)
	P5_LM_A6	0.080230236	G	T			coding (337/1020 nt)	INS
	P5_LM_A6	0.197505898	CCCGGTGGAGGCCA				coding (357-370/1020 nt)	DEL(14bp)
	P5_LM_A6	0.095425606	C	T	TAG	CAG	565	SNP(Q189*)
	P5_LM_A6	0.259467125	T	C	CTC	TTC	775	SNP(F259L)
Small_WM	P5_HM_W5	0.091964545	GCAGGGGAAGTC				coding (82-93/1020 nt)	DEL(12bp)
	P5_HM_W5	0.223884106	C	G	TAG	TAC	798	SNP(Y266*)
	P5_HM_W6	0.122768376	69-bp				coding (232-300/1020 nt)	AMP(69bp)
	P5_HM_W6	0.195212364	T	A	GAG	GTG	863	SNP(V288E)
	P5_HM_W7	0.090318494	G	CTGCC			coding (171/1020 nt)	INS
	P5_HM_W8	0.372941494	C				coding (320/1020 nt)	DEL(1bp)
	P5_HM_W8	0.369764328	G				coding (321/1020 nt)	DEL(1bp)
	P5_HM_W8	0.364094262	ACCCCGGTGGAGGCCA				coding (355-370/1020 nt)	DEL(16bp)
	P5_LM_W6	0.120898701	CAGGGGAAGTCCTG				coding (83-96/1020 nt)	DEL(14bp)
	P5_LM_W6	0.26842497	C	GCA			coding (847/1020 nt)	INS

Table B.1. List of mutations in the **mexS** gene in the small metapopulations (frequency threshold of 8%).

Treatment	sample	frequency	ref_seq	new_seq	codon_new_seq	codon_ref_seq	gene_position	Mutation_ID
Small_STAR	P5_HM_A5	0.080966617	AGTCCTACCTGGAAG				coding (347-361/564 nt)	DEL(15bp)
	P5_HM_A6	0.43322897	A	C	TGC	TGA	564	SNP(*188C)
	P5_HM_A7	0.180153847	A	C	TGC	TGA	564	SNP(*188C)
	P5_HM_A8	0.26293993	A	C	TGC	TGA	564	SNP(*188C)
	P5_LM_A5	0.264607119	GGG				coding (140-142/564 nt)	DEL(3bp)
	P5_LM_A5	0.289522171	C	A	TAA	TAC	459	SNP(Y153*)
	P5_LM_A5	0.189495087	A	C	TGC	TGA	564	SNP(*188C)
	P5_LM_A6	0.080730774	TCGAGGGCCACGGA				coding (161-174/564 nt)	DEL(14bp)
small_WM	P5_HM_W7	0.110305704	ACGCGGGACAA				coding (136-146/564 nt)	DEL(11bp)
	P5_LM_W5	0.252698898	A	C	TGC	TGA	564	SNP(*188C)
	P5_LM_W6	0.133255959	C				coding (129/564 nt)	DEL(1bp)
	P5_LM_W6	0.222690582	A	C	TGC	TGA	564	SNP(*188C)

Table B.2. List of mutations in the **nfxB** gene in the small metapopulations (frequency threshold of 8%).

sample	frequency	ref_seq	new_seq	codon_new_seq	codon_ref_seq	gene_position	Mutation_ID
P5_HM_A5	0.083703518	C	A	TAC	TCC	1397	SNP(S466Y)

Table B.3. List of mutations in the **gyrB** gene in the small metapopulations (frequency threshold of 8%). No mutations were detected in well-mixed metapopulations.

Treatment	sample	frequency	ref_seq	new_seq	codon_new_seq	codon_ref_seq	gene_position	Mutation_ID
Small_STAR	P5_HM_A5	0.399431705	A				coding (853/1008 nt)	DEL(1bp)
	P5_HM_A5	0.393784523	A				coding (854/1008 nt)	DEL(1bp)
	P5_HM_A7	0.49113512	T	G	AGC	ATC	8	SNP(I3S)
	P5_LM_A5	0.148963451	C				coding (831/1008 nt)	DEL(1bp)
	P5_LM_A6	0.241940759	ACGTGG				coding (143-148/1008 nt)	DEL(6bp)
	P5_LM_A6	0.151443481	T	G			coding (620/1008 nt)	INS
	P5_LM_A6	0.151422024	T	C			coding (620/1008 nt)	INS
small_WM	P5_HM_W6	0.187381744	C	G			coding (498/1008 nt)	INS
	P5_HM_W6	0.083902962	ATTATTGGCGT				coding (785-795/1008 nt)	DEL(11bp)
	P5_HM_W7	0.43863597	CAA				coding (852-854/1008 nt)	DEL(3bp)

Table B.4. List of mutations in the **wspF** gene in the small metapopulations (frequency threshold of 8%).

sample	frequency	ref_seq	new_seq	codon_new_seq	codon_ref_seq	gene_position	Mutation_ID
P5_HM_A6	0.156435617	84-bp				coding (855-938/1629 nt)	DEL(84bp)
P5_HM_A8	0.161041662	42-bp				coding (853-894/1629 nt)	DEL(42bp)

Table B.5. List of mutations in the **wspA** gene in the small STAR metapopulations (frequency threshold of 8%). No mutations were detected in the well-mixed metapopulations.

Treatment	sample	frequency	ref_seq	new_seq	codon_new_seq	codon_ref_seq	gene_position	Mutation_ID
Small_STAR	P5_HM_A8	0.361739635	T	A	CAG	CTG	3464	SNP(L1155Q)
	P5_LM_A5	0.208880901	A	T	CTG	CAG	2978	SNP(Q993L)
	P5_LM_A5	0.104067802	A	G	GAG	AAG	3367	SNP(K1123E)
Small_WM	P5_LM_W6	0.146544933	T	A	TAC	TTC	3041	SNP(F1014Y)

Table B.5. List of mutations in the **morA** gene in the small metapopulations (frequency threshold of 8%).

Treatment	sample	frequency	ref_seq	new_seq	codon_new_seq	codon_ref_seq	gene_position	Mutation_ID
Large_STAR	P7_HM_A8	1	A	G	GGC	GAC	260	SNP(D87G)
	P7_LM_A5	0.277235508	G	A	AAC	GAC	259	SNP(D87N)
	P7_LM_A6	0.522967339	A	G	GGC	GAC	260	SNP(D87G)
	P7_LM_A8	0.636086464	A	G	GGC	GAC	260	SNP(D87G)
	P7_LM_A8	0.158688545	T	G	GAT	TAT	964	SNP(Y322D)
Large_WM	P7_HM_W1	1	G	T	TAC	GAC	259	SNP(D87Y)
	P7_HM_W3	1	G	T	TAC	GAC	259	SNP(D87Y)
	P7_LM_W6	0.088499069	T	G	GAT	TAT	964	SNP(Y322D)
	P7_LM_W8	1	A	G	GGC	GAC	260	SNP(D87G)

Table B.6. List of mutations in the **gyrA** gene in the large metapopulations(frequency threshold of 8%).

Treatment	sample	frequency	ref_seq	new_seq	codon_new_seq	codon_ref_seq	gene_position	Mutation_ID
Large_STAR	P7_LM_A3	0.346958637	C	A	TAC	TCC	1397	SNP(S466Y)
	P7_LM_A5	0.499420166	C	A	TAC	TCC	1397	SNP(S466Y)
	P7_LM_A6	0.193561077	G	C	GAC	GAG	1404	SNP(E468D)
Large_WM	P7_LM_W5	0.442117691	C	A	TAC	TCC	1397	SNP(S466Y)

Table B.7. List of mutations in the **gyrB** gene in the large metapopulations(frequency threshold of 8%).

Treatment	sample	frequency	ref_seq	new_seq	codon_new_seq	codon_ref_seq	gene_position	Mutation_ID
Large_STAR	P7_HM_A3	0.08673673	ACGCTGGCAG				coding (339-348/564 nt)	DEL(10bp)
	P7_HM_A3	0.286056995	A	C	CCG	CAG	524	SNP(Q175P)
	P7_HM_A3	0.432704449	A	C	TGC	TGA	564	SNP(*188C)
	P7_LM_A3	0.336452007	T	G	CGG	CTG	440	SNP(L147R)
	P7_LM_A3	0.154998302	G	A	AGC	GGC	538	SNP(G180S)
	P7_LM_A3	0.119374275	A	C	TGC	TGA	564	SNP(*188C)
	P7_LM_A5	0.127055645	A	C	TGC	TGA	564	SNP(*188C)
	P7_LM_A6	0.163700581	A	C	TGC	TGA	564	SNP(*188C)
Large_WM	P7_LM_W5	0.22548008	A	C	TGC	TGA	564	SNP(*188C)
	P7_LM_W6	0.192060471	T	C	CCC	CTC	29	SNP(L10P)
	P7_LM_W6	0.179454803	G	A	AAA	GAA	436	SNP(E146K)
	P7_LM_W6	0.165957451	T	C	CCG	CTG	518	SNP(L173P)
	P7_LM_W6	0.258535385	G	T	TGC	GGC	538	SNP(G180C)
	P7_LM_W7	0.826631069	G	A	AGC	GGC	538	SNP(G180S)
	P7_LM_W7	0.093101978	A	C	TGC	TGA	564	SNP(*188C)

Table B.8. List of mutations in the **nfxB** gene in the large metapopulations (frequency threshold of 8%).

Treatment	sample	frequency	ref_seq	new_seq	codon_new_seq	codon_ref_seq	gene_position	Mutation_ID
Large_STAR	P7_HM_A3	0.335879803	T	C	GCG	GTG	2840	SNP(V947A)
	P7_HM_A3	0.083964348	T	A	CAG	CTG	3353	SNP(L1118Q)
	P7_LM_A6	0.458245402	GCA				coding (2918-2920/4248 nt)	DEL(3bp)
Large_WM	P7_LM_W5	0.178940773	G	A	AAA	GAA	3472	SNP(E1158K)
	P7_LM_W6	0.125416756	T	G	GAC	TAC	3946	SNP(Y1316D)

Table B.9. List of mutations in the **morA** gene in the large metapopulations(frequency threshold of 8%).

Treatment	sample	frequency	ref_seq	new_seq	codon_new_seq	codon_ref_seq	gene_position	Mutation_ID
Large_STAR	P7_HM_A3	0.255173566	GCGCGCACCATGC				coding (354-366/720 nt)	DEL(13bp)
	P7_HM_A3	0.135128415	CCATGCAGCGGCA				coding (347-359/720 nt)	DEL(13bp)
	P7_HM_A3	0.105674953	ACCAGGCCGGC				coding (322-332/720 nt)	DEL(11bp)
	P7_HM_A8	0.108437766	CCTCG				coding (414-418/720 nt)	DEL(5bp)
	P7_HM_A8	0.457137108	G				coding (60/720 nt)	DEL(1bp)
	P7_LM_A3	0.085239335	CGCACCATGCAGCG				coding (350-363/720 nt)	DEL(14bp)
	P7_LM_A5	0.173174381	A				coding (461/720 nt)	DEL(1bp)
	P7_LM_A5	0.196719351	A	GGACC			coding (443/720 nt)	INS
	P7_LM_A5	0.0837906	ATACACCAGGCC				coding (325-336/720 nt)	DEL(12bp)
	P7_LM_A8	0.165182987	TACGCGGCGG				coding (669-678/720 nt)	DEL(10bp)
	P7_LM_A8	0.17862739	TCCACGCTGAGGCT				coding (385-398/720 nt)	DEL(14bp)
	P7_LM_A8	0.126162556	ATACACCAGGCCGG				coding (323-336/720 nt)	DEL(14bp)
	P7_LM_A8	0.100872993	G				coding (60/720 nt)	DEL(1bp)
Large_WM	P7_HM_W1	1	CCAGGCGGCCG				coding (170-180/720 nt)	DEL(11bp)
	P7_HM_W3	0.098782539	T				coding (632/720 nt)	DEL(1bp)
	P7_HM_W3	0.091372264	T	GGAA			coding (632/720 nt)	INS
	P7_HM_W3	0.093834545	C	CCATA			coding (339/720 nt)	INS
	P7_HM_W3	0.176471277	GCGCCAGGCGGC				coding (172-183/720 nt)	DEL(12bp)
	P7_HM_W3	0.170723707	TTAGGCAACAGGC				coding (113-125/720 nt)	DEL(13bp)
	P7_LM_W5	0.414476648	GCT				coding (58-60/720 nt)	DEL(3bp)
	P7_LM_W6	0.236755848	C	G			coding (197/720 nt)	INS
	P7_LM_W6	0.236755848	C	G			coding (197/720 nt)	INS
	P7_LM_W6	0.085654886	TCGCCATCTT				coding (73-82/720 nt)	DEL(10bp)
	P7_LM_W7	0.470420837	A	C	GAC	TAC	166	SNP(Y56D)
	P7_LM_W8	0.290487766	G	A	TAG	CAG	478	SNP(Q160*)
	P7_LM_W8	0.103964806	C				coding (208/720 nt)	DEL(1bp)
	P7_LM_W8	0.166963215	C	CGGT			coding (198/720 nt)	INS
	P7_LM_W8	0.264792296	CCGACGATGAAG				coding (150-161/720 nt)	DEL(12bp)

Table B.10. List of mutations in the **lasR** gene in large metapopulations(frequency threshold of 8%).

Treatment	sample	frequency	ref_seq	new_seq	codon_new_seq	codon_ref_seq	gene_position	Mutation_ID
Large_STAR	P7_HM_A3	0.257416248	C	T	GTG	GCG	1265	SNP(A422V)
	P7_HM_A8	0.925330162	G	A	ATG	GTG	1228	SNP(V410M)
	P7_LM_A3	0.339353728	21-bp				coding (879-899/1629 nt)	DEL(21bp)
	P7_LM_A3	0.092446804	T	G	GGC	GTC	1358	SNP(V453G)
	P7_LM_A5	0.287717892	84-bp				coding (849-932/1629 nt)	DEL(84bp)
	P7_LM_A5	0.439920355	T	GCA			coding (1421/1629 nt)	INS
	P7_LM_A8	0.12610013	42-bp				coding (853-894/1629 nt)	DEL(42bp)
Large_WM	P7_HM_W3	0.322970812	84-bp				coding (849-932/1629 nt)	DEL(84bp)
	P7_LM_W5	0.136349245	84-bp				coding (849-932/1629 nt)	DEL(84bp)
	P7_LM_W6	0.487044238	84-bp				coding (849-932/1629 nt)	DEL(84bp)
	P7_LM_W7	0.850297567	84-bp				coding (849-932/1629 nt)	DEL(84bp)
	P7_LM_W8	0.317678013	84-bp				coding (849-932/1629 nt)	DEL(84bp)

Table B.11. List of mutations in the **wspA** gene in large metapopulations(frequency threshold of 8%).

sample	frequency	ref_seq	new_seq	codon_new_seq	codon_ref_seq	gene_position	Mutation_ID
P7_LM_W8	0.114372253	A	G	GTG	ATG	511	SNP(M171V)

Table B.12. List of mutations in the **wspR** gene in large well-mixed metapopulations (frequency threshold of 8%). No mutations were detected in Star metapopulations.

Treatment	sample	frequency	ref_seq	new_seq	gene_position	Mutation_ID
Large_STAR	P7_LM_A3	0.284551573	TCAA		coding (851-854/1008 nt)	DEL(4bp)
	P7_LM_A8	0.314595225	T	GGTGC	coding (422/1008 nt)	INS
	P7_LM_A8	0.213760736	CGAAGGCCGGCGGGGC		coding (431-446/1008 nt)	DEL(16bp)
	P7_LM_A8	0.082238802	CGGCGGGGCGC		coding (438-448/1008 nt)	DEL(11bp)
	P7_LM_A8	0.11243391	T		coding (716/1008 nt)	DEL(1bp)
	P7_LM_A8	0.094804287	A		coding (853/1008 nt)	DEL(1bp)
Large_WM	P7_HM_W1	1	T		coding (716/1008 nt)	DEL(1bp)
	P7_HM_W3	0.112259002	C	CGG	coding (821/1008 nt)	INS
	P7_HM_W3	0.443196666	T	GGGCC	coding (827/1008 nt)	INS
	P7_LM_W5	0.544695377	A		coding (853/1008 nt)	DEL(1bp)
	P7_LM_W5	0.101412773	A		coding (854/1008 nt)	DEL(1bp)
	P7_LM_W6	0.136858928	CAA		coding (852-854/1008 nt)	DEL(3bp)
	P7_LM_W8	0.140458653	CGAAGGCC		coding (431-438/1008 nt)	DEL(8bp)
	P7_LM_W8	0.276706182	G	GCGTGGCGAATTATTG	coding (791/1008 nt)	INS

Table B.13. List of mutations in the **wspF** gene in large metapopulations(frequency threshold of 8%).

Bibliography

Abel, S., P. A. zur Wiesch, B. M. Davis, and M. K. Waldor. 2015. Analysis of Bottlenecks in Experimental Models of Infection. PLOS Pathogens 11:e1004823. Public Library of Science.

Adlam, B., K. Chatterjee, and M. A. Nowak. 2015. Amplifiers of selection. Proc. R. Soc. A 471:20150114.

Aif, S., N. Appold, L. Kampman, O. Hallatschek, and J. Kayser. 2022. Evolutionary rescue of resistant mutants is governed by a balance between radial expansion and selection in compact populations. Nat Commun 13:7916. Nature Publishing Group.

Aitken, S. N., and M. C. Whitlock. 2013. Assisted Gene Flow to Facilitate Local Adaptation to Climate Change. Annu. Rev. Ecol. Evol. Syst. 44:367–388. Annual Reviews.

Amarasekare, P. 2003. Competitive coexistence in spatially structured environments: a synthesis. Ecology Letters 6:1109–1122.

Andersson, D. I., and D. Hughes. 2010. Antibiotic resistance and its cost: is it possible to reverse resistance? Nat Rev Microbiol 8:260–271. Nature Publishing Group.

Angert, A. L., M. G. Bontrager, and J. Ågren. 2020. What Do We Really Know About Adaptation at Range Edges? Annual Review of Ecology, Evolution, and Systematics 51:341–361.

Attrill, E. L., R. Claydon, U. Łapińska, M. Recker, S. Meaden, A. T. Brown, E. R. Westra, S. V. Harding, and S. Pagliara. 2021. Individual bacteria in structured environments rely on phenotypic resistance to phage. PLOS Biology 19:e3001406. Public Library of Science.

Azimi, S., G. R. Lewin, and M. Whiteley. 2022. The biogeography of infection revisited. Nat Rev Microbiol 20:579–592. Nature Publishing Group.

Bachmann, H., M. Fischlechner, I. Rabbers, N. Barfa, F. Branco dos Santos, D. Molenaar, and B. Teusink. 2013. Availability of public goods shapes the evolution of competing metabolic strategies. Proceedings of the National Academy of Sciences 110:14302–14307. Proceedings of the National Academy of Sciences.

Bailey, S. F., L. A. Alonso Morales, and R. Kassen. 2021a. Effects of Synonymous Mutations beyond Codon Bias: The Evidence for Adaptive Synonymous Substitutions from Microbial Evolution Experiments. Genome Biology and Evolution 13:evab141.

Bailey, S. F., and T. Bataillon. 2016. Can the experimental evolution programme help us elucidate the genetic basis of adaptation in nature? Molecular Ecology 25:203–218.

Bailey, S. F., F. Blanquart, T. Bataillon, and R. Kassen. 2017. What drives parallel evolution? BioEssays 39:e201600176.

Bailey, S. F., Q. Guo, and T. Bataillon. 2018. Identifying Drivers of Parallel Evolution: A Regression Model Approach. Genome Biology and Evolution 10:2801–2812.

Bailey, S. F., A. Hinz, and R. Kassen. 2014. Adaptive synonymous mutations in an experimentally evolved Pseudomonas fluorescens population. Nat Commun 5:4076. Nature Publishing Group.

Bailey, S. F., and R. Kassen. 2012. Spatial Structure of Ecological Opportunity Drives Adaptation in a Bacterium. The American Naturalist 180:270–283. The University of Chicago Press.

Bailey, S. F., A. Trudeau, K. Tulowiecki, M. McGrath, A. Belle, H. Fountain, and M. Akter. 2021b. Spatial structure affects evolutionary dynamics and drives genomic diversity in experimental populations of Pseudomonas fluorescens. bioRxiv, doi: 10.1101/2021.09.28.461808. Cold Spring Harbor Laboratory.

Barnard, F. M., and A. Maxwell. 2001. Interaction between DNA Gyrase and Quinolones: Effects of Alanine Mutations at GyrA Subunit Residues Ser83and Asp87. Antimicrobial Agents and Chemotherapy 45:1994–2000. American Society for Microbiology.

Barrick, J. E., D. S. Yu, S. H. Yoon, H. Jeong, T. K. Oh, D. Schneider, R. E. Lenski, and J. F. Kim. 2009. Genome evolution and adaptation in a long-term experiment with Escherichia coli. Nature 461:1243–1247. Nature Publishing Group.

Barton, N. H. 1993. The probability of fixation of a favoured allele in a subdivided population. Genetics Research 62:149–157.

Barton, N. H., and B. Charlesworth. 1984. Genetic Revolutions, Founder Effects, and Speciation. Annual Review of Ecology and Systematics 15:133–164.

Barton, N. H., and M. C. Whitlock. 1997. 9 - The Evolution of Metapopulations. Pp. 183–210 *in* I. Hanski and M. E. Gilpin, eds. Metapopulation Biology. Academic Press, San Diego.

Bates, D., M. Mächler, B. Bolker, and S. Walker. 2015. Fitting Linear Mixed-Effects Models Using lme4. Journal of Statistical Software 67:1–48.

Baym, M., T. D. Lieberman, E. D. Kelsic, R. Chait, R. Gross, I. Yelin, and R. Kishony. 2016. Spatiotemporal microbial evolution on antibiotic landscapes. Science 353:1147–1151.

Bell, G. 2008. Selection: The Mechanism of Evolution. OUP Oxford.

Bever, J. D., and E. L. Simms. 2000. Evolution of nitrogen fixation in spatially structured populations of Rhizobium. Heredity 85:366–372. Nature Publishing Group.

Blanquart, F., S. Gandon, and S. L. Nuismer. 2012. The effects of migration and drift on local adaptation to a heterogeneous environment. Journal of Evolutionary Biology 25:1351–1363.

Bolger, A. M., M. Lohse, and B. Usadel. 2014. Trimmomatic: a flexible trimmer for Illumina sequence data. Bioinformatics 30:2114–2120.

Boots, M., and A. Sasaki. 1999. ‘Small worlds’ and the evolution of virulence: infection occurs locally and at a distance. Proceedings of the Royal Society of London. Series B: Biological Sciences 266:1933–1938. Royal Society.

Boots and Sasaki. 2000. The evolutionary dynamics of local infection and global reproduction in host–parasite interactions. Ecology Letters 3:181–185.

Borer, B., D. Ciccarese, D. Johnson, and D. Or. 2020. Spatial organization in microbial range expansion emerges from trophic dependencies and successful lineages. Commun Biol 3:1–10. Nature Publishing Group.

Bosshard, L., I. Dupanloup, O. Tenaillon, R. Bruggmann, M. Ackermann, S. Peischl, and L. Excoffier. 2017. Accumulation of Deleterious Mutations During Bacterial Range Expansions. Genetics 207:669–684.

Brockhurst, M. A., A. Buckling, and P. B. Rainey. 2006. Spatial heterogeneity and the stability of host-parasite coexistence. Journal of Evolutionary Biology 19:374–379.

Brockhurst, M. A., A. D. Morgan, P. B. Rainey, and A. Buckling. 2003. Population mixing accelerates coevolution. Ecology Letters 6:975–979.

Buckingham, L. J., and B. Ashby. 2022. Coevolutionary theory of hosts and parasites. Journal of Evolutionary Biology 35:205–224.

Buckling, A., and M. A. Brockhurst. 2008. Kin selection and the evolution of virulence. Heredity 100:484–488. Nature Publishing Group.

Buttery, N. J., C. N. Jack, B. Adu-Oppong, K. T. Snyder, C. R. L. Thompson, D. C. Queller, and J. E. Strassmann. 2012. Structured growth and genetic drift raise relatedness in the social amoeba Dictyostelium discoideum. Biology Letters 8:794–797. Royal Society.

Cairns, J., L. Ruokolainen, J. Hultman, M. Tamminen, M. Virta, and T. Hiltunen. 2018. Ecology determines how low antibiotic concentration impacts community composition and horizontal transfer of resistance genes. Commun Biol 1:1–8. Nature Publishing Group.

Celik Ozgen, V., W. Kong, A. E. Blanchard, F. Liu, and T. Lu. 2018. Spatial interference scale as a determinant of microbial range expansion. Science Advances 4:eaau0695. American Association for the Advancement of Science.

Chadha, J., K. Harjai, and S. Chhibber. 2022. Revisiting the virulence hallmarks of Pseudomonas aeruginosa: a chronicle through the perspective of quorum sensing. Environmental Microbiology 24:2630–2656.

Chakraborty, P. P., L. R. Nemzer, and R. Kassen. 2023. Experimental evidence that network topology can accelerate the spread of beneficial mutations. Evolution Letters 7:447–456.

Chao, L., and B. R. Levin. 1981. Structured habitats and the evolution of anticompetitor toxins in bacteria. Proceedings of the National Academy of Sciences 78:6324–6328. Proceedings of the National Academy of Sciences.

Charlesworth, B., D. Charlesworth, and N. H. Barton. 2003. The Effects of Genetic and Geographic Structure on Neutral Variation. Annual Review of Ecology, Evolution, and Systematics 34:99–125.

Chen, P., and R. Kassen. 2020. The evolution and fate of diversity under hard and soft selection. Proceedings of the Royal Society B: Biological Sciences 287:20201111. Royal Society.

Cheptou, P.-O., A. L. Hargreaves, D. Bonte, and H. Jacquemyn. 2017. Adaptation to fragmentation: evolutionary dynamics driven by human influences. Philosophical Transactions of the Royal Society B: Biological Sciences 372:20160037. Royal Society.

Chevin, L.-M., G. Martin, and T. Lenormand. 2010. Fisher's model and the genomics of adaptation: restricted pleiotropy, heterogenous mutation, and parallel evolution. Evolution 64:3213–3231.

Choy, W.-K., L. Zhou, C. K.-C. Syn, L.-H. Zhang, and S. Swarup. 2004. MorA Defines a New Class of Regulators Affecting Flagellar Development and Biofilm Formation in Diverse Pseudomonas Species. Journal of Bacteriology 186:7221–7228. American Society for Microbiology.

Ciccarese, D., A. Zuidema, V. Merlo, and D. R. Johnson. 2020. Interaction-dependent effects of surface structure on microbial spatial self-organization. Philosophical Transactions of the Royal Society B: Biological Sciences 375:20190246. Royal Society.

Coberly, L. C., W. Wei, K. Y. Sampson, J. Millstein, H. A. Wichman, and S. M. Krone. 2009. Space, Time, and Host Evolution Facilitate Coexistence of Competing Bacteriophages: Theory and Experiment. Am. Nat. 173:E121–E138. Univ Chicago Press, Chicago.

Coenye, T., M. Bové, and T. Bjarnsholt. 2022. Biofilm antimicrobial susceptibility through an experimental evolutionary lens. npj Biofilms Microbiomes 8:1–12. Nature Publishing Group.

Constable, G. W. A., and A. J. McKane. 2014. Population genetics on islands connected by an arbitrary network: An analytic approach. Journal of Theoretical Biology 358:149–165.

Conte, G. L., M. E. Arnegard, C. L. Peichel, and D. Schluter. 2012. The probability of genetic parallelism and convergence in natural populations. Proceedings of the Royal Society B: Biological Sciences 279:5039–5047. Royal Society.

Coyne, J. A., N. H. Barton, and M. Turelli. 1997. Perspective: A Critique of Sewall Wright's Shifting Balance Theory of Evolution. Evolution 51:643–671. [Society for the Study of Evolution, Wiley].

Cremin, K., S. J. N. Duxbury, J. Rosko, and O. S. Soyer. 2023. Formation and emergent dynamics of spatially organized microbial systems. Interface Focus 13:20220062. Royal Society.

Dal Co, A., M. Ackermann, and S. van Vliet. 2019a. Metabolic activity affects the response of single cells to a nutrient switch in structured populations. Journal of The Royal Society Interface 16:20190182. Royal Society.

Dal Co, A., S. van Vliet, and M. Ackermann. 2019b. Emergent microscale gradients give rise to metabolic cross-feeding and antibiotic tolerance in clonal bacterial populations. Philosophical Transactions of the Royal Society B: Biological Sciences 374:20190080. Royal Society.

Dang, H., and C. R. Lovell. 2015. Microbial Surface Colonization and Biofilm Development in Marine Environments. Microbiology and Molecular Biology Reviews 80:91–138. American Society for Microbiology.

Datta, M. S., K. S. Korolev, I. Cvijovic, C. Dudley, and J. Gore. 2013. Range expansion promotes cooperation in an experimental microbial metapopulation. Proceedings of the National Academy of Sciences 110:7354–7359. Proceedings of the National Academy of Sciences.

Deatherage, D. E., and J. E. Barrick. 2014. Identification of mutations in laboratory-evolved microbes from next-generation sequencing data using breseq. Methods Mol Biol 1151:165–188.

Denk-Lobnig, M., and K. B. Wood. 2023. Antibiotic resistance in bacterial communities. Current Opinion in Microbiology 74:102306.

Desai, M. M., and D. S. Fisher. 2007. Beneficial Mutation–Selection Balance and the Effect of Linkage on Positive Selection. Genetics 176:1759–1798.

Desai, M. M., D. S. Fisher, and A. W. Murray. 2007. The Speed of Evolution and Maintenance of Variation in Asexual Populations. Current Biology 17:385–394.

Donker, T., J. Wallinga, and H. Grundmann. 2014. Dispersal of antibiotic-resistant high-risk clones by hospital networks: changing the patient direction can make all the difference. Journal of Hospital Infection 86:34–41.

Durão, P., R. S. Ramiro, C. Pereira, J. Jurič, D. Pereira, and I. Gordo. 2020. Radial Expansion Facilitates the Maintenance of Double Antibiotic Resistances. Antimicrobial Agents and Chemotherapy 64:10.1128/aac.00668-20. American Society for Microbiology.

Endler, J. A., 1947. 1977. Geographic Variation, Speciation, and Clines. Princeton, N.J. : Princeton University Press, 1977.

Estrela, S., and S. P. Brown. 2018. Community interactions and spatial structure shape selection on antibiotic resistant lineages. PLOS Computational Biology 14:e1006179. Public Library of Science.

Estrela, S., and S. P. Brown. 2013. Metabolic and Demographic Feedbacks Shape the Emergent Spatial Structure and Function of Microbial Communities. PLOS Computational Biology 9:e1003398. Public Library of Science.

Excoffier, L., M. Foll, and R. J. Petit. 2009. Genetic Consequences of Range Expansions. Annual Review of Ecology, Evolution, and Systematics 40:481–501.

Excoffier, L., and N. Ray. 2008. Surfing during population expansions promotes genetic revolutions and structuration. Trends in Ecology & Evolution 23:347–351. Elsevier.

Eyre-Walker, A., and P. D. Keightley. 2007. The distribution of fitness effects of new mutations. Nat Rev Genet 8:610–618. Nature Publishing Group.

Felsenstein, J. 1976. The Theoretical Population Genetics of Variable Selection and Migration. Annual Review of Genetics 10:253–280.

Fisher, R. A. 1930. The genetical theory of natural selection. Clarendon Press, Oxford, England.

France, M. T., A. Cornea, H. Kehlet-Delgado, and L. J. Forney. 2019a. Spatial structure facilitates the accumulation and persistence of antibiotic-resistant mutants in biofilms. Evolutionary Applications 12:498–507.

France, M. T., A. Cornea, H. Kehlet-Delgado, and L. J. Forney. 2019b. Spatial structure facilitates the accumulation and persistence of antibiotic-resistant mutants in biofilms. Evolutionary Applications 12:498–507.

France, M. T., and L. J. Forney. 2019. The Relationship between Spatial Structure and the Maintenance of Diversity in Microbial Populations. The American Naturalist 193:503–513. The University of Chicago Press.

France, M. T., B. J. Ridenhour, and L. J. Forney. 2018. Effects of Spatial Structure and Reduced Growth Rates on Evolution in Bacterial Populations. Pp. 175–197 *in* P. H.

Rampelotto, ed. Molecular Mechanisms of Microbial Evolution. Springer International Publishing, Cham.

Frank, S. A. 1998. Foundations of social evolution. Princeton University Press, Princeton, N.J.

Frank, S. A. 1996. Models of parasite virulence. Q Rev Biol 71:37–78.

Frank, S. A., and M. Slatkin. 1992. Fisher's fundamental theorem of natural selection. Trends Ecol Evol 7:92–95.

Frean Marcus, Rainey Paul B., and Traulsen Arne. 2013. The effect of population structure on the rate of evolution. Proceedings of the Royal Society B: Biological Sciences 280:20130211.

Fusco, D., M. Gralka, J. Kayser, A. Anderson, and O. Hallatschek. 2016. Excess of mutational jackpot events in expanding populations revealed by spatial Luria–Delbrück experiments. Nat Commun 7:12760. Nature Publishing Group.

Galanis, A., A. Göbel, L. A. Goldberg, J. Lapinskas, and D. Richerby. 2017. Amplifiers for the Moran Process. J. ACM 64:5:1-5:90.

García-Bayona, L., and L. E. Comstock. 2018. Bacterial antagonism in host-associated microbial communities. Science 361:eaat2456. American Association for the Advancement of Science.

Garoff, L., F. Pietsch, D. L. Huseby, T. Lilja, G. Brandis, and D. Hughes. 2020. Population Bottlenecks Strongly Influence the Evolutionary Trajectory to Fluoroquinolone Resistance in Escherichia coli. Molecular Biology and Evolution 37:1637–1646.

Gerrish, P. J., and R. E. Lenski. 1998. The fate of competing beneficial mutations in an asexual population. Genetica 102:127.

Gillespie, J. H. 1983. A simple stochastic gene substitution model. Theoretical Population Biology 23:202–215.

Gillespie, J. H. 1984. Molecular Evolution Over the Mutational Landscape. Evolution 38:1116–1129.

Gillespie, J. H. 1994. The Causes of Molecular Evolution. Oxford University Press.

Gomulkiewicz, R., D. M. Drown, M. F. Dybdahl, W. Godsoe, S. L. Nuismer, K. M. Pepin, B. J. Ridenhour, C. I. Smith, and J. B. Yoder. 2007. Dos and don'ts of testing the geographic mosaic theory of coevolution. Heredity 98:249–258. Nature Publishing Group.

Good, B. H., M. J. McDonald, J. E. Barrick, R. E. Lenski, and M. M. Desai. 2017. The dynamics of molecular evolution over 60,000 generations. Nature 551:45–50. Nature Publishing Group.

Gordo, I., and P. R. A. Campos. 2006. Adaptive evolution in a spatially structured asexual population. Genetica 127:217.

Gralka, M., F. Stiewe, F. Farrell, W. Möbius, B. Waclaw, and O. Hallatschek. 2016. Allele surfing promotes microbial adaptation from standing variation. Ecology Letters 19:889–898.

Granato, E. T., C. Ziegenhain, R. L. Marvig, and R. Kümmerli. 2018. Low spatial structure and selection against secreted virulence factors attenuates pathogenicity in Pseudomonas aeruginosa. ISME J 12:2907–2918. Nature Publishing Group.

Guillaume, F. 2011. MIGRATION-INDUCED PHENOTYPIC DIVERGENCE: THE MIGRATION–SELECTION BALANCE OF CORRELATED TRAITS. Evolution 65:1723–1738.

Ha, D.-G., and G. A. O'Toole. 2015. c-di-GMP and its Effects on Biofilm Formation and Dispersion: a Pseudomonas Aeruginosa Review. Pp. 301–317 *in* Microbial Biofilms. John Wiley & Sons, Ltd.

Ha, D.-G., M. E. Richman, and G. A. O'Toole. 2014. Deletion Mutant Library for Investigation of Functional Outputs of Cyclic Diguanylate Metabolism in Pseudomonas aeruginosa PA14. Applied and Environmental Microbiology 80:3384–3393. American Society for Microbiology.

Habets, M. G. J. L., T. Czárán, R. F. Hoekstra, and J. A. G. M. de Visser. 2007. Spatial structure inhibits the rate of invasion of beneficial mutations in asexual populations. Proceedings of the Royal Society B: Biological Sciences 274:2139–2143. Royal Society.

Habets, M. G. J. L., D. E. Rozen, R. F. Hoekstra, and J. A. G. M. de Visser. 2006. The effect of population structure on the adaptive radiation of microbial populations evolving in spatially structured environments. Ecology Letters 9:1041–1048.

Hajishengallis, G., R. J. Lamont, and H. Koo. 2023. Oral polymicrobial communities: Assembly, function, and impact on diseases. Cell Host & Microbe 31:528–538.

Hallatschek, O., P. Hersen, S. Ramanathan, and D. R. Nelson. 2007. Genetic drift at expanding frontiers promotes gene segregation. Proceedings of the National Academy of Sciences 104:19926–19930. Proceedings of the National Academy of Sciences.

Hall-Stoodley, L., J. W. Costerton, and P. Stoodley. 2004. Bacterial biofilms: from the Natural environment to infectious diseases. Nat Rev Microbiol 2:95–108. Nature Publishing Group.

Hamilton, W. D. 1972. Altruism and Related Phenomena, Mainly in Social Insects. Annual Review of Ecology and Systematics 3:193–232.

Hamilton, W. D. 1963. The Evolution of Altruistic Behavior. The American Naturalist 97:354–356. The University of Chicago Press.

Hamilton, W. D. 1964. The genetical evolution of social behaviour. I. Journal of Theoretical Biology 7:1–16.

Handel, A., and M. R. Bennett. 2008. Surviving the Bottleneck: Transmission Mutants and the Evolution of Microbial Populations. Genetics 180:2193–2200.

Hannan, T. J., M. Totsika, K. J. Mansfield, K. H. Moore, M. A. Schembri, and S. J. Hultgren. 2012. Host–pathogen checkpoints and population bottlenecks in persistent and intracellular uropathogenic Escherichia coli bladder infection. FEMS Microbiology Reviews 36:616–648.

Hansen, S. K., P. B. Rainey, J. A. J. Haagensen, and S. Molin. 2007. Evolution of species interactions in a biofilm community. Nature 445:533–536. Nature Publishing Group.

Hanski, I. A., and M. E. Gilpin (eds). 1997. Metapopulation Biology: Ecology, Genetics, and Evolution. 1st edition. Academic Press, San Diego, Calif.

Harcombe, W. 2010. NOVEL COOPERATION EXPERIMENTALLY EVOLVED BETWEEN SPECIES. Evolution 64:2166–2172.

Harris, K. B., K. M. Flynn, and V. S. Cooper. 2021. Polygenic Adaptation and Clonal Interference Enable Sustained Diversity in Experimental Pseudomonas aeruginosa Populations. Molecular Biology and Evolution 38:5359–5375.

Harrison, J. J., H. Almblad, Y. Irie, D. J. Wolter, H. C. Eggleston, T. E. Randall, J. O. Kitzman, B. Stackhouse, J. C. Emerson, S. Mcnamara, T. J. Larsen, J. Shendure, L. R. Hoffman, D. J. Wozniak, and M. R. Parsek. 2020. Elevated exopolysaccharide levels in Pseudomonas aeruginosa flagellar mutants have implications for biofilm growth and chronic infections. PLOS Genetics 16:e1008848. Public Library of Science.

Harrison, S., and A. Hastings. 1996. Genetic and evolutionary consequences of metapopulation structure. Trends in Ecology & Evolution 11:180–183.

Hedrick, P. W. 1986. Genetic Polymorphism in Heterogeneous Environments: A Decade Later. Annual Review of Ecology and Systematics 17:535–566.

Hindersin, L., and A. Traulsen. 2015. Most Undirected Random Graphs Are Amplifiers of Selection for Birth-Death Dynamics, but Suppressors of Selection for Death-Birth Dynamics. PLOS Computational Biology 11:e1004437. Public Library of Science.

Høiby, N., T. Bjarnsholt, M. Givskov, S. Molin, and O. Ciofu. 2010. Antibiotic resistance of bacterial biofilms. International Journal of Antimicrobial Agents 35:322–332.

Hol, F. J. H., P. Galajda, K. Nagy, R. G. Woolthuis, C. Dekker, and J. E. Keymer. 2013. Spatial Structure Facilitates Cooperation in a Social Dilemma: Empirical Evidence from a Bacterial Community. PLOS ONE 8:e77042. Public Library of Science.

Hol, F. J. H., P. Galajda, R. G. Woolthuis, C. Dekker, and J. E. Keymer. 2015. The idiosyncrasy of spatial structure in bacterial competition. BMC Res Notes 8:245.

Houchmandzadeh, B., and M. Vallade. 2013. Exact results for fixation probability of bithermal evolutionary graphs. Biosystems 112:49–54.

Houchmandzadeh, B., and M. Vallade. 2011. The fixation probability of a beneficial mutation in a geographically structured population. New J. Phys. 13:073020.

Hughes, D., and D. I. Andersson. 2017. Evolutionary Trajectories to Antibiotic Resistance. Annual Review of Microbiology 71:579–596. Annual Reviews.

Jacoby, G. A. 2005. Mechanisms of Resistance to Quinolones. Clinical Infectious Diseases 41:S120–S126.

Jamieson-Lane, A., and C. Hauert. 2015. Fixation probabilities on superstars, revisited and revised. Journal of Theoretical Biology 382:44–56.

Jenal, U., A. Reinders, and C. Lori. 2017. Cyclic di-GMP: second messenger extraordinaire. Nat Rev Microbiol 15:271–284. Nature Publishing Group.

Kassen, R. 2014. Experimental evolution and the nature of biodiversity. Roberts and Company, Greenwood Village, Colorado.

Kassen, R. 2019. Experimental Evolution of Innovation and Novelty. Trends Ecol Evol 34:712–722.

Kassen, R. 2002. The experimental evolution of specialists, generalists, and the maintenance of diversity. Journal of Evolutionary Biology 15:173–190.

Kassen, R., and T. Bataillon. 2006. Distribution of fitness effects among beneficial mutations before selection in experimental populations of bacteria. Nat Genet 38:484–488. Nature Publishing Group.

Katharios-Lanwermeyer, S., G. B. Whitfield, P. L. Howell, and G. A. O'Toole. 2021. Pseudomonas aeruginosa Uses c-di-GMP Phosphodiesterases RmcA and MorA To Regulate Biofilm Maintenance. mBio 12:10.1128/mbio.03384-20. American Society for Microbiology.

Kawecki, T. J., and D. Ebert. 2004. Conceptual issues in local adaptation. Ecology Letters 7:1225–1241.

Kawecki, T. J., R. E. Lenski, D. Ebert, B. Hollis, I. Olivieri, and M. C. Whitlock. 2012. Experimental evolution. Trends in Ecology & Evolution 27:547–560. Elsevier.

Kayser, J., C. F. Schreck, M. Gralka, D. Fusco, and O. Hallatschek. 2019. Collective motion conceals fitness differences in crowded cellular populations. Nat Ecol Evol 3:125–134. Nature Publishing Group.

Kelly, E., and B. L. Phillips. 2016. Targeted gene flow for conservation. Conserv Biol 30:259–267.

Kerr, B., C. Neuhauser, B. J. M. Bohannan, and A. M. Dean. 2006. Local migration promotes competitive restraint in a host–pathogen “tragedy of the commons.” Nature 442:75–78. Nature Publishing Group.

Kerr, B., M. A. Riley, M. W. Feldman, and B. J. M. Bohannan. 2002. Local dispersal promotes biodiversity in a real-life game of rock–paper–scissors. Nature 418:171–174. Nature Publishing Group.

Keymer, J. E., P. Galajda, G. Lambert, D. Liao, and R. H. Austin. 2008. Computation of mutual fitness by competing bacteria. Proceedings of the National Academy of Sciences 105:20269–20273. Proceedings of the National Academy of Sciences.

Keymer, J. E., P. Galajda, C. Muldoon, S. Park, and R. H. Austin. 2006. Bacterial metapopulations in nanofabricated landscapes. PNAS 103:17290–17295.

Khademi, S. M. H., P. Sazinas, and L. Jelsbak. 2019. Within-Host Adaptation Mediated by Intergenic Evolution in Pseudomonas aeruginosa. Genome Biology and Evolution 11:1385–1397.

Kim, H. J., J. Q. Boedicker, J. W. Choi, and R. F. Ismagilov. 2008. Defined spatial structure stabilizes a synthetic multispecies bacterial community. Proc Natl Acad Sci USA 105:18188.

Kim, W., F. Racimo, J. Schluter, S. B. Levy, and K. R. Foster. 2014. Importance of positioning for microbial evolution. Proceedings of the National Academy of Sciences 111:E1639–E1647. Proceedings of the National Academy of Sciences.

Korolev, K. S., M. Avlund, O. Hallatschek, and D. R. Nelson. 2010. Genetic demixing and evolution in linear stepping stone models. Rev. Mod. Phys. 82:1691–1718. American Physical Society.

Korolev, K. S., M. J. I. Müller, N. Karahan, A. W. Murray, O. Hallatschek, and D. R. Nelson. 2012. Selective sweeps in growing microbial colonies. Phys. Biol. 9:026008. IOP Publishing.

Korolev, K. S., J. B. Xavier, and J. Gore. 2014. Turning ecology and evolution against cancer. Nat Rev Cancer 14:371–380. Nature Publishing Group.

Korona, R., C. H. Nakatsu, L. J. Forney, and R. E. Lenski. 1994. Evidence for multiple adaptive peaks from populations of bacteria evolving in a structured habitat. Proceedings of the National Academy of Sciences 91:9037–9041. Proceedings of the National Academy of Sciences.

Kottler, E. J., E. E. Dickman, J. P. Sexton, N. C. Emery, and S. J. Franks. 2021. Draining the Swamping Hypothesis: Little Evidence that Gene Flow Reduces Fitness at Range Edges. Trends in Ecology & Evolution 36:533–544. Elsevier.

Kraemer, S. A., and P. J. Boynton. 2017. Evidence for microbial local adaptation in nature. Molecular Ecology 26:1860–1876.

Krieger, M. S., C. E. Denison, T. L. Anderson, M. A. Nowak, and A. L. Hill. 2020. Population structure across scales facilitates coexistence and spatial heterogeneity of antibiotic-resistant infections. PLOS Computational Biology 16:e1008010. Public Library of Science.

Kryazhimskiy, S., D. P. Rice, and M. M. Desai. 2012. Population Subdivision and Adaptation in Asexual Populations of Saccharomyces Cerevisiae. Evolution 66:1931–1941.

Kümmerli, R., A. S. Griffin, S. A. West, A. Buckling, and F. Harrison. 2009. Viscous medium promotes cooperation in the pathogenic bacterium Pseudomonas aeruginosa. Proceedings of the Royal Society B: Biological Sciences 276:3531–3538. Royal Society.

Lambert, G., D. Liao, S. Vyawahare, and R. H. Austin. 2011. Anomalous Spatial Redistribution of Competing Bacteria under Starvation Conditions. Journal of Bacteriology 193:1878–1883. American Society for Microbiology.

Lang, G. I., D. P. Rice, M. J. Hickman, E. Sodergren, G. M. Weinstock, D. Botstein, and M. M. Desai. 2013. Pervasive genetic hitchhiking and clonal interference in forty evolving yeast populations. Nature 500:571–574. Nature Publishing Group.

Leale, A. M., and R. Kassen. 2018. The emergence, maintenance, and demise of diversity in a spatially variable antibiotic regime. Evolution Letters 2:134–143.

Lenormand, T. 2002. Gene flow and the limits to natural selection. Trends in Ecology & Evolution 17:183–189. Elsevier.

Lenormand, T., L.-M. Chevin, and T. Bataillon. 2016. 8. Parallel Evolution: What Does It (Not) Tell Us and Why Is It (Still) Interesting? Pp. 196–220 *in* 8. Parallel Evolution: What Does It (Not) Tell Us and Why Is It (Still) Interesting? University of Chicago Press.

Lenski, R. E. 2017. Experimental evolution and the dynamics of adaptation and genome evolution in microbial populations. ISME J 11:2181–2194. Nature Publishing Group.

Lenth, R. V. 2020. emmeans: Estimated Marginal Means, aka Least-Squares Means.

Levin, B. R. 1981. PERIODIC SELECTION, INFECTIOUS GENE EXCHANGE AND THE GENETIC STRUCTURE OF E. COLI POPULATIONS. Genetics 99:1–23.

Levin, B. R., V. Perrot, and N. Walker. 2000. Compensatory Mutations, Antibiotic Resistance and the Population Genetics of Adaptive Evolution in Bacteria. Genetics 154:985–997.

Lieberman, E., C. Hauert, and M. A. Nowak. 2005. Evolutionary dynamics on graphs. Nature 433:312.

Limdi, A., A. Pérez-Escudero, A. Li, and J. Gore. 2018. Asymmetric migration decreases stability but increases resilience in a heterogeneous metapopulation. Nat Commun 9:2969. Nature Publishing Group.

Lion, S., and M. van Baalen. 2008. Self-structuring in spatial evolutionary ecology. Ecology Letters 11:277–295.

Lion, S., and S. Gandon. 2015. Evolution of spatially structured host–parasite interactions. Journal of Evolutionary Biology 28:10–28.

Lipinski, K. A., L. J. Barber, M. N. Davies, M. Ashenden, A. Sottoriva, and M. Gerlinger. 2016. Cancer Evolution and the Limits of Predictability in Precision Cancer Medicine. Trends in Cancer 2:49–63. Elsevier.

Ma, L. Z., D. Wang, Y. Liu, Z. Zhang, and D. J. Wozniak. 2022. Regulation of Biofilm Exopolysaccharide Biosynthesis and Degradation in Pseudomonas aeruginosa. Annual Review of Microbiology 76:413–433.

MacLean, R. C., and A. Buckling. 2009. The Distribution of Fitness Effects of Beneficial Mutations in Pseudomonas aeruginosa. PLOS Genetics 5:e1000406. Public Library of Science.

MacLean, R. C., and I. Gudelj. 2006. Resource competition and social conflict in experimental populations of yeast. Nature 441:498–501. Nature Publishing Group.

Mahrt, N., A. Tietze, S. Künzel, S. Franzenburg, C. Barbosa, G. Jansen, and H. Schulenburg. 2021. Bottleneck size and selection level reproducibly impact evolution of antibiotic resistance. Nat Ecol Evol 5:1233–1242. Nature Publishing Group.

Marchal, M., F. Goldschmidt, S. N. Derksen-Müller, S. Panke, M. Ackermann, and D. R. Johnson. 2017. A passive mutualistic interaction promotes the evolution of spatial structure within microbial populations. BMC Evol Biol 17:106.

Marrec, L., I. Lamberti, and A.-F. Bitbol. 2021. Toward a Universal Model for Spatially Structured Populations. Phys. Rev. Lett. 127:218102. American Physical Society.

Martens, E. A., R. Kostadinov, C. C. Maley, and O. Hallatschek. 2011. Spatial structure increases the waiting time for cancer. New J. Phys. 13:115014. IOP Publishing.

Martin, G., and T. Lenormand. 2006. A General Multivariate Extension of Fisher's Geometrical Model and the Distribution of Mutation Fitness Effects Across Species. Evolution 60:893–907.

Martin, G., and T. Lenormand. 2008. The Distribution of Beneficial and Fixed Mutation Fitness Effects Close to an Optimum. Genetics 179:907–916.

Martínez, J. L., and F. Baquero. 2014. Emergence and spread of antibiotic resistance: setting a parameter space. Upsala Journal of Medical Sciences 119:68–77. Taylor & Francis.

Maruyama, T. 1970. On the fixation probability of mutant genes in a subdivided population*. Genetics Research 15:221–225.

Maynard Smith, J. 1997. The major transitions in evolution. Oxford University Press, Oxford ;

McDonald, M. J. 2019. Microbial Experimental Evolution – a proving ground for evolutionary theory and a tool for discovery. EMBO reports 20:e46992. John Wiley & Sons, Ltd.

McDougald, D., S. A. Rice, N. Barraud, P. D. Steinberg, and S. Kjelleberg. 2012. Should we stay or should we go: mechanisms and ecological consequences for biofilm dispersal. Nat Rev Microbiol 10:39–50. Nature Publishing Group.

McNally, L., E. Bernardy, J. Thomas, A. Kalziqi, J. Pentz, S. P. Brown, B. K. Hammer, P. J. Yunker, and W. C. Ratcliff. 2017. Killing by Type VI secretion drives genetic phase separation and correlates with increased cooperation. Nat Commun 8:14371.

Melnyk, A. H., N. McCloskey, A. J. Hinz, J. Dettman, and R. Kassen. 2017. Evolution of Cost-Free Resistance under Fluctuating Drug Selection in Pseudomonas aeruginosa. mSphere 2:10.1128/msphere.00158-17. American Society for Microbiology.

Michod, R. E., and D. Roze. 2001. Cooperation and conflict in the evolution of multicellularity. Heredity 86:1–7. Nature Publishing Group.

Miralles, R., A. Moya, and S. F. Elena. 1999. Effect of population patchiness and migration rates on the adaptation and divergence of vesicular stomatitis virus quasispecies populations. Journal of General Virology 80:2051–2059. Microbiology Society,.

Mitri, S., E. Clarke, and K. R. Foster. 2016. Resource limitation drives spatial organization in microbial groups. ISME J 10:1471–1482. Nature Publishing Group.

Momeni, B., A. J. Waite, and W. Shou. 2013. Spatial self-organization favors heterotypic cooperation over cheating. eLife 2:e00960.

Moradali, M. F., S. Ghods, and B. H. A. Rehm. 2017. Pseudomonas aeruginosa Lifestyle: A Paradigm for Adaptation, Survival, and Persistence. Frontiers in Cellular and Infection Microbiology 7.

Moran, P. A. P. (Patrick A. P. 1962. The statistical processes of evolutionary theory. Clarendon Press, Oxford.

Murrell, D. J. 2005. Local Spatial Structure and Predator-Prey Dynamics: Counterintuitive Effects of Prey Enrichment. The American Naturalist 166:354–367. The University of Chicago Press.

Nadell, C. D., K. Drescher, and K. R. Foster. 2016. Spatial structure, cooperation and competition in biofilms. Nat Rev Microbiol 14:589–600. Nature Publishing Group.

Nadell, C. D., K. R. Foster, and J. B. Xavier. 2010. Emergence of Spatial Structure in Cell Groups and the Evolution of Cooperation. PLOS Computational Biology 6:e1000716. Public Library of Science.

Nadell, C. D., D. Ricaurte, J. Yan, K. Drescher, and B. L. Bassler. 2017. Flow environment and matrix structure interact to determine spatial competition in Pseudomonas aeruginosa biofilms. eLife 6:e21855. eLife Sciences Publications, Ltd.

Nagy, K., Á. Ábrahám, J. E. Keymer, and P. Galajda. 2018. Application of Microfluidics in Experimental Ecology: The Importance of Being Spatial. Front. Microbiol. 9.

Nahum, J. R., P. Godfrey-Smith, B. N. Harding, J. H. Marcus, J. Carlson-Stevermer, and B. Kerr. 2015. A tortoise–hare pattern seen in adapting structured and unstructured populations suggests a rugged fitness landscape in bacteria. Proceedings of the National Academy of Sciences 112:7530–7535. Proceedings of the National Academy of Sciences.

Nash, J. C. 2016. nlmrt: Functions for Nonlinear Least Squares Solutions.

Noble, R., D. Burri, C. Le Sueur, J. Lemant, Y. Viossat, J. N. Kather, and N. Beerenwinkel. 2022. Spatial structure governs the mode of tumour evolution. Nat Ecol Evol 6:207–217. Nature Publishing Group.

Nowak, M. A. 2006a. Evolutionary dynamics: exploring the equations of life. Belknap Press of Harvard University Press, Cambridge, Mass.

Nowak, M. A. 2006b. Five rules for the evolution of cooperation. Science 314:1560–1563.

Nowak, M. A., and R. M. May. 1992. Evolutionary games and spatial chaos. Nature 359:826–829.

Oksanen, J., G. L. Simpson, F. G. Blanchet, R. Kindt, P. Legendre, P. R. Minchin, R. B. O'Hara, P. Solymos, M. H. H. Stevens, E. Szoecs, H. Wagner, M. Barbour, M. Bedward, B. Bolker, D. Borcard, G. Carvalho, M. Chirico, M. D. Caceres, S. Durand, H. B. A. Evangelista, R. FitzJohn, M. Friendly, B. Furneaux, G. Hannigan, M. O. Hill, L. Lahti, D. McGlinn, M.-H. Ouellette, E. R. Cunha, T. Smith, A. Stier, C. J. F. T. Braak, and J. Weedon. 2022. vegan: Community Ecology Package.

Oliver, A., and A. Mena. 2010. Bacterial hypermutation in cystic fibrosis, not only for antibiotic resistance. Clin Microbiol Infect 16:798–808.

Orr, H. A. 2003. The Distribution of Fitness Effects Among Beneficial Mutations. Genetics 163:1519–1526.

Orr, H. A. 2005a. The genetic theory of adaptation: a brief history. Nat Rev Genet 6:119–127. Nature Publishing Group.

Orr, H. A. 2002. The Population Genetics of Adaptation: The Adaptation of Dna Sequences. Evolution 56:1317–1330.

Orr, H. A. 1998. The Population Genetics of Adaptation: The Distribution of Factors Fixed during Adaptive Evolution. Evolution 52:935–949.

Orr, H. A. 2005b. The Probability of Parallel Evolution. Evolution 59:216–220.

Orr, H. A. 2005c. Theories of adaptation: what they do and don't say. Genetica 123:3–13.

Pande, S., F. Kaftan, S. Lang, A. Svatoš, S. Germerodt, and C. Kost. 2016. Privatization of cooperative benefits stabilizes mutualistic cross-feeding interactions in spatially structured environments. ISME J 10:1413–1423. Nature Publishing Group.

Pannell, J. R., and B. Charlesworth. 2000. Effects of metapopulation processes on measures of genetic diversity. Philosophical Transactions of the Royal Society of London. Series B: Biological Sciences 355:1851–1864. Royal Society.

Papkou, A., C. S. Gokhale, A. Traulsen, and H. Schulenburg. 2016. Host–parasite coevolution: why changing population size matters. Zoology 119:330–338.

Patwa Z and Wahl L.M. 2008. The fixation probability of beneficial mutations. Journal of The Royal Society Interface 5:1279–1289.

Pavlogiannis, A., J. Tkadlec, K. Chatterjee, and M. A. Nowak. 2018. Construction of arbitrarily strong amplifiers of natural selection using evolutionary graph theory. Communications Biology 1:71.

Perfeito, L., L. Fernandes, C. Mota, and I. Gordo. 2007a. Adaptive Mutations in Bacteria: High Rate and Small Effects. Science 317:813–815. American Association for the Advancement of Science.

Perfeito, L., M. I. Pereira, P. R. A. Campos, and I. Gordo. 2007b. The effect of spatial structure on adaptation in Escherichia coli. Biology Letters 4:57–59. Royal Society.

Pfeiffer, T., and S. Bonhoeffer. 2003. An evolutionary scenario for the transition to undifferentiated multicellularity. Proceedings of the National Academy of Sciences 100:1095–1098. Proceedings of the National Academy of Sciences.

Poltak, S. R., and V. S. Cooper. 2011. Ecological succession in long-term experimentally evolved biofilms produces synergistic communities. ISME J 5:369–378.

Ponciano, J. M., H.-J. La, P. Joyce, and L. J. Forney. 2009. Evolution of Diversity in Spatially Structured Escherichia coli Populations. Applied and Environmental Microbiology 75:6047–6054. American Society for Microbiology.

Poole, K. 2007. Efflux pumps as antimicrobial resistance mechanisms. Annals of Medicine 39:162–176. Taylor & Francis.

Poole, K. 2005. Efflux-mediated antimicrobial resistance. Journal of Antimicrobial Chemotherapy 56:20–51.

Poole, K. 2004. Efflux-mediated multiresistance in Gram-negative bacteria. Clinical Microbiology and Infection 10:12–26.

Queller, D. C. 1992. Does population viscosity promote kin selection? Trends in Ecology & Evolution 7:322–324.

Queller, D. C. 1994. Genetic relatedness in viscous populations. Evol Ecol 8:70–73.

R Core Team. 2020. R: A Language and Environment for Statistical Computing. R Foundation for Statistical Computing, Vienna, Austria.

R Core Team. 2022. R: A Language and Environment for Statistical Computing. R Foundation for Statistical Computing, Vienna, Austria.

Rainey, P. B., and M. Travisano. 1998. Adaptive radiation in a heterogeneous environment. Nature 394:69–72. Nature Publishing Group.

Ramos, C. H., E. Rodríguez-Sánchez, J. A. A. Del Angel, A. V. Arzola, M. Benítez, A. E. Escalante, A. Franci, G. Volpe, and N. Rivera-Yoshida. 2021. The environment

topography alters the way to multicellularity in Myxococcus xanthus. Science Advances 7:eabh2278. American Association for the Advancement of Science.

Rehman, A., W. M. Patrick, and I. L. Lamont. 2019. Mechanisms of ciprofloxacin resistance in Pseudomonas aeruginosa: new approaches to an old problem. J Med Microbiol 68:1–10.

Richardot, C., P. Juarez, K. Jeannot, I. Patry, P. Plésiat, and C. Llanes. 2016. Amino Acid Substitutions Account for Most MexS Alterations in Clinical nfxC Mutants of Pseudomonas aeruginosa. Antimicrobial Agents and Chemotherapy 60:2302–2310. American Society for Microbiology.

Römling, U., M. Y. Galperin, and M. Gomelsky. 2013. Cyclic di-GMP: the First 25 Years of a Universal Bacterial Second Messenger. Microbiol Mol Biol Rev 77:1–52.

Rose, C. J., K. Hammerschmidt, Y. Pichugin, and P. B. Rainey. 2020. Meta-population structure and the evolutionary transition to multicellularity. Ecology Letters 23:1380–1390.

Rousset, F. 2004. Genetic Structure and Selection in Subdivided Populations. Princeton University Press.

Roychoudhury, P., N. Shrestha, V. R. Wiss, and S. M. Krone. 2014. Fitness benefits of low infectivity in a spatially structured population of bacteriophages. Proc. R. Soc. B-Biol. Sci. 281:20132563. Royal Soc, London.

Rozen, D. E., J. A. G. M. de Visser, and P. J. Gerrish. 2002. Fitness Effects of Fixed Beneficial Mutations in Microbial Populations. Current Biology 12:1040–1045.

Ruiz, J. 2003. Mechanisms of resistance to quinolones: target alterations, decreased accumulation and DNA gyrase protection. Journal of Antimicrobial Chemotherapy 51:1109–1117.

Rumbaugh, K. P., J. A. Griswold, and A. N. Hamood. 2000. The role of quorum sensing in the in vivo virulence of Pseudomonas aeruginosa. Microbes and Infection 2:1721–1731.

Rumbaugh, K. P., and K. Sauer. 2020. Biofilm dispersion. Nat Rev Microbiol 18:571–586. Nature Publishing Group.

Ryder, C., M. Byrd, and D. J. Wozniak. 2007. Role of polysaccharides in Pseudomonas aeruginosa biofilm development. Current Opinion in Microbiology 10:644–648.

Sanders, L. H., A. Rockel, H. Lu, D. J. Wozniak, and M. D. Sutton. 2006. Role of Pseudomonas aeruginosa dinB-encoded DNA polymerase IV in mutagenesis. J Bacteriol 188:8573–8585.

Santos-Lopez, A., C. W. Marshall, M. R. Scribner, D. J. Snyder, and V. S. Cooper. 2019. Evolutionary pathways to antibiotic resistance are dependent upon environmental structure and bacterial lifestyle. eLife 8:e47612. eLife Sciences Publications, Ltd.

Saxer, G., M. Doebeli, and M. Travisano. 2009. Spatial Structure Leads to Ecological Breakdown and Loss of Diversity. Proceedings: Biological Sciences 276:2065–2070. Royal Society.

Schenk, M. F., M. P. Zwart, S. Hwang, P. Ruelens, E. Severing, J. Krug, and J. A. G. M. de Visser. 2022. Population size mediates the contribution of high-rate and large-benefit mutations to parallel evolution. Nat Ecol Evol 6:439–447. Nature Publishing Group.

Schick, A., S. Shewaramani, and R. Kassen. 2022. Genomics of Diversification of Pseudomonas aeruginosa in Cystic Fibrosis Lung-like Conditions. Genome Biology and Evolution 14:evac074.

Schoustra, S. E., T. Bataillon, D. R. Gifford, and R. Kassen. 2009. The Properties of Adaptive Walks in Evolving Populations of Fungus. PLOS Biology 7:e1000250.

Schrag, S. J., and J. E. Mittler. 1996. Host-Parasite Coexistence: The Role of Spatial Refuges in Stabilizing Bacteria-Phage Interactions. The American Naturalist 148:348–377. The University of Chicago Press.

Schuster, M., and E. Peter Greenberg. 2006. A network of networks: Quorum-sensing gene regulation in Pseudomonas aeruginosa. International Journal of Medical Microbiology 296:73–81.

Scribner, M. R., A. C. Stephens, J. L. Huong, A. R. Richardson, and V. S. Cooper. 2022. The Nutritional Environment Is Sufficient To Select Coexisting Biofilm and Quorum Sensing Mutants of Pseudomonas aeruginosa. Journal of Bacteriology 204:e00444-21. American Society for Microbiology.

Seferbekova, Z., A. Lomakin, L. R. Yates, and M. Gerstung. 2023. Spatial biology of cancer evolution. Nat Rev Genet 24:295–313. Nature Publishing Group.

Sexton, J. P., P. J. McIntyre, A. L. Angert, and K. J. Rice. 2009. Evolution and Ecology of Species Range Limits. Annu. Rev. Ecol. Evol. Syst. 40:415–436. Annual Reviews.

Shaer Tamar, E., and R. Kishony. 2022. Multistep diversification in spatiotemporal bacterial-phage coevolution. Nat Commun 13:7971. Nature Publishing Group.

Shapiro, J. T., G. Leboucher, A.-F. Myard-Dury, P. Girardo, A. Luzzati, M. Mary, J.-F. Sauzon, B. Lafay, O. Dauwalder, F. Laurent, G. Lina, C. Chidiac, S. Couray-Targe, F. Vandenesch, J.-P. Flandrois, and J.-P. Rasigade. 2020. Metapopulation ecology links antibiotic resistance, consumption, and patient transfers in a network of hospital wards. eLife 9:e54795. eLife Sciences Publications, Ltd.

Sharma, N., S. Yagoobi, and A. Traulsen. 2023. Self-loops in evolutionary graph theory: Friends or foes? PLOS Computational Biology 19:e1011387. Public Library of Science.

Shi, H., Q. Shi, B. Grodner, J. S. Lenz, W. R. Zipfel, I. L. Brito, and I. De Vlaminck. 2020. Highly multiplexed spatial mapping of microbial communities. Nature 588:676–681. Nature Publishing Group.

Slatkin, M. 1981. Fixation Probabilities and Fixation Times in a Subdivided Population. Evolution 35:477–488.

Slatkin, M. 1987. Gene Flow and the Geographic Structure of Natural Populations. Science 236:787–792. American Association for the Advancement of Science.

Slatkin, M. 1985. Gene Flow in Natural Populations. Annual Review of Ecology and Systematics 16:393–430. Annual Reviews.

Smith, W. P. J., Y. Davit, J. M. Osborne, W. Kim, K. R. Foster, and J. M. Pitt-Francis. 2017. Cell morphology drives spatial patterning in microbial communities. Proc Natl Acad Sci U S A 114:E280–E286.

Sniegowski, P. D., and P. J. Gerrish. 2010. Beneficial mutations and the dynamics of adaptation in asexual populations. Philos Trans R Soc Lond B Biol Sci 365:1255–1263.

Sprouffske, K., L. M. F. Merlo, P. J. Gerrish, C. C. Maley, and P. D. Sniegowski. 2012. Cancer in Light of Experimental Evolution. Current Biology 22:R762–R771.

Stacy, A., L. McNally, S. E. Darch, S. P. Brown, and M. Whiteley. 2016. The biogeography of polymicrobial infection. Nat Rev Microbiol 14:93–105. Nature Publishing Group.

Steenackers, H. P., I. Parijs, K. R. Foster, and J. Vanderleyden. 2016. Experimental evolution in biofilm populations. FEMS Microbiology Reviews 40:373–397.

Susan F. Bailey, Andrew Trudeau, Katherine Tulowiecki, Morgan McGrath, Aria Belle, Herbert Fountain, and Mahfuza Akter. 2021. Spatial structure affects evolutionary dynamics and drives genomic diversity in experimental populations of Pseudomonas fluorescens. bioRxiv 2021.09.28.461808.

Svensson, E. I., and R. Calsbeek. 2012. The adaptive landscape in evolutionary biology. University Press, Oxford.

Taylor, P. D. 1992. Altruism in viscous populations — an inclusive fitness model. Evol Ecol 6:352–356.

Tenaillon, O., J. E. Barrick, N. Ribeck, D. E. Deatherage, J. L. Blanchard, A. Dasgupta, G. C. Wu, S. Wielgoss, S. Cruveiller, C. Médigue, D. Schneider, and R. E. Lenski. 2016. Tempo and mode of genome evolution in a 50,000-generation experiment. Nature 536:165–170. Nature Publishing Group.

Testa, S., S. Berger, P. Piccardi, F. Oechslin, G. Resch, and S. Mitri. 2019. Spatial structure affects phage efficacy in infecting dual-strain biofilms of Pseudomonas aeruginosa. Commun Biol 2:1–12. Nature Publishing Group.

Thompson, J. N. 2005. The geographic mosaic of coevolution. University of Chicago Press, Chicago.

Thorpe, H. A., S. C. Bayliss, L. D. Hurst, and E. J. Feil. 2017. Comparative Analyses of Selection Operating on Nontranslated Intergenic Regions of Diverse Bacterial Species. Genetics 206:363–376.

Tilman, D., and P. M. Kareiva. 1997. Spatial ecology: the role of space in population dynamics and interspecific interactions. Princeton University Press, Princeton, N.J.

Tkadlec, J., A. Pavlogiannis, K. Chatterjee, and M. A. Nowak. 2021. Fast and strong amplifiers of natural selection. Nat Commun 12:4009.

Tkadlec, J., A. Pavlogiannis, K. Chatterjee, and M. A. Nowak. 2020. Limits on amplifiers of natural selection under death-Birth updating. PLOS Computational Biology 16:e1007494. Public Library of Science.

Trubenová, B., D. Roizman, A. Moter, J. Rolff, and R. R. Regoes. 2022. Population genetics, biofilm recalcitrance, and antibiotic resistance evolution. Trends in Microbiology 30:841–852.

Urban, M. C., M. A. Leibold, P. Amarasekare, L. De Meester, R. Gomulkiewicz, M. E. Hochberg, C. A. Klausmeier, N. Loeuille, C. de Mazancourt, J. Norberg, J. H. Pantel, S. Y. Strauss, M. Vellend, and M. J. Wade. 2008. The evolutionary ecology of metacommunities. Trends in Ecology & Evolution 23:311–317.

Van den Bergh, B., T. Swings, M. Fauvart, and J. Michiels. 2018. Experimental Design, Population Dynamics, and Diversity in Microbial Experimental Evolution. Microbiology and Molecular Biology Reviews 82:10.1128/mmbr.00008-18. American Society for Microbiology.

Van Dyken, J. D., M. J. I. Müller, K. M. L. Mack, and M. M. Desai. 2013. Spatial Population Expansion Promotes the Evolution of Cooperation in an Experimental Prisoner's Dilemma. Current Biology 23:919–923.

Vega, N. M., and J. Gore. 2018. Simple organizing principles in microbial communities. Current Opinion in Microbiology 45:195–202.

Velicer, G. J., L. Kroos, and R. E. Lenski. 1998. Loss of social behaviors by Myxococcus xanthus during evolution in an unstructured habitat. Proceedings of the National Academy of Sciences 95:12376–12380. Proceedings of the National Academy of Sciences.

Venables, W. N., and B. D. Ripley. 2002. Modern Applied Statistics with S. Fourth. Springer, New York.

Venail, P. A., R. C. MacLean, T. Bouvier, M. A. Brockhurst, M. E. Hochberg, and N. Mouquet. 2008. Diversity and productivity peak at intermediate dispersal rate in evolving metacommunities. Nature 452:210–214. Nature Publishing Group.

Vogwill, T., A. Fenton, and M. A. Brockhurst. 2010. HOW DOES SPATIAL DISPERSAL NETWORK AFFECT THE EVOLUTION OF PARASITE LOCAL ADAPTATION? Evolution 64:1795–1801.

Vogwill, T., R. L. Phillips, D. R. Gifford, and R. C. MacLean. 2016. Divergent evolution peaks under intermediate population bottlenecks during bacterial experimental evolution. Proceedings of the Royal Society B: Biological Sciences 283:20160749. Royal Society.

Wade, M. J., and C. J. Goodnight. 1998. Perspective: The Theories of Fisher and Wright in the Context of Metapopulations: When Nature Does Many Small Experiments. Evolution 52:1537–1553.

Wein, T., and T. Dagan. 2019. The Effect of Population Bottleneck Size and Selective Regime on Genetic Diversity and Evolvability in Bacteria. Genome Biology and Evolution 11:3283–3290.

Werner, G. D. A., J. E. Strassmann, A. B. F. Ivens, D. J. P. Engelmoer, E. Verbruggen, D. C. Queller, R. Noë, N. C. Johnson, P. Hammerstein, and E. T. Kiers. 2014. Evolution of

microbial markets. Proceedings of the National Academy of Sciences 111:1237–1244. Proceedings of the National Academy of Sciences.

Whitlock, M. C. 2003. Fixation Probability and Time in Subdivided Populations. Genetics 164:767–779.

Wiegand, I., A. K. Marr, E. B. M. Breidenstein, K. N. Schurek, P. Taylor, and R. E. W. Hancock. 2008. Mutator genes giving rise to decreased antibiotic susceptibility in Pseudomonas aeruginosa. Antimicrob Agents Chemother 52:3810–3813.

Wild, G., A. Gardner, and S. A. West. 2009. Adaptation and the evolution of parasite virulence in a connected world. Nature 459:983–986. Nature Publishing Group.

Williams, P., and M. Cámara. 2009. Quorum sensing and environmental adaptation in Pseudomonas aeruginosa: a tale of regulatory networks and multifunctional signal molecules. Current Opinion in Microbiology 12:182–191.

Winsor, G. L., E. J. Griffiths, R. Lo, B. K. Dhillon, J. A. Shay, and F. S. L. Brinkman. 2016. Enhanced annotations and features for comparing thousands of Pseudomonas genomes in the Pseudomonas genome database. Nucleic Acids Research 44:D646–D653.

Wong, A., and R. Kassen. 2011. Parallel evolution and local differentiation in quinolone resistance in Pseudomonas aeruginosa. Microbiology 157:937–944. Microbiology Society,.

Wong, A., N. Rodrigue, and R. Kassen. 2012. Genomics of Adaptation during Experimental Evolution of the Opportunistic Pathogen Pseudomonas aeruginosa. PLOS Genetics 8:e1002928.

Wood, T. K. 2014. Biofilm dispersal: deciding when it is better to travel. Molecular Microbiology 94:747–750.

Wright, S. 1932. The Roles of Mutation, Inbreeding, crossbreeding and Selection in Evolution. Proceedings of the XI International Congress of Genetics 8:209–222.

Yagoobi, S., and A. Traulsen. 2021. Fixation probabilities in network structured meta-populations. Sci Rep 11:17979.

Yanni, D., P. Márquez-Zacarías, P. J. Yunker, and W. C. Ratcliff. 2019. Drivers of Spatial Structure in Social Microbial Communities. Current Biology 29:R545–R550.

Yeaman, S., A. C. Gerstein, K. A. Hodgins, and M. C. Whitlock. 2018. Quantifying how constraints limit the diversity of viable routes to adaptation. PLoS Genet 14:e1007717.

Yeaman, S., and S. P. Otto. 2011. ESTABLISHMENT AND MAINTENANCE OF ADAPTIVE GENETIC DIVERGENCE UNDER MIGRATION, SELECTION, AND DRIFT. Evolution 65:2123–2129.

Yoshida, H., M. Bogaki, M. Nakamura, and S. Nakamura. 1990a. Quinolone resistance-determining region in the DNA gyrase gyrA gene of Escherichia coli. Antimicrobial Agents and Chemotherapy 34:1271–1272. American Society for Microbiology.

Yoshida, H., M. Nakamura, M. Bogaki, and S. Nakamura. 1990b. Proportion of DNA gyrase mutants among quinolone-resistant strains of Pseudomonas aeruginosa. Antimicrobial Agents and Chemotherapy 34:1273–1275. American Society for Microbiology.

Yuan, Y. 2016. Spatial Heterogeneity in the Tumor Microenvironment. Cold Spring Harb Perspect Med 6:a026583.

Zhang, Q., G. Lambert, D. Liao, H. Kim, K. Robin, C. Tung, N. Pourmand, and R. H. Austin. 2011. Acceleration of Emergence of Bacterial Antibiotic Resistance in Connected Microenvironments. Science 333:1764–1767.